CANADIAN THESES ON MICROFICHE

THÈSES CANADIENNES SUR MICROFICHE

National Library of Canada
Collections Development Branch

Canadian Theses on
Microfiche Service

Ottawa, Canada
K1A 0N4

Bibliothèque nationale du Canada
Direction du développement des collections

Service des thèses canadiennes
sur microfiche

NOTICE

The quality of this microfiche is heavily dependent upon the quality of the original thesis submitted for microfilming. Every effort has been made to ensure the highest quality of reproduction possible.

If pages are missing, contact the university which granted the degree.

Some pages may have indistinct print especially if the original pages were typed with a poor typewriter ribbon or if the university sent us an inferior photocopy.

Previously copyrighted materials (journal articles, published tests, etc.) are not filmed.

Reproduction in full or in part of this film is governed by the Canadian Copyright Act, R.S.C. 1970, c. C-30. Please read the authorization forms which accompany this thesis.

AVIS

La qualité de cette microfiche dépend grandement de la qualité de la thèse soumise au microfilmage. Nous avons tout fait pour assurer une qualité supérieure de reproduction.

S'il manque des pages, veuillez communiquer avec l'université qui a conféré le grade.

La qualité d'impression de certaines pages peut laisser à désirer, surtout si les pages originales ont été dactylographiées à l'aide d'un ruban usé ou si l'université nous a fait parvenir une photocopie de qualité inférieure.

Les documents qui font déjà l'objet d'un droit d'auteur (articles de revue, examens publiés, etc.) ne sont pas microfilmés.

La reproduction, même partielle, de ce microfilm est soumise à la Loi canadienne sur le droit d'auteur, SRC 1970, c. C-30. Veuillez prendre connaissance des formules d'autorisation qui accompagnent cette thèse.

THIS DISSERTATION HAS BEEN MICROFILMED EXACTLY AS RECEIVED

LA THÈSE A ÉTÉ MICROFILMÉE TELLE QUE NOUS L'AVONS REÇUE

Canada

NL 339 (r. 85/09)

(138)

0-315-21332-9

National Library of Canada
Canadian Theses Division
Ottawa, Canada
K1A 0N4

Bibliothèque nationale du Canada
Division des thèses canadiennes

PERMISSION TO MICROFILM — AUTORISATION DE MICROFILMER

• Please print or type — Écrire en lettres moulées ou dactylographier

Full Name of Author — Nom complet de l'auteur

KEVIN MICHAEL ANSDELL

Date of Birth — Date de naissance

31-01-61

Country of Birth — Lieu de naissance

UNITED KINGDOM

Permanent Address — Résidence fixe

21 EAST GROVE ROAD, SHEFFIELD, SOUTH YORKSHIRE, S10 2NN ENGLAND

Title of Thesis — Titre de la thèse

FLUID INCLUSION AND STABLE ISOTOPE STUDY OF THE TOM BA-PB-ZN DEPOSIT, YUKON TERRITORY, CANADA

University — Université

UNIVERSITY OF ALBERTA

Degree for which thesis was presented — Grade pour lequel cette thèse fut présentée

MASTER OF SCIENCE

Year this degree conferred — Année d'obtention de ce grade

1985

Name of Supervisor — Nom du directeur de thèse

DR. BRUCE E. NESBITT

Permission is hereby granted to the NATIONAL LIBRARY OF CANADA to microfilm this thesis and to lend or sell copies of the film.

The author reserves other publication rights, and neither the thesis nor extensive extracts from it may be printed or otherwise reproduced without the author's written permission.

L'autorisation est, par la présente, accordée à la BIBLIOTHÈQUE NATIONALE DU CANADA de microfilmer cette thèse et de prêter ou de vendre des exemplaires du film.

L'auteur se réserve les autres droits de publication; ni la thèse ni de longs extraits de celle-ci ne doivent être imprimés ou autrement reproduits sans l'autorisation écrite de l'auteur.

Date

29 November 1984

Signature

Kevin M. Ansdell

NL-91 (4/77)

THE UNIVERSITY OF ALBERTA

Fluid inclusion and stable isotope study of the Tom Ba-Pb-Zn deposit, Yukon Territory, Canada

by

Kevin Michael Ansdell

(C)

A THESIS

SUBMITTED TO THE FACULTY OF GRADUATE STUDIES AND RESEARCH

IN PARTIAL FULFILMENT OF THE REQUIREMENTS FOR THE DEGREE

Of Master of Science

Geology

EDMONTON, ALBERTA

Spring, 1985

THE UNIVERSITY OF ALBERTA

RELEASE FORM

NAME OF AUTHOR Kevin Michael Ansdell

TITLE OF THESIS Fluid inclusion and stable isotope study of the Tom Ba-Pb-Zn deposit, Yukon Territory, Canada

DEGREE FOR WHICH THESIS WAS PRESENTED Master of Science

YEAR THIS DEGREE GRANTED Spring, 1985

Permission is hereby granted to THE UNIVERSITY OF ALBERTA LIBRARY to reproduce single copies of this thesis and to lend or sell such copies for private, scholarly or scientific research purposes only.

The author reserves other publication rights, and neither the thesis nor extensive extracts from it may be printed or otherwise reproduced without the author's written permission.

(SIGNED) Kevin M. Ansdell

PERMANENT ADDRESS:

21 East Grove Road

Sheffield, Sth Yorks, S10 2NN

ENGLAND

DATED 19 Nov 1984

THE UNIVERSITY OF ALBERTA

FACULTY OF GRADUATE STUDIES AND RESEARCH

The undersigned certify that they have read, and recommend to the Faculty of Graduate Studies and Research, for acceptance, a thesis entitled Fluid inclusion and stable isotope study of the Tom Ba-Pb-Zn deposit, Yukon Territory, Canada submitted by Kevin Michael Ansdell in partial fulfilment of the requirements for the degree of Master of Science.

Bruce Nesbitt

Supervisor

Date 19th November 1984

Dedication

To friends

Abstract

The Tom Ba-Pb-Zn deposit is a typical, sediment-hosted, stratiform, exhalative, massive sulfide deposit, hosted by carbonaceous mudstones, turbiditic sand-banded mudstones, and debris flow chert pebble conglomerates of the Upper Devonian Earn Group. The deposit consists of a lens of massive sulfides (pyrrhotite-galena-Fe-rich sphalerite-ankerite-chalcopyrite) which passes vertically and laterally into laminated sulfides (Fe-poor sphalerite-galena-pyrite-barite-chert). In the footwall units below the massive sulfides is an area of ankerite, and quartz veining, interpreted by Carne (1979) to represent the feeder zone for the mineralizing fluids. Ankerite veins are related to mineralization, whereas fluid inclusion and stable isotope data suggest that the quartz veins formed during one of the post-mineralization, deformation events.

Homogenization temperatures from ankerite and quartz exhibit a range from 125° to 335°C. The range is due to variable leakage from all inclusions during deformation. Leakage increases the measured homogenization temperature and so the average ankerite homogenization temperature (258°C) represents an upper limit for the temperature of the mineralizing fluid. However, fluid inclusion analysis allows distinction of the mineralizing fluid from the deformation fluid on the basis of inclusion type and salinity. Ankerite was deposited from an aqueous solution of salinity 9.1 ± 3.4 wt.% NaCl equiv., while the tectonic quartz was deposited from fluids with a high and variable CO_2 (± CH_4) content and salinity of 4.8 ± 1.3 wt.% NaCl equiv. The CO_2 content of inclusions within a given quartz grain are usually similar, but there are distinctive inter-grain, and inter-sample variations. This is a function of local variations in the proportion of secondary ankerite cement in the adjacent rocks.

The lack of variation in the oxygen isotopic compositions of mudstones, and <2μm mineral fractions, plus the absence of an alteration halo around the mineralization, implies that the extent of interaction between the mineralizing fluid and the country rock was small. This may be due to a low water/rock ratio, a high fluid flow rate and/or a low temperature (~150°C) for the mineralizing fluid. Pure clay samples were not obtained, but a depletion in ^{18}O in kaolinite-rich samples does suggest that the isotopic composition of the kaolinite is a result of interaction with the hydrothermal fluid.

The isotopic compositions of the ankerite- and quartz-forming fluids were calculated for temperatures ranging from 100° to 250°C, by assuming equilibrium fractionation between the minerals and water. At a given temperature, the isotopic composition of the quartz-forming fluid is enriched in ^{18}O relative to the ankerite-forming fluid. Both fluids were probably formation waters.

The mineral assemblages and paragenesis suggest that early mineral deposition (fine-grained quartz, ankerite) occurred in a sulfur-deficient environment. Local production of reduced sulfur eventually allowed the precipitation of sulfides. The mineral zonation exhibited by the massive and laminated ore is typical of hot, reduced hydrothermal fluids mixing with cooler, more oxygenated water.

Acknowledgements

Throughout the duration of this project, numerous people have provided advice, encouragement, assistance and friendship, and to everyone I am extremely grateful. I particularly thank my supervisor, Bruce Nesbitt, for initiating the project and providing much needed guidance. Fred Longstaffe kindly allowed me unlimited access to his clay mineralogy laboratory and X-ray diffractometer, and shared much of his knowledge of stable isotopes with me. Roger Morton is thanked for teaching me the fundamentals of fluid inclusion analysis.

Thanks are due to Diane Caird because the stable isotope section of this project would not have been completed without her tireless efforts. She performed all the stable isotope analyses and did much of the time-consuming preparatory work. I also thank Steve Launspach for assistance with the electron microprobe analyses, and Peter Black for preparing all my normal and polished thin sections. The Experimental Petrology Laboratory of Chris Scarfe kindly allowed me to use their polishing wheel in the preparation of numerous fluid inclusion plates.

The project would not have got off the ground without the co-operation of the owners of the Tom property, Hudson's Bay Exploration and Development Company Ltd., and Gerry Bidwell of the Whitehorse office in particular. They allowed me unlimited access to drillcore stored at the property and at the H. S. Bostock Core Library in Whitehorse, and provided food and accommodation during my time in the field for which I am very grateful. Ken McClay of Goldsmiths College, London, and Bob Turner of Stanford University are thanked for friendship in the field and for numerous fruitful discussions.

Financial support for this project was provided by the Boreal Institute for Northern Studies, and by a Department of Energy, Mines and Resources grant to Fred Longstaffe. I also gratefully acknowledge receipt of a Canadian Reverse Rhodes Scholarship for the period 1982-83, and a teaching assistantship from the Department of Geology.

Finally, I am grateful for the friendship provided by the faculty, fellow graduates, and undergraduates in the Department. Simon J. Hook is especially thanked for his continuous encouragement, support, and friendship.

Table of Contents

Chapter		Page
1.	INTRODUCTION	1
2.	REGIONAL GEOLOGY	4
	2.1 Introduction	4
	2.2 Selwyn Basin	4
	2.2.1 Stratigraphy and tectonic setting	4
	2.2.2 Regional Ba-Pb-Zn mineralization	8
	2.3 Stratigraphy and structure of the MacMillan Pass Graben	9
3.	GEOLOGY OF THE TOM DEPOSIT	16
	3.1 Introduction	16
	3.2 General geology and structure	16
	3.3 Petrological features of the ore and associated rocks	21
	3.3.1 Footwall rocks	21
	3.3.2 Sulfide mineralization	24
	3.3.3 Hangingwall rocks	30
	3.3.4 Deformation features	35
	3.3.5 Paragenesis	36
4.	FLUID INCLUSIONS	41
	4.1 Introduction	41
	4.2 Analytical procedure	41
	4.3 Inclusion petrography and classification	44
	4.4 Freezing measurements	49
	4.5 Heating measurements	60
	4.6 Discussion of results	65
	4.7 Conclusions	70
5.	ISOTOPE GEOCHEMISTRY	71
	5.1 Introduction	71
	5.2 Analytical procedure	71
	5.3 Results	72
	5.4 Discussion of results	76

6. DISCUSSION AND CONCLUSIONS ON THE DEVELOPMENT OF THE TOM DEPOSIT 83

6.1 Genesis of the deposit 83

6.1.1 Features relevant to the formation of the deposit 83

6.1.2 Composition, temperature and origin of the mineralizing fluid 84

6.1.3 Constraints on the depositional environment 86

6.2 Determination of the timing of quartz veins 89

6.3 Conclusions on the nature of the fluids present during deformation 90

REFERENCES 92

APPENDIX 1. SECTIONS ACROSS THE TOM WEST ZONE 105

APPENDIX 2. PREPARATION OF CLAY SAMPLES 115

APPENDIX 3. RELATIVE INTENSITIES OF KAOLINITE AND ILLITE PEAKS ON X.R.D. CHARTS 117

APPENDIX 4. FLUID INCLUSION MEASUREMENTS 118

List of Tables

Table 1. Correlation and description of lithologies in the vicinity of Tom 20

Table 2. Structural characteristics of the Tom 22

Table 3. Electron microprobe analyses of iron carbonates 23

Table 4. Electron microprobe analyses of sphalerite 32

Table 5. Salinities of Type 1 inclusions 55

Table 6. Composition of Type 2 inclusions 58

Table 7. Oxygen and carbon isotope data 73

Table 8. Calculated isotopic composition of the ankerite-forming fluid 78

Table 9. Calculated isotopic composition of the quartz-forming fluid 80

List of Figures

Figure 1. Major tectonic elements of the northern Canadian Cordillera, and location of important Pb-Zn camps 2

Figure 2. Schematic stratigraphic sections across the Selwyn Basin 5

Figure 3. Geology of the MacMillan Fold Belt 10

Figure 4. Structural cross-sections across the MacMillan Fold Belt 12

Figure 5. Geology of the Tom deposit 17

Figure 6. Schematic isopach map of the Tom deposit 19

Figure 7. Typical stratigraphy of the West Zone mineralization, and metal grade patterns from TS84 31

Figure 8. Paragenesis of the Tom deposit 39

Figure 9. Freezing-and-heating stage calibration curve 43

Figure 10. Melting temperatures from Type 1 inclusions 50

Figure 11. CO_2 and clathrate melting temperatures 51

Figure 12. CO_2 homogenization temperatures in Type 2 inclusions 52

Figure 13. Temperature-composition diagram at 1 bar in the system H_2O-NaCl 54

Figure 14. Graph showing the affect of adding NaCl and CH_4 to the H_2O-CO_2 system 61

Figure 15. Homogenization and decrepitation temperatures from Type 1 and 2 inclusions in quartz and ankerite 63

Figure 16. Boiling point curve for a H_2O-NaCl solution of salinity 9 wt.% NaCl 68

Figure 17. Simplified longitudinal cross-section through the Tom West Zone to allow location of stable isotope samples 75

List of Plates

Plate 1. Replacement by ankerite in the chert pebble conglomerate 25

Plate 2. Photograph showing relationship between ankerite replacement of the country rock, ankerite veins, pyrrhotite veins, and arsenopyrite euhedra 25

Plate 3. Pyrrhotite vein infiltrating along cleavage in ankerite 28

Plate 4. Bird's eye replacement of pyrrhotite by pyrite 28

Plate 5. Pyrite framboids in the laminated ore 33

Plate 6. Barite grain aligned oblique to primary banding 33

Plate 7. Quartz-carbonate vein cutting chert pebble conglomerate 37

Plate 8. Pressure solution cleavage in chert pebble conglomerate 37

Plate 9. Type 1 inclusion in quartz 45

Plate 10. Two-phase type 2 inclusion in quartz 45

Plate 11. Three-phase type 2 inclusion in quartz 47

Plate 12. Typical morphology of ankerite inclusions 47

1. INTRODUCTION

The Tom deposit situated at 63°10' N, 130°12' W forms part of the MacMillan Pass base-metal camp and is one of a number of large Ba-Pb-Zn resources in the Selwyn Basin, Yukon Territory (Fig. 1) (Carne and Cathro, 1982). The deposit, which is presently owned by Hudson Bay Exploration and Development, was discovered by prospectors in 1951, and provided the spark for extensive exploration activity in the MacMillan Pass area leading to the discovery of numerous other Ba-Pb-Zn occurrences.

The deposit is classified as a sediment-hosted, stratiform, base metal deposit (Large, 1983). The mineralization consists of two zones, the West and East Zones, hosted by a sequence of clastic rocks of the Upper Devonian, lower Earn Group (Gordey et al., 1982). Present-day reserves are estimated at 9.8 million tonnes, grading 7.5 percent Zn, 6.4 percent Pb, and 74 g/tonne Ag (McClay, 1984). Previous contributions to our knowledge of the geology, geochemistry, and structure of the deposit have been made by Carne (1979), Large (1981), and McClay (1984). Large (1981) attempted to define the boundary conditions of the hydrothermal fluid and the depositional environment, based on mineralogical, and geochemical observations.

The objective of this study was to determine the source, composition, and temperature of the mineralizing fluid, its interaction with the host rock, and the physicochemical conditions of the depositional environment by using fluid inclusions and stable isotopes. Similar studies have been completed recently at the neighbouring Jason deposit (Longstaffe et al., 1982; Gardner, 1983), and so it was hoped to compare and contrast their results with those obtained at Tom. Many similarities were expected considering the spatial and temporal proximity of the two deposits. Carne (1979) delineated a funnel-shaped, stockwork zone of quartz, carbonate, and sulfide veins, underlying the massive sulfides of the West Zone. He interpreted these veins to represent the conduits for the mineralizing fluids, and so this part of the deposit was considered the most suitable for unravelling the nature, and affects of the mineralizing, hydrothermal fluids. Sampling was thus concentrated in this area.

Sampling and detailed observations were completed over a total period of five weeks from drillcore stored at the property, and at the H.S. Bostock Core Library, Whitehorse. Few surface samples were collected because of the paucity of mineralized

Figure 1. Major tectonic elements of the northern Canadian Cordillera, and location of the important Pb-Zn camps.

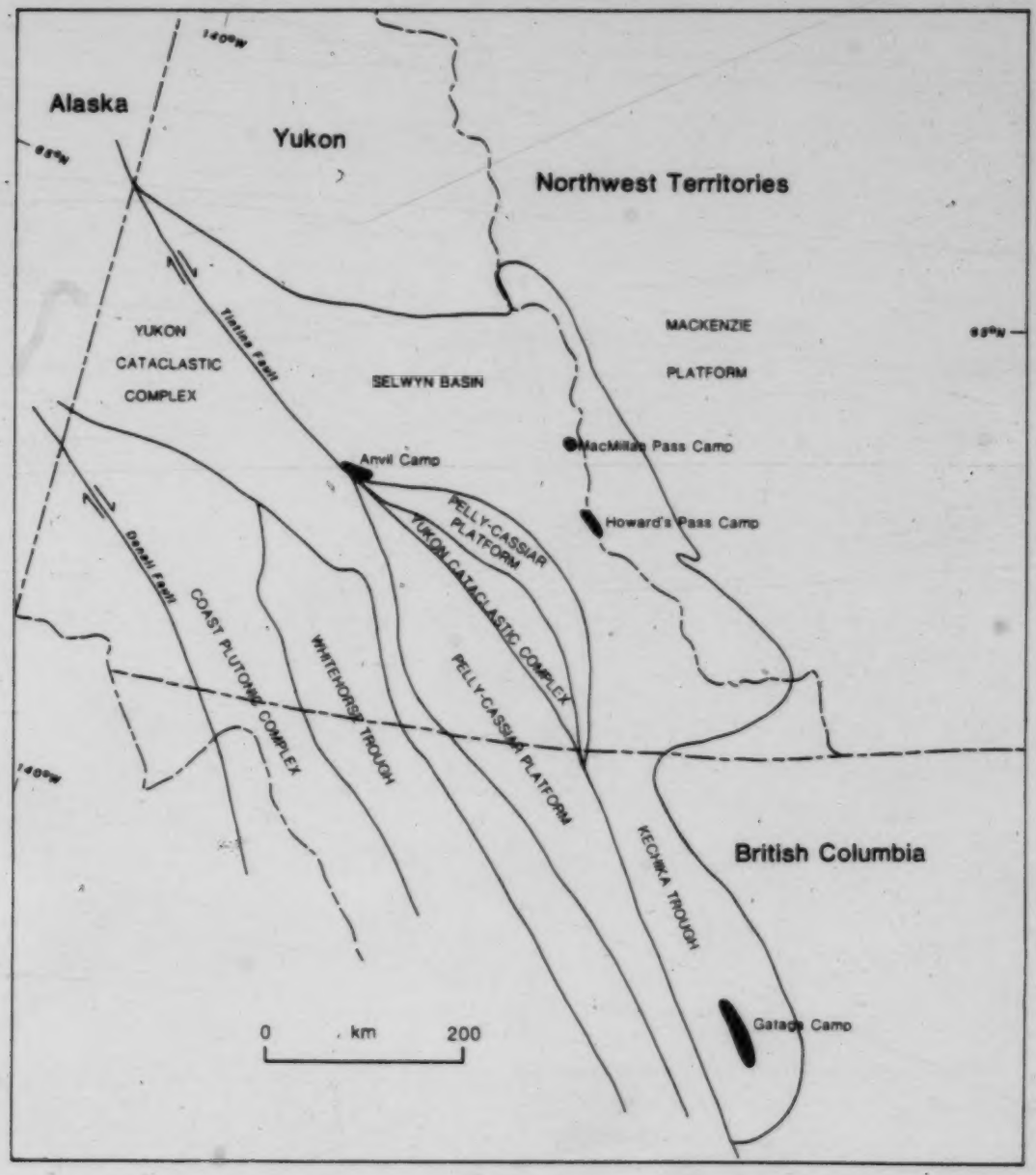

outcrops, and rocks immediately adjacent to the mineralization. The underground workings were completely flooded and so observation underground was impossible.

A paragenetic history was compiled after preparing normal- and polished-thin sections. The timing of the many quartz veins relative to mineralization was difficult to determine initially. However, from fluid inclusion and stable isotope analyses the veins were finally interpreted to have formed post-mineralization, during one of the three deformation periods described by McClay (1984). It was therefore also possible to provide information on the nature of the fluids present during deformation, as well as during mineralization.

2. REGIONAL GEOLOGY

2.1 Introduction

The following descriptions and interpretations of the stratigraphy and structure of the Selwyn Basin and MacMillan Pass Graben are based on a review of pertinent literature. According to Large's (1983) classification of the host basins for sediment-hosted massive sulfide lead-zinc deposits, these two would represent first and second order basins respectively.

2.2 Selwyn Basin

2.2.1 Stratigraphy and tectonic setting

The Selwyn Basin, a term first proposed by Gabrielse (1967), is an important tectonostratigraphic unit of the northern Canadian Cordillera. It is an arcuate, elongate feature that parallels the other main tectonic elements of the Cordillera (Fig. 1). The definition of the Selwyn Basin is still a matter of controversy, and so the limits of the Selwyn Basin, as defined by Carne and Cathro (1982), are used in this review.

The oldest lithologic unit in this region is the "Grit Unit" (Fig. 2) (Roddick and Green, 1961), an Hadrynian sequence of quartzofeldspathic sandstones, shales and minor limestones (Gabrielse et al., 1973). These rocks are thought to have been deposited as a sedimentary wedge on the north-western margin of the North American continent (Douglas et al., 1970).

During Lower Cambrian time, gentle downwarping of this passive, Atlantic-type, continental margin, parallel to the craton edge, formed the trough-like Selwyn Basin (Blusson, 1976). This shallow trough was bounded to the north and east by shallow-water, platform carbonates of the Mackenzie platform, and to the south-west by the incipient Pelly-Cassiar platform (Figs. 1 and 2). The development of the Pelly-Cassiar platform as a positive topographic feature around the Cambro-Ordovician boundary is related either to Late Cambrian volcanism (Templeman-Kluit and Blusson, 1977), or to the rapid build-up of carbonates (Jennings et al., 1980), and resulted in the restriction of the Selwyn Basin from the open ocean. The Lower Cambrian Sekwi Formation represents the

Figure 2. Schematic stratigraphic sections across the Selwyn Basin (after Templeman-Kluit, 1977; Gordey, 1980; Gordey et al., 1981; Gordey et al., 1982).

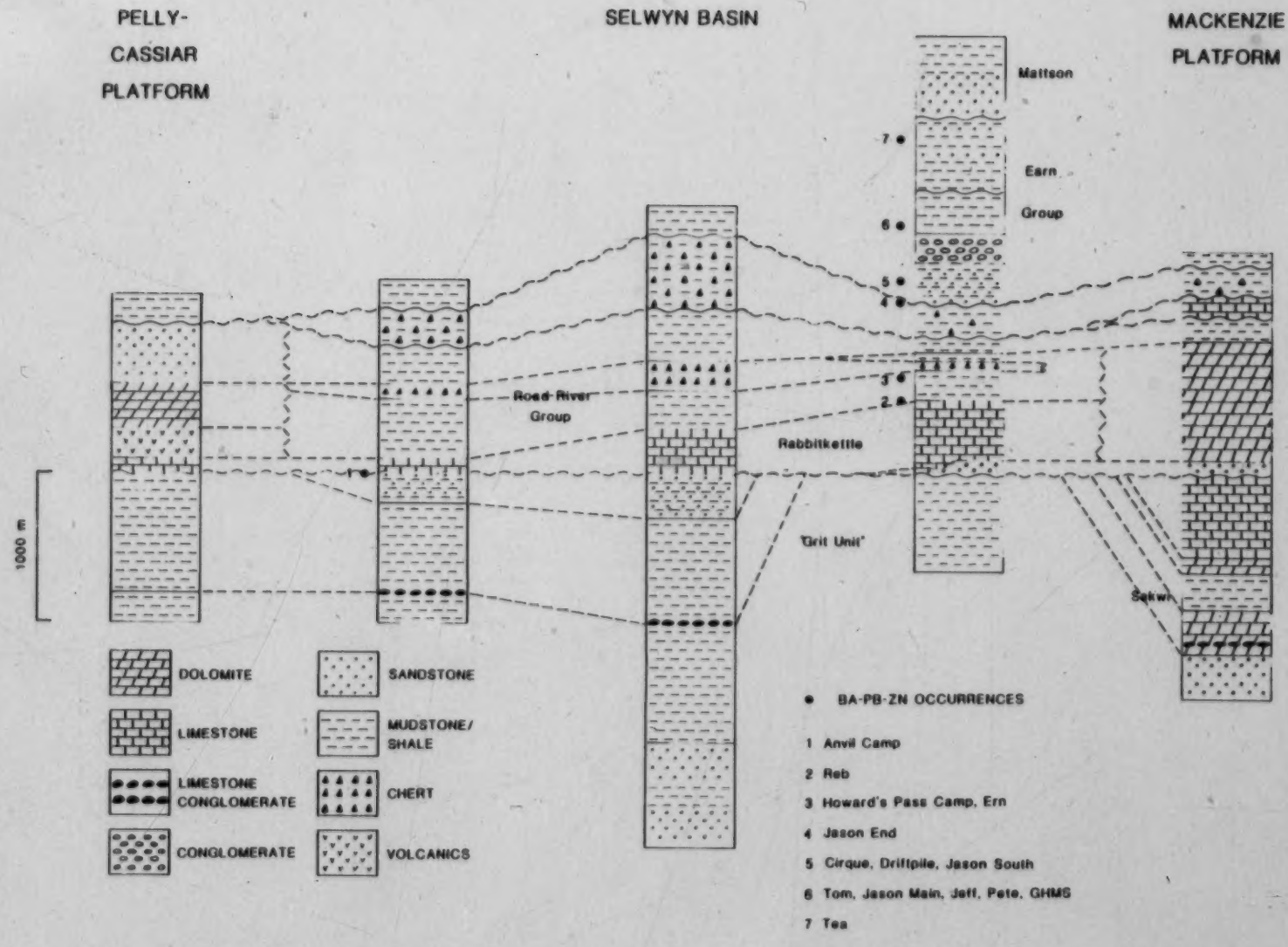
PELLY-
CASSIAR
PLATFORM
SELWYN BASIN
MACKENZIE
PLATFORM
Mattson
Earn
Group
Road River
Group
Rabbitkettle
'Grit Unit'
Sekwi
1000 m
DOLOMITE
LIMESTONE
LIMESTONE
CONGLOMERATE
CONGLOMERATE
SANDSTONE
MUDSTONE/
SHALE
CHERT
VOLCANICS
BA-PB-ZN OCCURRENCES
1 Anvil Camp
2 Reb
3 Howard's Pass Camp, Ern
4 Jason End
5 Cirque, Driftpile, Jason South
6 Tom, Jason Main, Jeff, Pete, GHMS
7 Tea

first indication of a basinal feature, with facies variations from calcareous shales and gray mudstones in the basin center to limestones, dolomites and siltstones of the Mackenzie platform (Fig. 2) (Gordey, 1980).

The eventual development of a quiet, euxinic, restricted environment is indicated by the Rabbitkettle Formation and the Road River Group (Fig. 2). The former consists of argillaceous limestones and calcareous siltstones, while the latter is typified by black, graptolitic, siliceous shales and thinly-bedded limestones. The black shale of the Road River Group grades into cherts in the central portion of the trough (Blusson, 1976). These lithologies are relatively thin when compared to the coeval carbonate successions of the Mackenzie and Pelly-Cassiar platforms (Gordey, 1980; Carne and Cathro, 1982).

An important change in the tectonic and sedimentary regime occurred during the Middle Devonian. At this time the Selwyn Basin was affected by unstable, extensional tectonics resulting in block faulting, rifting, and basinal uplift and an associated complicated package of clastic sediments. This package is termed the Earn Group (Gordey et al., 1982), and exhibits frequent thickness and facies changes throughout the Selwyn Basin making correlation difficult (Fig. 2). The lower Earn Group consists of gun-blue weathering, siliceous shale, siltstone and chert with localized occurrences of chert pebble conglomerate. The upper Earn Group of Upper Devonian to Middle Mississippian age rests unconformably on the lower Earn Group, and consists of similar lithologies except that they weather a brown color. The Earn Group marks the end of the Selwyn Basin as a distinctive sedimentary basin.

The Earn Group is unconformably overlain by a quartz sandstone, which is correlated with the Mattson Formation, and marks the return to normal, shallow-marine, clastic sedimentation typical of continental shelves (Gordey et al., 1982).

The region was inactive tectonically until the Late Jurassic. The Columbian Orogeny then affected the whole of the Selwyn Basin area, initiating open folding, faulting, and the intrusion of granodioritic and quartz monzonitic stocks. These Mesozoic structures were then overprinted and rejuvenated during the Early Tertiary Laramide Orogeny.

2.2.2 Regional Ba-Pb-Zn mineralization

About twenty, sedimentary, exhalative, barium-lead-zinc deposits have been discovered in the Selwyn Basin, most of which are concentrated in four major areas :- Anvil, Howard's Pass, Gataga, and MacMillan Pass (Fig. 1) (Carne and Cathro, 1982). The latter includes the Tom and Jason deposits, and will be discussed in more detail later. The stratigraphic positions of the deposits are shown on Figure 2.

The eight deposits in the Anvil camp are all Lower Cambrian in age, and associated with a graphitic phyllite transition zone between non-calcareous phyllites and schists (Mt.Mye Formation equivalent to upper "Grit Unit"), and calcareous phyllites (Vangorda Formation equivalent to Rabbitkettle Formation) (Jennings and Jilson, 1983). The mineralization occurs at the base of a mafic volcanic sequence, although a connection between mineralization and volcanism has not been confirmed.

The Lower Silurian, Howard's Pass deposits (Op, Anniv, XY) are low grade, but an estimated tonnage of several hundred million tonnes makes them one of the world's largest lead-zinc resources. The mineralization is hosted in the Lower Silurian Active member of the Howard's Pass Formation (Road River Group), which is exceedingly thick in the vicinity of the deposits (Morganti, 1983). The thickened Howard's Pass Formation defines the sub-basins in which mineralization was concentrated.

The Gataga camp consists of sulfide deposits ranging from Ordovician to Late Devonian in age (MacIntyre, 1983). The larger deposits (Cirque, Driftpile, Elf) are hosted in Late Devonian cherts and argillites which are typical of a starved basinal environment (Jefferson et al., 1983) Northwest-trending depositional troughs, indicated by rapid facies changes, have been suggested as the sub-basins in which mineralizing brines collected.

Significant occurrences of Pb-Zn mineralization of Early Silurian (ERN) and Middle Ordovician (Reb) age, have been found in the Gataga district. Both are associated with black graptolitic shales (MacIntyre, 1983).

Stratiform barite occurrences are found throughout the Selwyn Basin stratigraphy, although they are generally concentrated in Earn Group rocks (Dawson, 1983). Barium is frequently associated with lead-zinc occurrences, but also occurs alone in thick stratiform baritites and thin nodular deposits. Identification of conodonts from associated limestones has allowed Dawson and Orchard (1982) to pick out three major intervals of

barite deposition in the MacMillan Pass, and Howard's Pass areas. The major interval is a regional Upper Devonian (Frasnian) horizon, and includes the Jeff, GHMS, Pete, and Gargantua North occurrences. The latter two are thought to represent the distal part of the MacMillan Pass lead-zinc mineralization, while the other two were the products of a separate exhalative event. Middle Devonian, and Mississippian barite intervals are also important. The large Tea deposit (Lydon et al., 1979) occurs in the latter interval.

This brief description of sediment-hosted mineralization in the Selwyn Basin, and the location of occurrences throughout the stratigraphy of the region (Fig. 2), indicates the long-ranging and widespread extent of hydrothermal activity in this important lead-zinc province.

2.3 Stratigraphy and structure of the MacMillan Pass Graben

The MacMillan Pass area of the eastern Selwyn Basin has been intensively explored in recent years following the discovery of the Tom and Jason Ba-Pb-Zn deposits, and numerous barite occurrences. Regional geological mapping in the area has culminated in the production of an Open File Report by D.I.A.N.D. (Abbott, 1983), and so only a synthesis of the geology will be given here.

Abbott (1982) showed that all the deposits in the MacMillan Pass area occur in a structural feature, 30 km wide by 60 km long, that trends west-north-west oblique to the structural trends in the Selwyn Basin. This belt, the MacMillan Fold Belt, is split into three blocks based on structural style and Devonian stratigraphy. The geology of the fold belt and structural cross-sections across the belt are shown in Figures 3 and 4, with the boundaries to the three blocks superimposed.

The rocks of the area range from Late Proterozoic to Triassic. Underlying the Road River Group is a conformable sequence of maroon, green, brown, and gray shales, gray limestones, and limestone conglomerate. The latter is thought to be derived from the Mackenzie carbonate platform to the east. Conodonts and graptolites suggest that the limestones are time equivalents of the Rabbitkettle Formation.

The Road River Group consists of three divisions (Abbott, 1982). From base to top the three divisions are:

Figure 3. Geology of the MacMillan Fold Belt (from Abbott, 1982).

Legend
Kg - Cretaceous granitoid rocks
Ppt - Permian cherty shale
Cl - Carboniferous bioclastic limestone
Cq - Carboniferous sandstone
Csp - Carboniferous shale
Msp - Upper Earn Group
muDpt - Lower Earn Group(LEG) silver blue shale
muDcg - Late Devonian LEG chert pebble conglomerate
muDps - Late Devonian LEG brown shale
emDpt - Early Devonian LEG black to dark blue chert
SDv - Silurian/Devonian alkaline volcanics
OSDpt - Road River Group
COp - Rabbitkettle Formation and "Grit Unit"

The information on this page has been removed due to copyright restrictions. Description of the material is found on the preceding page

Figure 4. Structural cross-sections across the MacMillan Fold Belt (from Abbott, 1982). Legend as for Figure 3.

The information on this page has been removed due to copyright restrictions. Description of the material is found on the preceding page.

(1) cherts and black graphitic slates,

(2) bioturbated, flaser-bedded mudstones,

(3) dark silty limestone.

Within the Central Block the silty limestone is cut by, and interbedded with orange-weathering volcaniclastics.

The Middle to Upper Devonian lower Earn Group unconformably overlies the Road River Group. Within the lower Earn Group, there are distinctive stratigraphic variations within, and between, blocks. In the Central Block a series of clastic rocks (turbiditic sand-banded mudstones, overlain by chert pebble conglomerates) are bracketed by a siliceous shale facies. This clastic facies is thought to represent a turbidite fan complex, which has a westerly source (Winn et al., 1981). The conglomerate is confined to the Central Block, where it also thickens eastwards and towards the center of its depositional basin. Silver-weathering, graphitic, siliceous shales overlie the conglomerate, and range in thickness from 10 to 300 m towards the middle of the Central Block.

The lower contact of the upper Earn Group is an unconformity, and may account for some of the variations in thickness exhibited by the siliceous facies of the lower Earn Group in the Central Block. The upper Earn Group consists of ripple cross-laminated sandstones, siltstones, and shales, passing up into black shales. Within the Central Block the ripple cross-laminated unit dies out, and the whole of the upper Earn Group thins westwards. The greatest thickness (450 m) of the ripple cross-laminated unit occurs at the eastern end of the South Block, suggesting that the Central Block was no longer the focus of deposition at this time.

Post-Selwyn Basin sedimentary rocks are represented by Carboniferous quartz sandstones, Permian shales and cherts, and Triassic shales and sandstones (Gordey et al., 1982).

The structural styles in the three blocks can be seen in Figure 4, and are described in detail by Abbott (1982). The North Block consists of southerly-directed, imbricate, thrust faults that dip steeply north-westwards. The Central Block is the most complex structurally. High angle, northerly-directed, reverse faults which are genetically related to folding appear to make up the oldest deformation event. There appear to be two sets of tight upright folding, trending west-north-west and east-north-east, which are

superimposed towards the eastern end of the Central Block. Randomly oriented, steeply dipping faults cut the above structures. However, in some cases, these faults appear to have influenced fold development on either side. Abbott (1982) suggests that they may be tear faults that developed during later deformation as a result of sharp changes in the thickness of lower Earn Group rocks. Some of the faults may also be rejuvenated Devonian structures, although it is difficult to relate facies thickness changes with a given fault. However, at the Jason deposit, a Devonian synsedimentary fault is indicated by the presence of slump breccias involving locally deposited sediments, which are associated with the mineralization (Winn et al., 1981). The position of the mineralization is related to the presence of this fault. The southern boundary of the Central Block is also marked approximately by the trace of this fault. The South Block consists solely of large scale, tight, north-west trending folds that are cut by normal faults.

Structural features in the MacMillan Pass area are probably the result of regional Jurassic-Cretaceous deformation events. The complexity of the structure within the Central Block suggests that the Central Block may have been a zone of Devonian faulting, which influenced the later deformation events. A fault-dominated environment during the Devonian can be implied from the confinement of Devonian clastics to the Central Block, the presence of volcaniclastics, and rapid facies thickness variations. The concentration of lead, zinc, and barium mineralization within the Central Block must also be related to the presence of widespread faulting and basin development.

3. GEOLOGY OF THE TOM DEPOSIT

3.1 Introduction

The emphasis in this chapter is on the mineralogy, chemistry, and paragenesis of the ore and gangue minerals in the deposit and its host rocks. A detailed description of the deposit is unnecessary, because of the work of Carne (1979) on the general geology, Large (1981) on the host rock geochemistry, and McClay (1984) on the structural history of the area. The following section is a summary of the general geology and structure of the deposit based on this previous work. The remaining sections of the chapter detail the observations made during this study which will be used later when considering the formation and development of the deposit.

The surface geology, and the positions of the sampled surface drill holes are shown on Figure 5. Sections across the West Zone are shown in Appendix 1, with sample positions also marked. Drillhole intersections with the mineralization are used to construct a schematic isopach map of the deposit (Fig. 6).

3.2 General geology and structure

The Tom deposit consists of two mineralized zones, the West, and the East Zone, which are hosted in clastic sedimentary rocks of the lower Earn Group. Carne (1979) originally divided the sedimentary rocks of the deposit into a number of informal units. These units are correlatable with the lithological divisions of the Earn Group in the MacMillan Pass area (Gordey et al., 1982). The correlations are shown in Table 1, along with a description of the lithologies in the vicinity of the mineralized zones. For simplicity, the unit numbers, as defined by Carne (1979), will be used.

The footwall rocks are mainly detrital in origin (Large, 1981), and are interpreted to be distal turbidites, except for unit 2, the chert pebble conglomerate, which is typical of a debris flow deposit (Carne, 1979). Large (1981) showed that units 2 and 3a are intercalated in the vicinity of the deposit and suggested that they should be considered as a stratigraphic package. However, to the east, such interbedding is not seen. Large (1981) and McClay (1984) relate this facies variation to the presence of a synsedimentary fault at the time of deposition of the chert pebble conglomerate. Further contemporaneous

Figure 5. Geology of the Tom deposit showing positions of surface diamond drillholes (after Carne, 1979; Large, 1981; McClay, 1984).

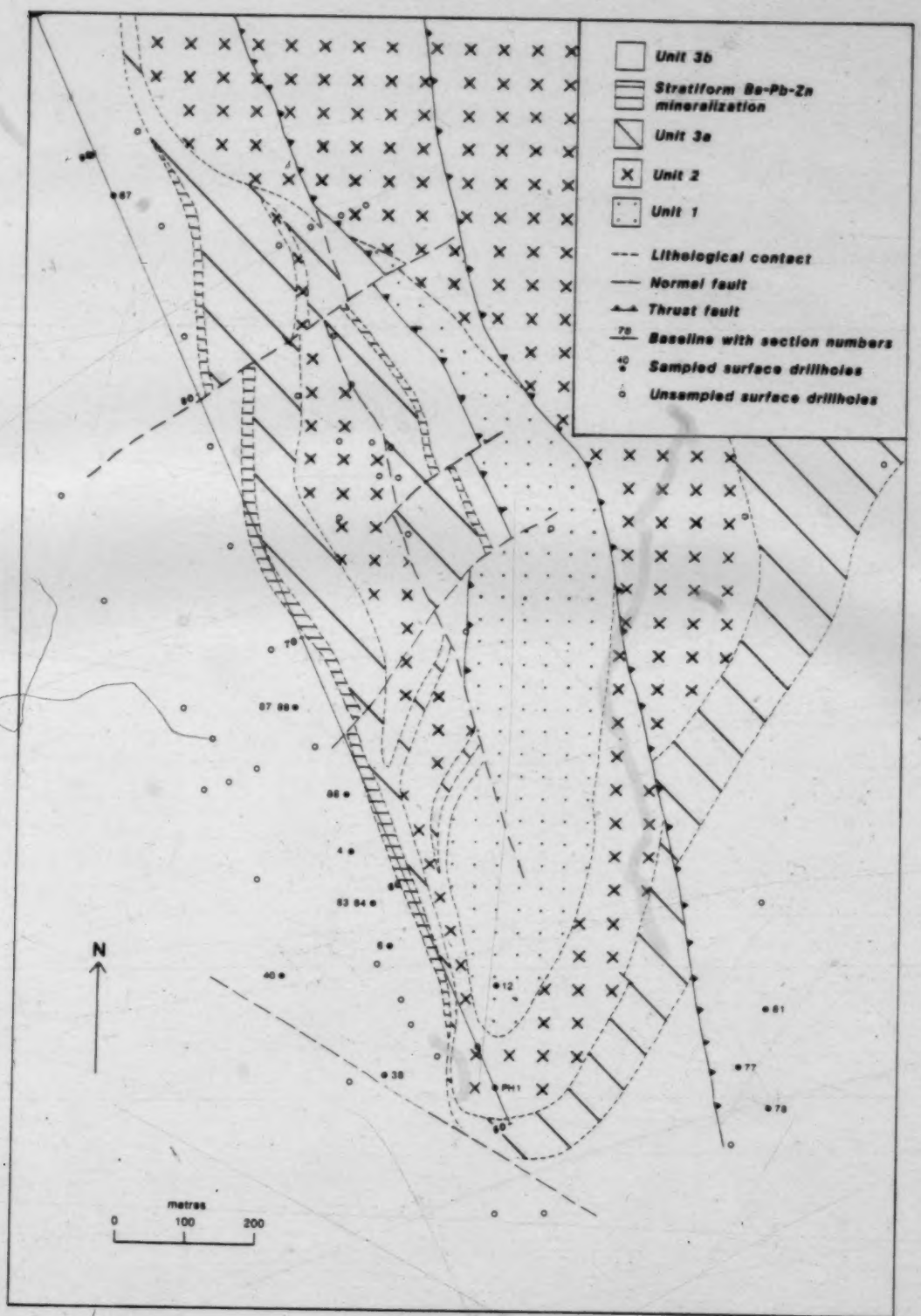
Unit 3b
Stratiform Ba-Pb-Zn mineralization
Unit 3a
Unit 2
Unit 1
Lithological contact
Normal fault
Thrust fault
Baseline with section numbers
Sampled surface drillholes
Unsampled surface drillholes
N
metres
0
100
200

Figure 6. Schematic isopach map of the Tom deposit. The boundary of the mineralization is not known because the down dip extensions of the West and East Zones remain open.

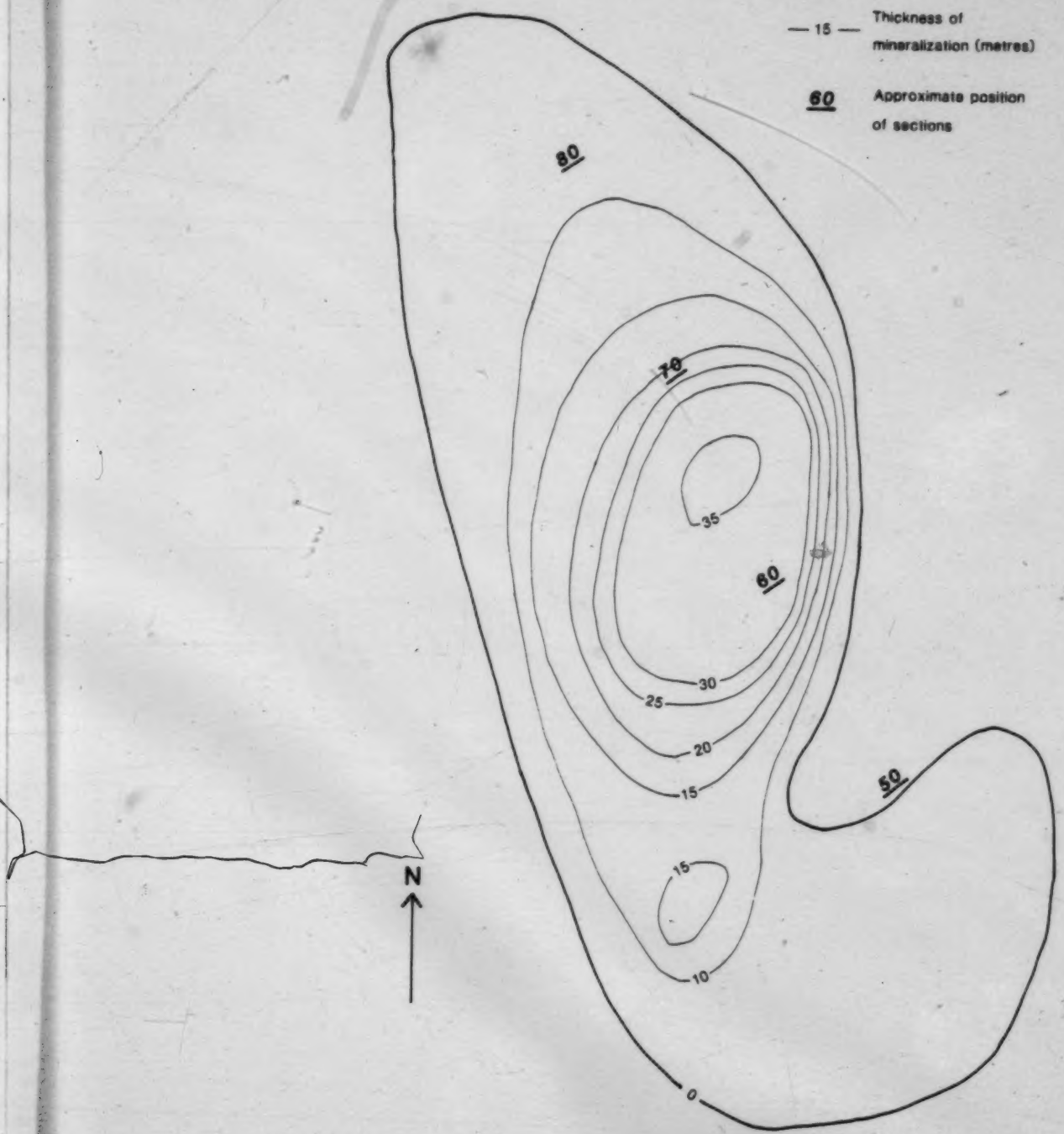

Table 1. Correlation and description of lithologies in the vicinity of Tom.

Carne, 1979	Gordey et al., 1982	Lithology
4	Upper Earn Group	Brown-weathering, ripple cross-laminated siltstones and mudstones
3b		Silver-gray-weathering, carbonaceous, siliceous mudstone
		Stratiform Ba-Pb-Zn mineralization
3a	Lower Earn Group	Laminated, pyritic, silty sandstones and mudstone
2		Chert pebble conglomerate
1		Sand-laminated siltstone and mudstone, with minor sandstone and conglomerate beds

faulting is also suggested by extreme thickening of unit 3b in the vicinity of Tom (Large, 1981). The stratiform mineralization probably formed within a sub-basin (third-order basin of the classification scheme of Large (1983)) bounded by these synsedimentary faults.

The West and East Zones occur at the contact between units 3a and 3b. The West Zone is a slightly folded, tabular body that dips steeply westwards at 70°, consisting of stratiform sphalerite-galena-barite mineralization that extends vertically, and laterally away from a zone of massive sulfides at the southern end of the zone. Carne (1979) outlined a funnel-shaped feeder zone below the massive sulfides.

The East Zone consists of intensely folded, fault-bounded pods. McClay (1984) correlates the East Zone with the laminated mineralization above the massive sulfides of the West Zone..

Geochemically, the major indication of hydrothermal activity is provided by the high Ba concentration of the host mudstones (Large, 1981). The hangingwall mudstones (5300 ppm) are more enriched than the footwall mudstones (3500 ppm) suggesting that submarine exhalations certainly continued after the formation of the stratiform mineralization. Surprisingly, the Pb and Zn content of the adjacent rocks are similar to values from regional samples (Large, 1981).

The area is structurally complex, and McClay (1984) has determined three phases of post-mineralization deformation, the major characteristics of which are outlined in Table 2.

3.3 Petrological features of the ore and associated rocks

3.3.1 Footwall rocks

The massive chert pebble conglomerate consists of clasts up to 7 cm long, cemented by a fine siliceous cement. The finer-grained lithologies of units 1 and 3a are also heavily silicified. The coarser-grained horizons (silt-size upwards) in the footwall appear to have been the locus of a secondary ankerite cement that weathers a distinctive red-brown colour. The chemistry of the ankerite is shown in Table 3 (analyses (11)-(14)). These ankerites have a similar composition to those found in the massive sulfides, or in

Table 2. Structural characteristics of the Tom deposit.

Deformation event	Characteristics of the deformation event
F_1	NW-SE isoclinal folding (e.g. Tom anticline), produces bedding parallel slaty cleavage - pre-unit 4
F_2	E-W folding - warps F_1, produces penetrative (often spaced) cleavage
F_3	N-S kink folds, produces fracture cleavage superimposed on F_1 structures

Table 3. Electron microprobe analyses of iron carbonates.[1]

Sample no.	TU60-18(1)	TU60-18(2)	TU60-18(3)	TU60-10B(4)
$CaCO_3$[2]	49.48	49.03	50.65	51.00
$MgCO_3$	32.80	26.62	26.27	27.23
$FeCO_3$	12.74	20.99	24.19	20.42
$MnCO_3$	4.99	3.37	0.90	1.37

Sample no.	TU70-7Y(5)	TU60-17(6)	TU71-11B(7)	TU70-7Y(8)
$CaCO_3$	50.47	50.25	51.13	1.91
$MgCO_3$	27.38	24.67	24.96	7.92
$FeCO_3$	20.97	24.03	22.76	87.45
$MnCO_3$	1.19	1.06	1.15	2.74

Sample no.	TU71-16(9)	TU60-17(10)	TU28-28(11)	TS12-56(12)
$CaCO_3$	2.20	1.79	49.49	51.63
$MgCO_3$	8.91	9.98	26.26	25.12
$FeCO_3$	84.71	86.06	23.23	23.15
$MnCO_3$	4.19	2.18	1.01	0.01

Sample no.	TU69-30(13)	TU75-21(14)
$CaCO_3$	51.03	50.00
$MgCO_3$	25.17	28.30
$FeCO_3$	23.21	21.00
$MnCO_3$	0.01	0.01

Sample descriptions - (1)-(7) Vein ankerites below the massive sulfides, (8)-(10) Remobilized stringers of siderite cutting above ankerites, (11)-(14) Ankerite in chert pebble conglomerate (analyzed by Qin Gongjiong).

[1] Operating conditions:- accelerating voltage - 15 kV, probe current - 4.0 nA, raster size - 20 μm, live time - 240 s. Data processed using EDATA2 (Smith and Gold, 1979).

[2] Mole percent carbonates calculated to 100 %.

veins underlying the massive sulfides. Small-scale veining, patchy replacement, and complete replacement of the siliceous cement can be seen (Plate 1). Replacement of the rims of chert clasts can also be seen in unit 2.

Pyrite euhedra are scattered throughout the coarser units, as well as the dark mudstones of unit 3a. They post-date the ankerite cement, but pre-date any deformation effects, suggesting a late diagenetic origin for these pyrites. In some cases the pyrite euhedra may be the result of recrystallization of framboidal pyrite.

Clay mineralogy of the mudstones around the deposit was investigated using standard X-ray diffraction techniques. Well-crystallized illite is the dominant clay mineral in the footwall, although the proportion of authigenic to detrital illite is indeterminable. Kaolinite was found in certain samples and where it does occur there is a general increase in the kaolinite / illite ratio towards the deposit (Appendices 2 and 3).

As the base of the deposit is approached from the footwall the percentage of pyrite in both the mudstones and the coarser laminae increases, as does the extent of silicification (Carne, 1979). The organic-carbon content in the footwall mudstones rises to 2 percent just below the deposit, suggesting that a locally reducing environment had developed prior to mineralization (Large, 1981). Geochemical haloes below the deposit are poorly developed (Large, 1981), although a sphalerite-rich zone is found 3 m below the base of the deposit (sample TU28-13), and a barium-bearing mineral, cymrite ($BaAlSi_3O_8(OH)$) has been identified by X-ray diffraction (sample TS38-153).

3.3.2 Sulfide mineralization

Sulfide mineralization in the West Zone can be divided into two major types:

(1) massive sulfide mineralization consisting chiefly of sphalerite, pyrrhotite, galena, and ankerite,

(2) stratiform laminated barite, sphalerite, galena, pyrite, ankerite, and chert, which overlies and extends laterally away from the massive sulfides at the southern end.

Detailed analysis of all drillcore in the zone below the massive sulfides failed to outline a well-defined feeder zone. Extensive ankerite and quartz veining was encountered in some drillholes in this area, but similar veining was also seen in the footwall rocks to the north. Also, many of the veins, especially the quartz-bearing veins, could not

Plate 1. Replacement of silica cement by ankerite in the chert pebble conglomerate. The rim of the top right hand clast is replaced by euhedral ankerite. Sample TS12-56. Transmitted light, crossed polars. Scale bar - 0.5 mm.

Plate 2. Host rock at the base of the photograph is replaced by fine-grained, iron-carbonate. This is cut by an ankerite vein, which itself is cut by a pyrrhotite vein. Euhedral arsenopyrites appear to be later than both the carbonate-replacement of the host rock and the ankerite vein. Sample TU60-18. Transmitted light, plane polars. Scale bar - 0.5 mm.

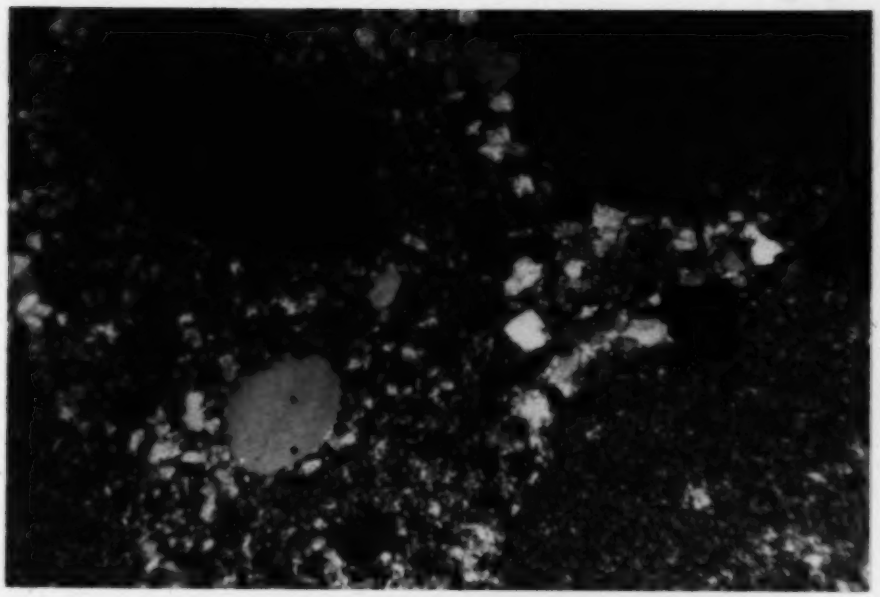

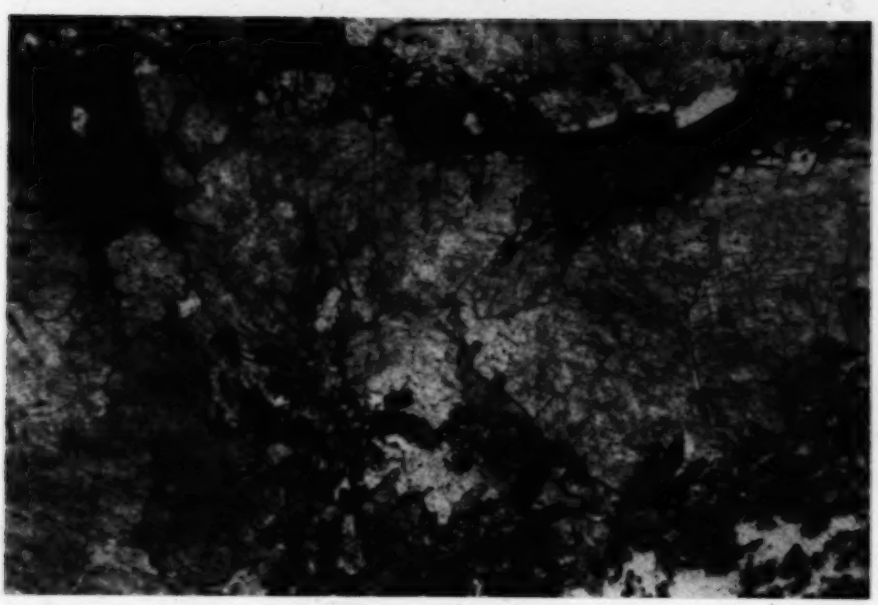

COLOURED PICTURES
Images en couleur

be unambiguously related to mineralization. Quartz vein relationships and origins are considered in more detail in section 3.3.4.

The immediate footwall to much of the southern end of the West Zone is characterized by a sugary appearance. This is caused by a partial or complete replacement of the initially silicified host rock by ankerite. No quantitative data on the composition of these ankerites could be obtained by electron microprobe because of the fine grain size and its intimate association with the initial fine-grained silica. In some samples the lithological banding in the original rock is still discernible. There does appear to be a rough correlation between the thickness of this sugary replacement zone and proximity to the suggested vent area. The replacement zone thins northwards from a maximum thickness of 15 m. Other secondary minerals found within this zone are celsian and adularia, both of which are pre-ankerite replacement. Arsenopyrite is frequently found as scattered, diamond-shaped euhedra that cut the secondary ankerites (Plate 2), and rarely, it occurs intimately associated with coarsely-recrystallized pyrite.

Coarsely-crystalline ankerite veins (chemistry, Table 3) cut these altered host rocks, and are themselves cut by pyrrhotite and pyrite stringers. These stringers characteristically infiltrate along the well-developed cleavage of the ankerite (Plates 2 and 3). Pyrrhotite is often replaced by an intimate intergrowth of pyrite, marcasite, and siderite (Plate 4). Minor sphalerite, galena, and chalcopyrite are also associated with the pyrrhotite.

The massive sulfides consist of a chaotic mixture of galena, sphalerite, pyrrhotite, pyrite, and ankerite, with minor chalcopyrite, and arsenopyrite. Rare, primary lithological banding is outlined by pyrite framboids suggests that the massive sulfides may be a replacement body, rather than being deposited immediately above the hydrothermal vent. Locally, pyrrhotite and pyrite appear to have formed together, but commonly pyrrhotite is replaced by pyrite.

Stratiform Ba-Pb-Zn mineralization gradationally overlies and extends laterally away from the massive sulfides. Pb grades are highest in the massive sulfides and at the base of a section of laminated ore. The highest Ag grades correlate with the high Pb grades. Zn grades generally exhibit a double maxima, one just above the footwall sediments, and another about half-way up the section. The stratigraphy and metal grade pattern of a

Plate 3. Pyrrhotite infiltrating along ankerite cleavage planes. Sample TU40-92. Transmitted light, plane polars. Scale bar - 0.5 mm.

Plate 4. Bird's eye replacement of pyrrhotite by pyrite. Sample TU60-18. Reflected light, plane polars. Scale bar - 0.1 mm.

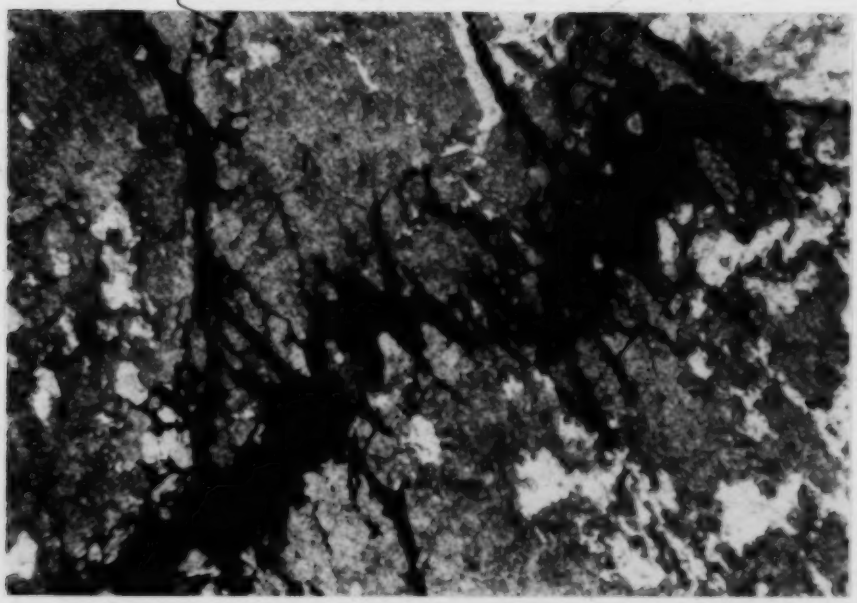

COLOURED PICTURES
Images en couleur

typical section through the laminated ore is shown in Figure 7.

The laminations dominantly consist of sphalerite, galena, barite, pyrite, quartz, and ankerite. Monomineralic laminae are rare, although no mineral preferentially occurs with any other.

Sphalerite in the laminated mineralization is a green-brown color in transmitted light and iron-poor, while the sphalerite in the massive sulfides is a red color and iron-rich (Table 4).

The majority of the pyrite in the laminated ore was originally precipitated as framboids in distinct bands (Plate 5). The bands of more euhedral pyrite probably represent diagenetic recrystallization of pyrite framboids.

Barite, quartz and ankerite are the dominant, non-sulfide, minerals. Ankerite-rich laminae are common just above the massive sulfides, while barite and quartz-rich laminae are more important away from the massive sulfides. Chert bands become more common up-section and away from the vent zone. Many of the cherts are rich in organic matter, and are partially composed of recrystallized radiolarian tests.

Celsian and carbonates are the dominant secondary minerals. Celsian occurs as euhedral, rhombic crystals that locally disrupt the laminae. They are found associated with barite, ankerite, and sphalerite, either concentrated within one zone, or as scattered crystals. The carbonates are interpreted to be slightly later than the celsian, because many celsian crystals are partially replaced along cleavage planes by carbonate. The carbonate mineralogy is complicated and consists mainly of barium carbonates. Witherite ($BaCO_3$), and norsethite ($BaMg(CO_3)_2$) have been identified. Barytocalcite ($CaBa(CO_3)_2$) and benstonite ($Ca_7Ba_6(CO_3)_{13}$) have been reported previously (Large, 1981), but were not identified in this study.

3.3.3 Hangingwall rocks

Hangingwall rocks are enriched in organic carbon (up to 4 %), and vanadium (400 ppm), which suggests that the sediments were deposited in an euxinic environment (Large, 1981).

The rocks are well-silicified and in some places contains 0.2 mm, recrystallized, spumellinid radiolaria (Goodbody, pers. comm., 1984). Pyritic laminae are common and

Figure 7. Typical stratigraphy of the West Zone mineralization, and metal grade patterns taken from drillhole TS84.

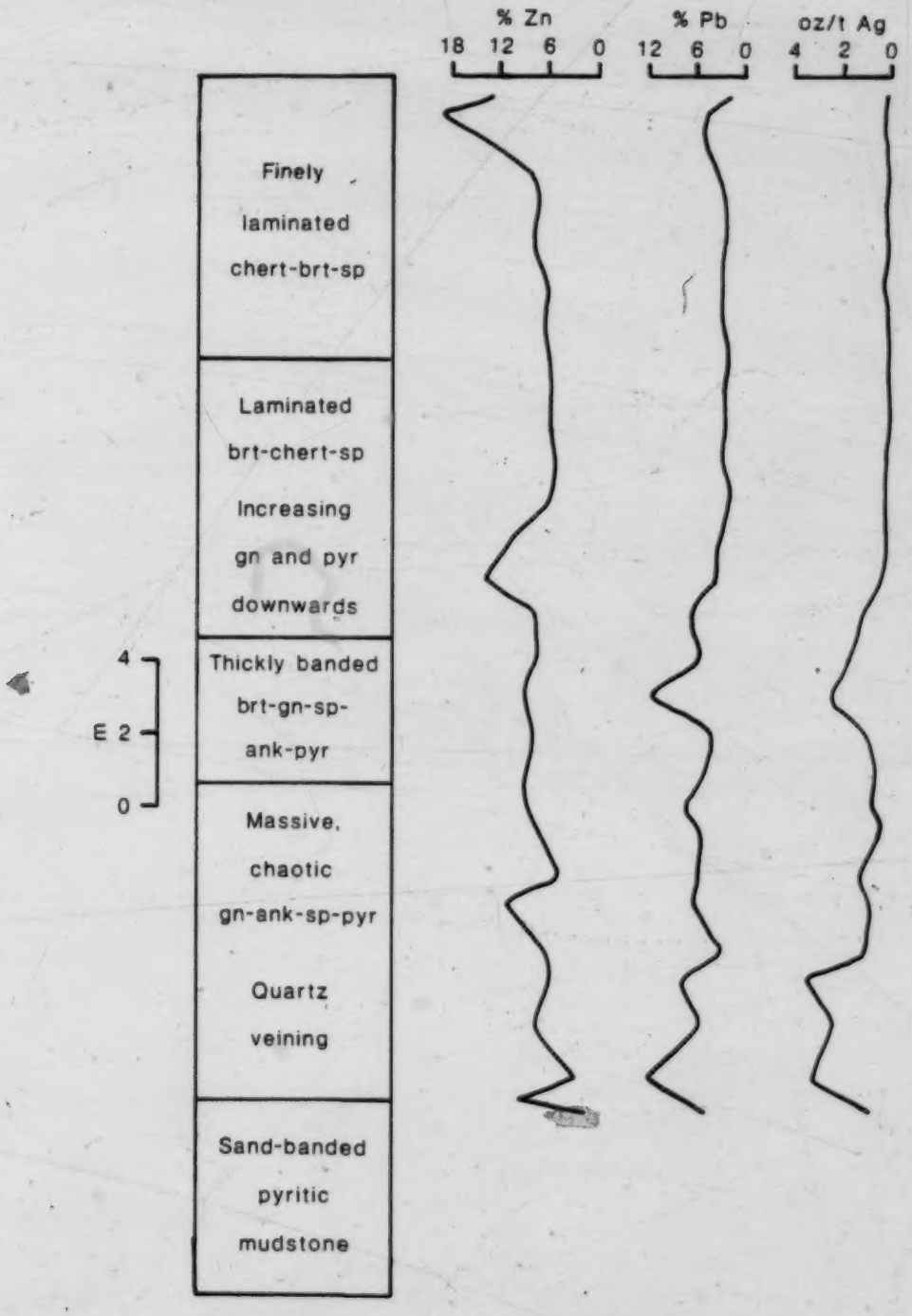

Table 4. Electron microprobe analyses of sphalerite.[1]

Sample no.	TU70-7Y(1)	TU70-7Y(2)	TU70-7Y(3)	TU71-11B(4)
ZnS[2]	85.28	85.38	85.08	85.21
FeS	14.72	14.62	14.92	14.79
CdS	na	na	na	na
Total[3]	99.26	99.84	100.13	100.79

Sample no.	TU71-11B(5)	TU70-3(6)	TU70-3(7)	TU15-5(8)
ZnS	86.56	89.88	90.16	97.28
FeS	13.44	9.08	8.83	1.71
CdS	na	1.04	1.01	1.01
Total	100.22	98.25	98.32	99.31

Sample no.	TU15-5(9)	TU15-5(10)	TU39-39(11)	TU39-39(12)
ZnS	97.32	98.02	98.72	98.67
FeS	1.66	0.85	0.10	0.17
CdS	1.02	1.12	1.18	1.16
Total	99.86	98.86	98.95	98.88

Sample no.	TU39-39(13)	TS84-59(14)
ZnS	98.93	98.89
FeS	0.00	0.00
CdS	1.07	1.11
Total	98.93	99.67

na - not analyzed for in this sample. Sample descriptions - (1)-(5) Sphalerite in massive sulfides, (6)-(14) Sphalerite in laminated ore.

[1] Operating conditions:- energy dispersive analysis, accelerating voltage - 15 kV, probe current - 4.0 nA, point beam, live time - 240 s. Data processed using EDATA2 (Smith and Gold, 1979).

[2] Mole percent sulfides calculated to 100 %.

[3] Actual analysis totals.

Plate 5. Pyrite framboids in the laminated ore. Sample TS83-21. Reflected light, plane polars. Scale bar - 0.1 mm.

Plate 6. Barite grains aligned oblique to the primary banding as a result of recrystallization during deformation. Sample TU17-6.. Transmitted light, crossed polars. Scale bar - 0.5 mm.

COLOURED PICTURES
Images en couleur

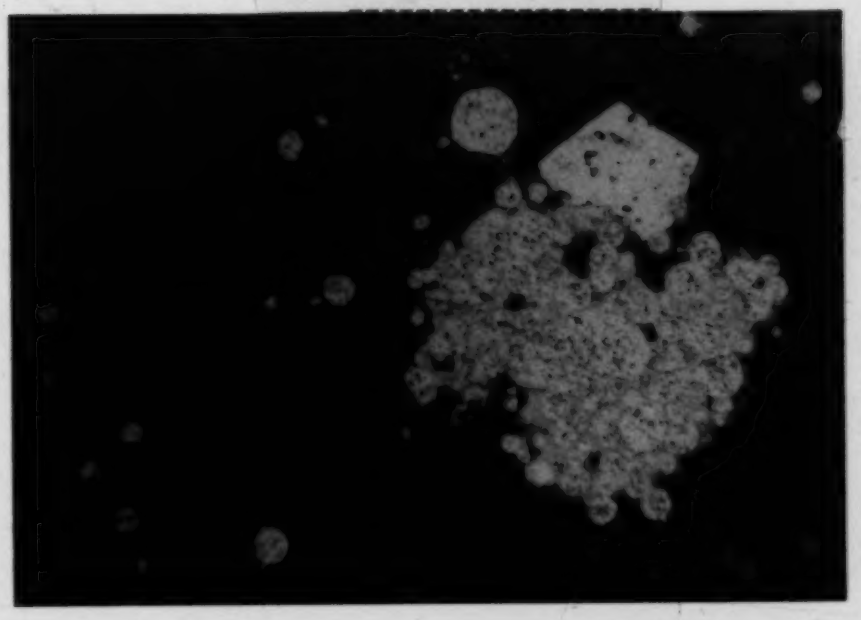

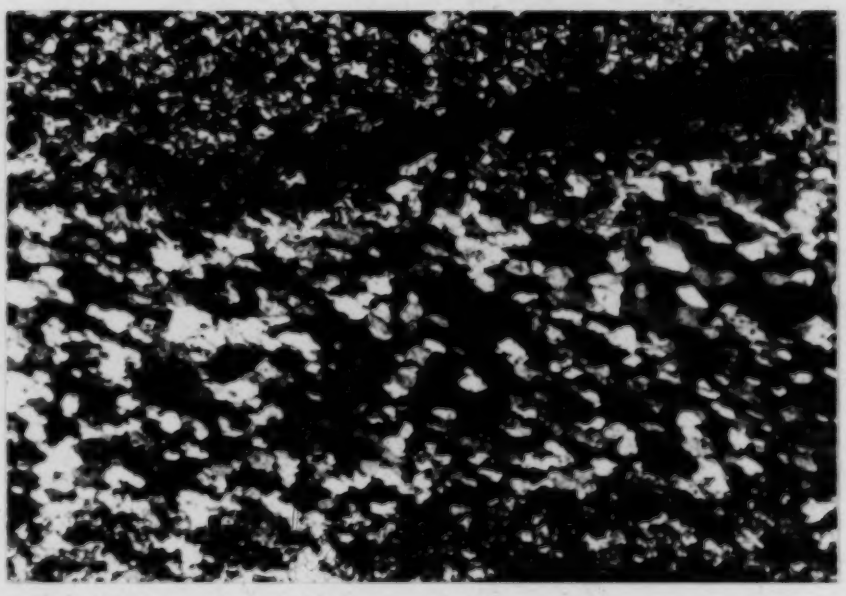

consist of partially or completely recrystallized, pyrite framboids. During diagenesis patchy replacement of the host rock by ferroan dolomite occurred. The major barium-bearing mineral is cymrite, which always occurs as isolated, cross-shaped euhedral crystals.

Kaolinite occurs more frequently in the hangingwall mudstones than in the footwall rocks. However, illite is still the dominant clay mineral in all samples, except TU39-29. As in the footwall units, there is an increase in the kaolinite / illite ratio towards the deposit (Appendices 2 and 3).

3.3.4 Deformation features

The Tom deposit area has undergone three phases of deformation (McClay, 1984). The criteria used to distinguish sedimentary and tectonic structures are those of McClay (1982). Recrystallization of barite, and pyrite framboids may have taken place during diagenesis, but this is then masked by minor remobilization and recrystallization during later deformation. The more obvious deformational features are:

(1) brecciated euhedral pyrite,

(2) remobilized galena cross-cutting adjacent laminae, and infilling brecciated pyrite,

(3) small cross-cutting veinlets infilled by locally-derived, remobilized barite and calcite,

(4) barite grains are often aligned oblique to the primary banding defining a foliation (Plate 6),

(5) sphalerite has been locally remobilized into cleavage planes.

Quartz ± carbonate ± sulfide veins are common throughout the area, but appear to be concentrated in the vicinity of the feeder zone described by Carne (1979). All these quartz veins are late in the paragenesis, but no cross-cutting relationships between quartz veins could be seen. In thin section many of the veins cut across cleavage, but all quartz grains exhibited signs of later deformation, such as undulose extinction, development of sub-grains and sutured grain boundaries. The features described above suggest that most of the quartz veins were probably formed during a later tectonic event rather than during mineralization, but this could not be proven conclusively for all veins.

The mode of formation of some of the quartz veins is clearly shown in thin section. Crystals elongated perpendicular to vein walls, the presence of bands of inclusions parallel to the vein wall, syntaxial overgrowth on wall minerals (Plate 7), and the presence of textures indicative of pressure solution in the surrounding rock (Plate 8), all suggest that the veins were formed by the crack-seal process described by Ramsay (1980).

3.3.5 Paragenesis

The paragenesis of the ores and gangue of the deposit is shown in Figure 8. It must be remembered that the deposit has undergone three deformation events, during which time small-scale remobilization, and recrystallization of the sulfides and barite has occurred. Small sulfide, calcite and barite veins which are interpreted to have been the result of late diagenetic and/or tectonic remobilization are ignored in the paragenesis. Quartz veins are also not included, since their timing relative to mineralization is still uncertain.

The paragenesis within the footwall, and within the stratiform mineralization was easily determined, but it was very difficult to accurately relate the two. For this reason the parageneses are separated, but suggested relationships are indicated in the text below.

Although the mineralogy of the deposit is simple, the absolute time relationship between the various stages of alteration, replacement, stratiform nimeralization, and veining cannot be accurately determined. For example, two thin sections from different stratigraphic positions in the laminated ore may both show diagenetic celsians. Because of the stratiform nature of the deposit however, the celsian in the lower sample may have been forming at the same time as the laminae in the higher sample were being deposited.

The ankerite veins are certainly early, but are suggested to be related to the mineralizing event only because of the presence of ankerite bands in the massive sulfides and the immediately overlying laminated ore, and because they are folded by one of the deformation events.

In the footwall rocks the sequence of alteration (silicification, carbonatization, pyritization) is easily determined, but the timing of the alteration stages relative to stratiform mineralization is difficult to ascertain. Within the footwall rocks it is likely that

Plate 7. Quartz-carbonate vein cutting chert pebble conglomerate. Vein crystals are elongated perpendicular to the vein walls. Note that vein carbonate is found adjacent to the secondary carbonate in the rock, at the left of the photograph. Sample TU69-30. Transmitted light, crossed polars. Scale bar - 0.5 mm.

Plate 8. Typical pressure solution cleavage in chert pebble conglomerate picked out by immobile, carbonaceous films. TU28-25. Transmitted light, plane polars. Scale bar - 0.5 mm.

COLOURED PICTURES
Images en couleur

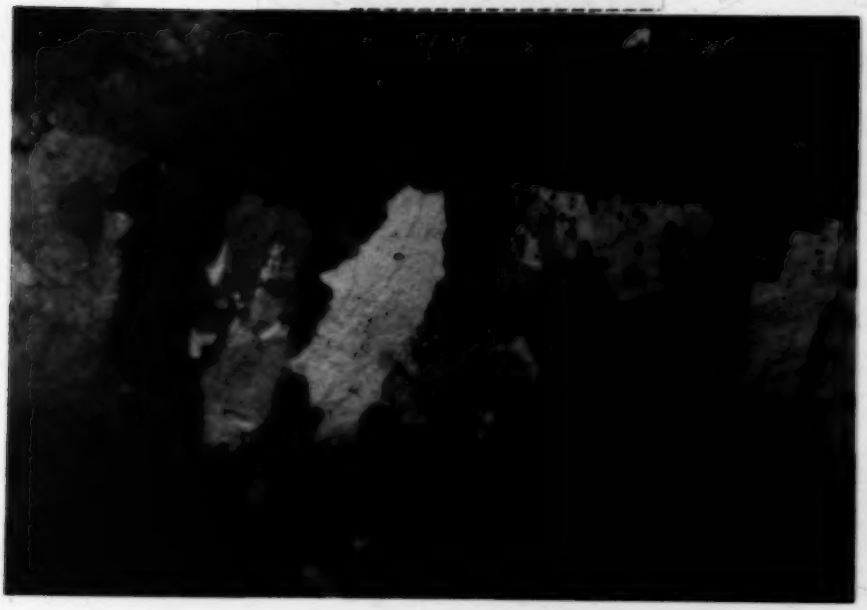

Figure 8. Paragenesis of the Tom deposit.

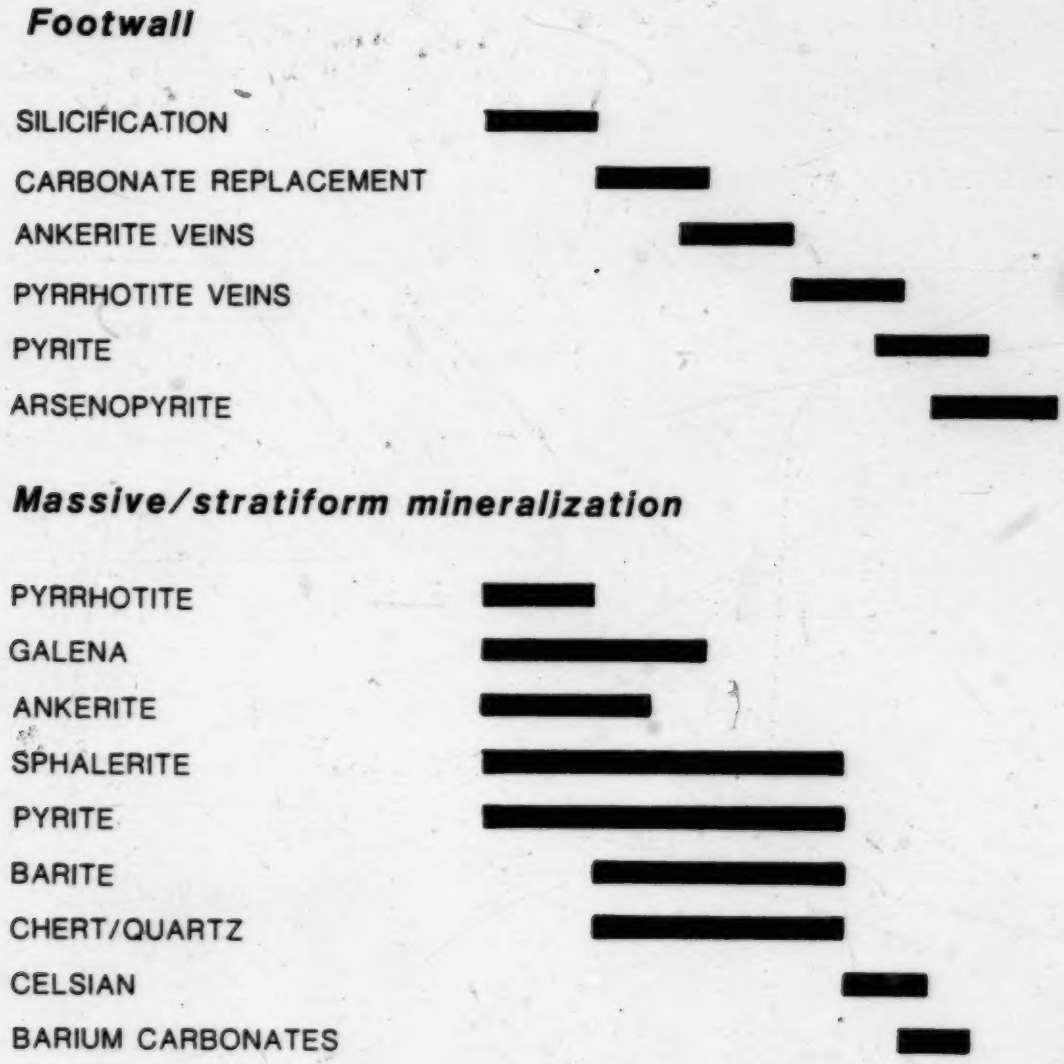

different silt/sand/pebble beds were altered at different stages, as the altering fluids could not have affected all the footwall rocks simultaneously.

4. FLUID INCLUSIONS

4.1 Introduction

The object of this fluid inclusion study was to determine, by microthermometric methods, the composition and temperature of the fluids at the time of formation of the Tom deposit. Suitable fluid inclusions were only found in the cross-cutting ankerite- and quartz-veins underlying the southern end of the Tom West Zone. Due to the fine-grained, recrystallized nature of the laminated sphalerite and barite, no workable inclusions could be found in this part of the deposit.

The classification and paragenesis of the veins have been outlined in Chapter 3. Ankerite veins are interpreted to be related to mineralization, and so primary inclusions in the ankerite could give information concerning the nature of the ore-forming fluids. Primary inclusions in tectonic quartz veins were analyzed for purposes of comparison, and to obtain information about the fluid conditions at the time of subsequent deformation and remobilization of the sulfides.

For extensive reviews of the methodology and applications of fluid inclusion analysis the reader is referred to Hollister and Crawford (1981), and Roedder (1984).

4.2 Analytical procedure

Doubly-polished chips were prepared, which varied in thickness from 30 to 500 μm. The ankerite chips generally had to be the thinnest due to the cloudiness of the mineral.

A Chaixmeca heating-and-cooling stage (Poty et al., 1976) attached to an Ortholuxll Leitz microscope was used for microthermometry. Inclusions were observed using 25X periplan oculars in combination with either 32X, or 40X objectives. The 32X objective was fitted with a water-cooled jacket for high temperature use, while the 40X objective was fitted with a plastic sleeve to reduce the amount of moisture reaching the sample during low temperature use. These high power objectives had to be used due to the small size (<10 μm) of most fluid inclusions analyzed. The instrumentation at the University of Alberta is described in more detail by English (1981).

Calibration of the stage was performed, using solid melting point standards, to improve the accuracy of the temperature measurements, since the platinum resistance thermometric probe used to measure the stage temperature is offset slightly from the centre of the stage. The resulting calibration curve is shown in Figure 9, and indicates that the calibration correction increases with increasing temperature. The standards employed at the University of Alberta are listed by English (1981).

Preliminary observations on all samples showed that CO_2-rich inclusions were the dominant primary inclusion type. Rarer, primary aqueous inclusions frequently had a high degree of filling. Lawler and Crawford (1983) show that on freezing, stretching occurs in inclusions exhibiting high degrees of filling. This occurs when the volume of expansion of water on freezing exceeds the volume of the vapor bubble. The volume of the inclusion is thus increased, which decreases the degree of filling and thus increases the homogenization temperature. On the other hand, homogenization of H_2O-CO_2 inclusions is frequently difficult to achieve because the internal pressure generated in such inclusions on heating is frequently high enough to decrepitate the inclusions (Burruss, 1981a). Leroy (1979) found that the internal pressure necessary for decrepitation decreased with increasing inclusion size. Due to the high percentage of CO_2-rich inclusions, it was decided to perform freezing measurements first on all inclusions, and to note the occurrence of probable stretching in those aqueous inclusions in which the vapor bubble completely disappeared upon freezing.

Freezing of most samples was accomplished by cooling to -120°C. The inclusions were then allowed to slowly warm to room temperature, during which time melting measurements were made. The calibration standard for pure CO_2 was measured under the same conditions giving the error indicated in Figure 9. For determinations of homogenization temperatures, the sample was allowed to equilibrate below the possible homogenization temperature. The inclusions were then heated slowly (0.5°C / min) up to the temperature of homogenization.

All measurements were repeated at least twice to check for reproducibility. CO_2 melting temperatures and CO_2 homogenization temperatures are reproducible to ±0.1°C. The small size of many of the inclusions meant that ice and CO_2 clathrates just prior to melting were very fine-grained, making precise observation difficult. Frequently the

Figure 9. Calibration curve showing corrections that must be applied to observed measurements.

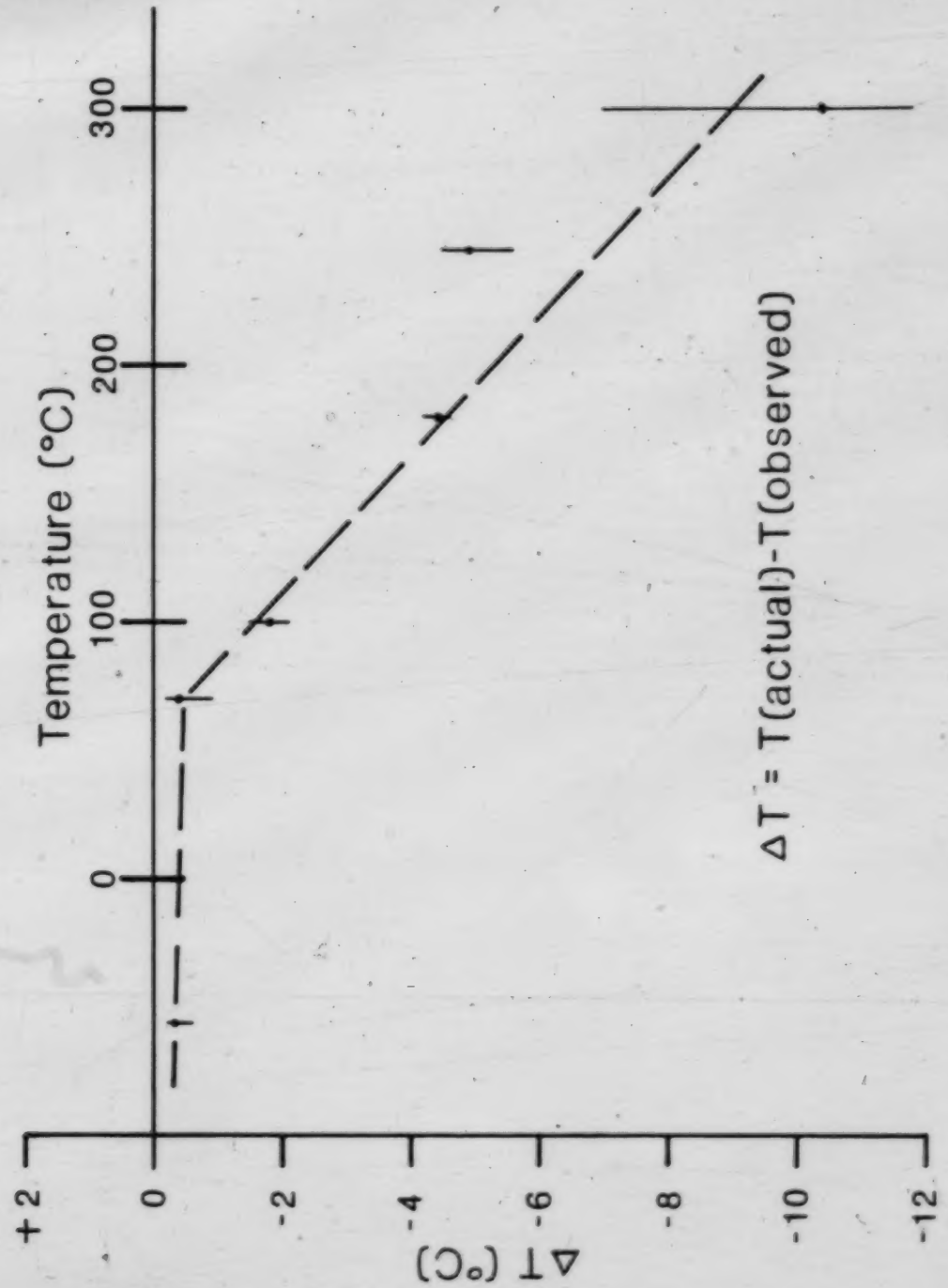

errors were as high as ±1.0°C, which have repercussions as far as determinations of salinities are concerned. The small inclusion size and reduction in optical quality on heating, also resulted in imprecision in many homogenization temperatures of up to ±5.0°C.

4.3 Inclusion petrography and classification

Only primary inclusions in ankerite, quartz, and calcite were described and analyzed. The criteria suggested by Roedder (1979) were used as a standard for distinguishing such inclusions. In all cases those inclusions that were isolated and definitely not forming part of a planar array were assumed to be primary. All inclusions in planes were assumed to be secondary. No primary growth directions or growth zonations could be determined. The calcite and many of the quartz samples frequently have areas with very high densities of inclusions (Touret, 1981) which made it difficult to distinguish primary from secondary inclusions.

All primary inclusions can be classified into two distinct types:

(1) aqueous inclusions with degrees of filling at room temperature varying from 55 to 95 %, although most have a degree of filling between 70 and 80 % (Plate 9),

(2) CO_2-rich inclusions which have a variable degree of filling. No classification distinction is made between pure CO_2 inclusions and those with only 2 % CO_2 by volume since, in any given sample, there is a wide range in degree of filling. Neither is a distinction made between CO_2-rich inclusions that are two-phase (aqueous phase and CO_2 fluid) at room temperature (Plate 10), and those that are three-phase (aqueous phase, CO_2 liquid, and CO_2 vapor) (Plate 11), as this is solely a function of the homogenization temperature of CO_2 relative to room temperature.

No daughter crystals were seen in any inclusion.

The size and shape of fluid inclusions are controlled by the physical properties of the host minerals. In ankerite and calcite, inclusions are small (<7 μm), rectangular and oriented parallel to cleavage directions (Plate 12). In quartz, primary inclusions are up to 40 μm long. The smaller inclusions (<20 μm) are rounded or have a negative crystal shape, while the larger inclusions (20 to 40 μm) are more irregular.

Plate 9. Type 1 inclusion in quartz. Sample TU70-17. Scale bar - 0.05 mm.

Plate 10. Type 2 inclusion in quartz that is two-phase at room temperature. Sample TS83-28. Scale bar - 0.05 mm.

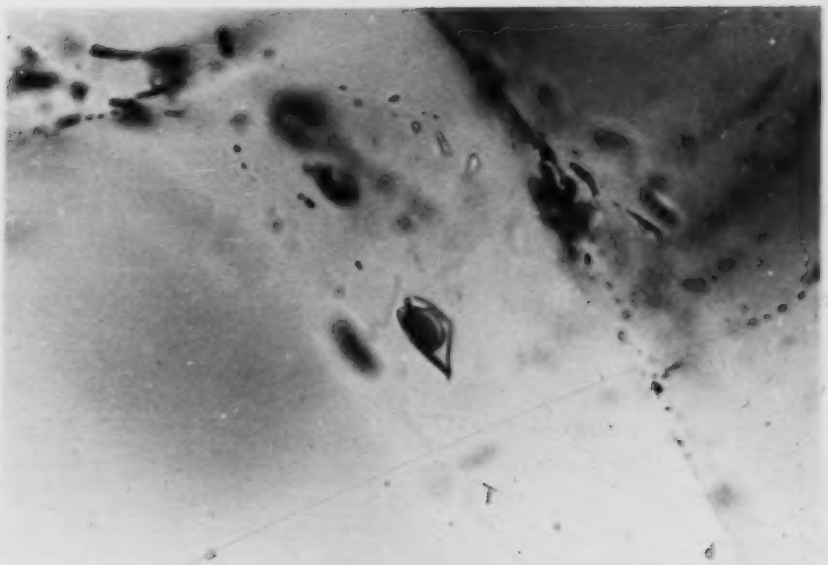

Plate 11. Type 2 inclusion in quartz that is three-phase at room temperature. Sample TS83-28. Scale bar - 0.05 mm.

Plate 12. Rare type 2 inclusion in ankerite. The morphology of this inclusion is typical of all inclusions in ankerite. Sample TU70-6. Scale bar - 0.05 mm.

The dominant inclusion type in the carbonates is Type 1 (80-90 %), while in quartz the dominant type is Type 2 (90-95 %). Primary inclusions of both types are often found together in three-dimensional groups in quartz. Also, within a given group, the CO_2-inclusions exhibit varying degrees of filling.

Evidence for necking and possible leakage was common. Such inclusions were ignored. The inclusions most affected by necking were those in the carbonates and the large irregular inclusions in quartz. In the carbonates the presence of thin tails extending away from an inclusion along a cleavage direction was taken as an indication of leakage.

Secondary inclusions are smaller and more common than primary inclusions, and consist of both inclusion types. No obvious compositional differences can be qualitatively detected between primary and secondary inclusions.

4.4 Freezing measurements

Freezing measurements were made on fluid inclusions in order to determine their composition. Measurements were obtained on a total of 129 inclusions. Many more measurements were attempted, especially in the carbonates, but the small size of many inclusions made accurate observation difficult. Attempts were made, where applicable, to observe the following :

-melting temperature of CO_2 ($TmCO_2$),

-ice eutectic temperature (Te),

-melting temperature of ice (TmIce),

-melting temperature of clathrate (TmClath),

-homogenization temperature of CO_2 ($ThCO_2$).

All measurements are included in Appendix 4, and displayed in histograms in Figures 10, 11 and 12.

The liquid phase in aqueous inclusions is usually assumed to be a dilute sodium chloride brine. The addition of other ions can be detected by determining the temperature of first melting of the ice (Te). For a H_2O-NaCl solution, Te is -20.8°C (Potter et al., 1978). Crawford (1981) lists the effects on the eutectic temperature of the addition of other common ions, e.g. Mg^{2+}, K^+, and Ca^{2+}. From Figure 10 there appears to be a range in Te from -20°C, which suggests that Na^+ is the dominant cation, to -45°C. This range implies

Figure 10. Melting temperatures from Type 1 inclusions.

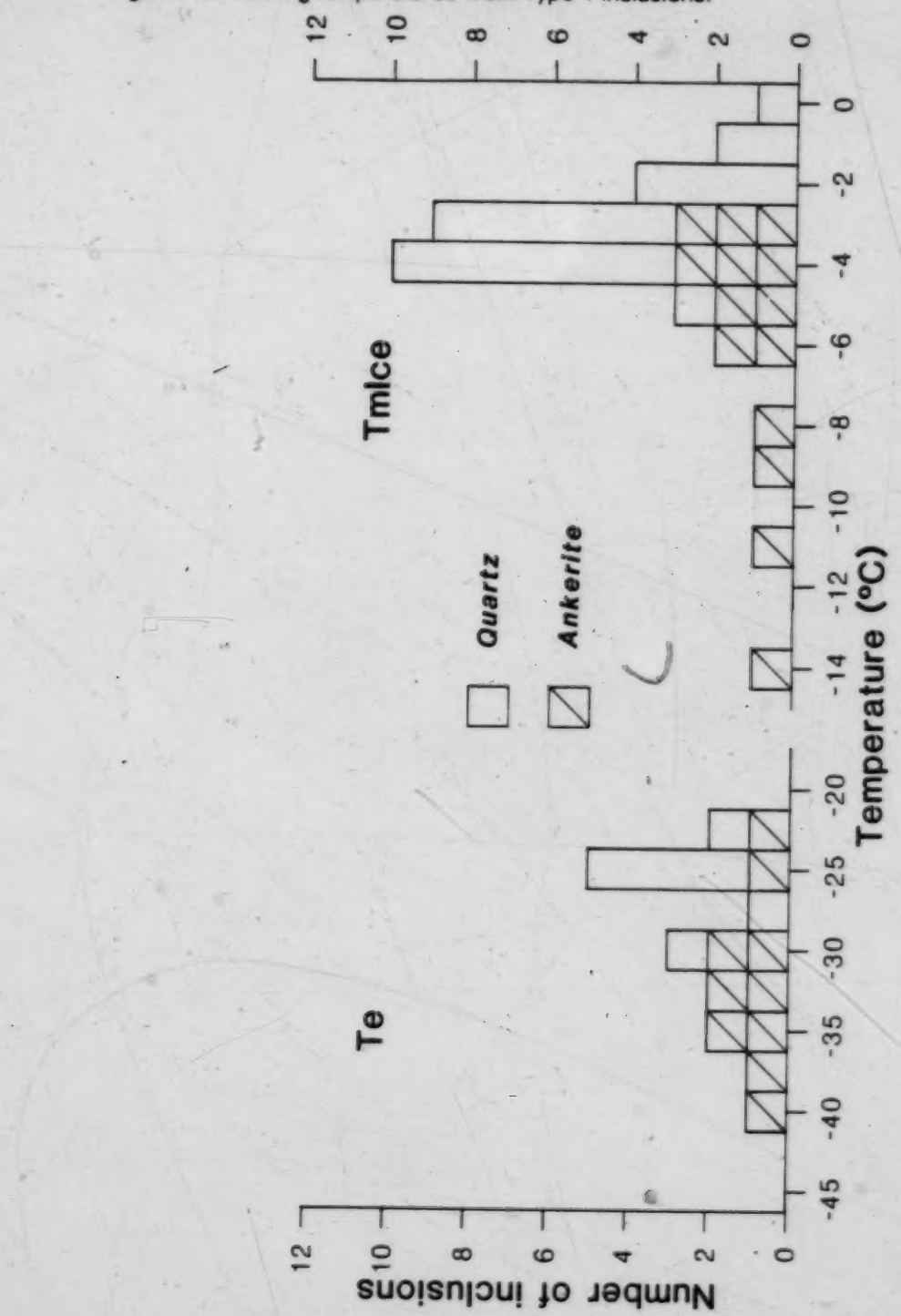

Figure 11. CO_2 and clathrate melting temperatures from Type 2 inclusions. Five inclusions in quartz exhibit $TmCO_2$ lower than -62°C (-86.5°C, -86.0°C, -73.0°C, -69.9°C, -64.5°C).

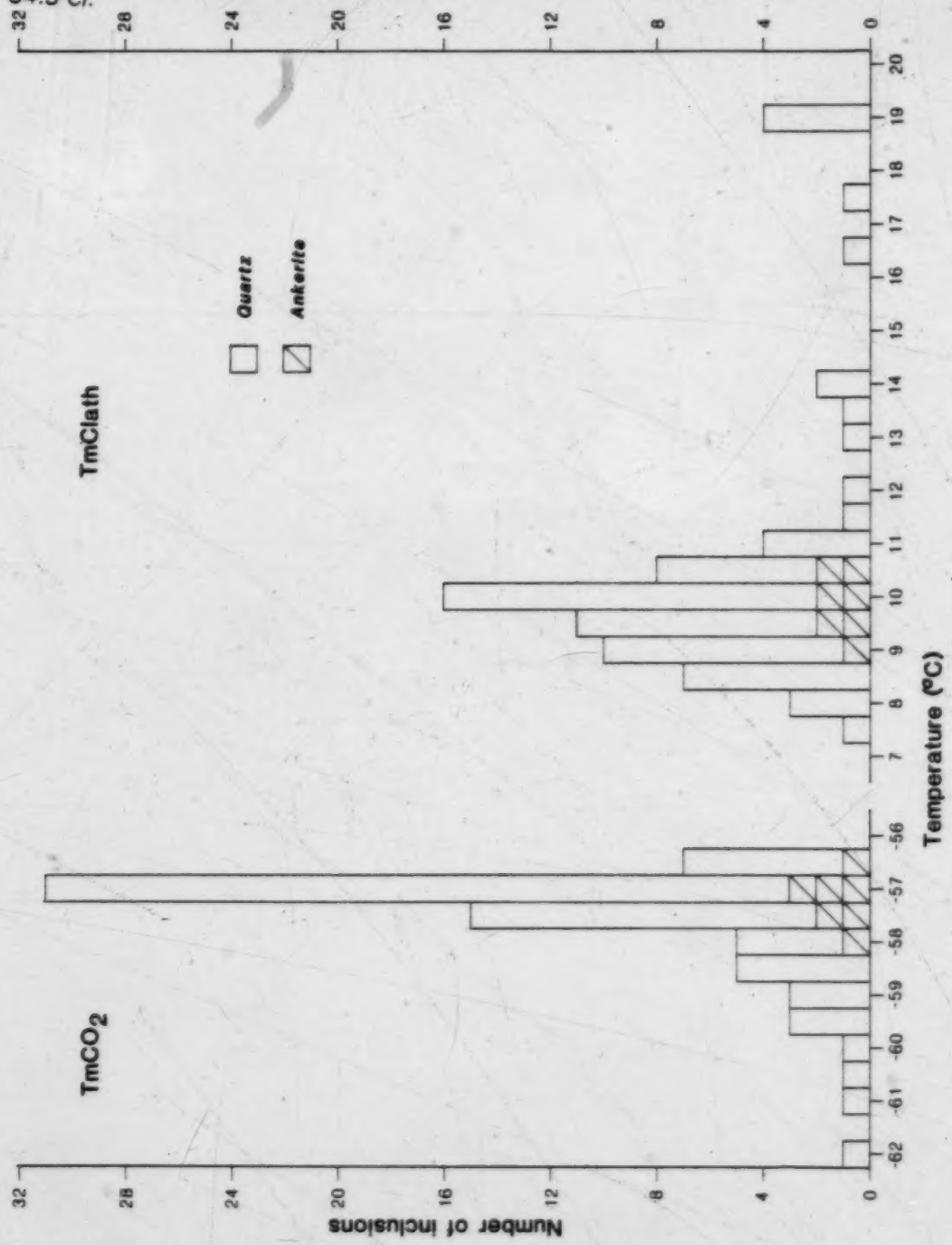

Figure 12. CO_2 homogenization temperatures in Type 2 inclusions.

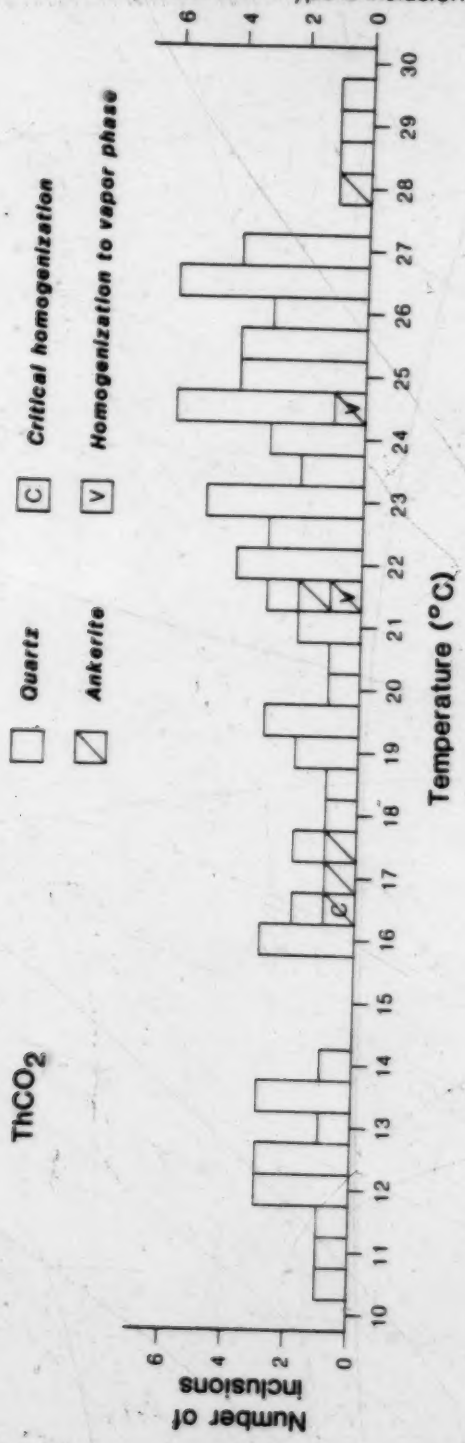

that some inclusions have trapped fluids that contain Ca^{2+} and/or Mg^{2+}, as well as Na^{+}. Generally Te measurements on aqueous inclusions in quartz had a smaller range (-20° to -30°C) than those in ankerite indicating a purer NaCl solution.

In Type 1 inclusions salinities were determined from Tmice, and phase equilibria in the system H_2O-NaCl (Potter et al., 1978). The T-X diagram at 1 bar for this system is shown in Figure 13, and Tmice are plotted as a histogram in Figure 10. As can be seen the Tmice gives ambiguous salinities if the solid phase cannot be identified. On freezing the vapor bubble shrinks, while on warming, in many of the inclusions, the solid phase coarsens above the eutectic temperature. These observations suggest that the solid phase is ice and that the fluid is less saline than the eutectic (Crawford, 1981). The salinities were then calculated using the formula of Potter et al. (1978):

$$W = 0.00 + 1.76958T - (4.2384 \times 10^{-2})T^2 + (5.2778 \times 10^{-4})T^3$$

where W = weight percent NaCl in solution, and T = freezing point depression (°C) = 0 - Tmice, and are shown in Table 5. All salinities are reported as weight percent NaCl equivalents. The errors that result from the presence of other salts is small, particularly at the low salinities of the aqueous fluids in this study (Clynne and Potter, 1977; Crawford, 1981). Ankerite Type 1 inclusions have salinities ranging from 5.0 to 18.3 weight percent NaCl equivalent with an average of 9.1 ± 3.4 weight percent NaCl equivalent, whereas quartz and calcite Type 1 inclusions are less saline, ranging from 0.1 to 7.6 weight percent NaCl equivalent with an average of 4.8 ± 1.3 weight percent NaCl equivalent.

Type 2 inclusions exhibit many more phase transitions, which have to be interpreted in terms of the quaternary system H_2O-CO_2-NaCl-CH_4. The phase equilibria in this system is outlined by Hollister and Burruss (1976) and Burruss (1981a).

Salinity determinations in these inclusions are not as straightforward as in Type 1 inclusions, due to the formation of a clathrate, CO_2 hydrate (CO_2.5.75H_2O). Collins (1979) summarizes the chemistry of gas hydrates, and explains why the formation of this clathrate invalidates the use of the freezing point depression of ice to determine the salinity of the aqueous phase. However, the salinity can be estimated from the freezing point depression of the clathrate in the presence of CO_2 liquid and gas (Collins, 1979).

Figure 13. Temperature-composition diagram at 1 bar in the system H_2O-NaCl (data after Potter et al., 1978).

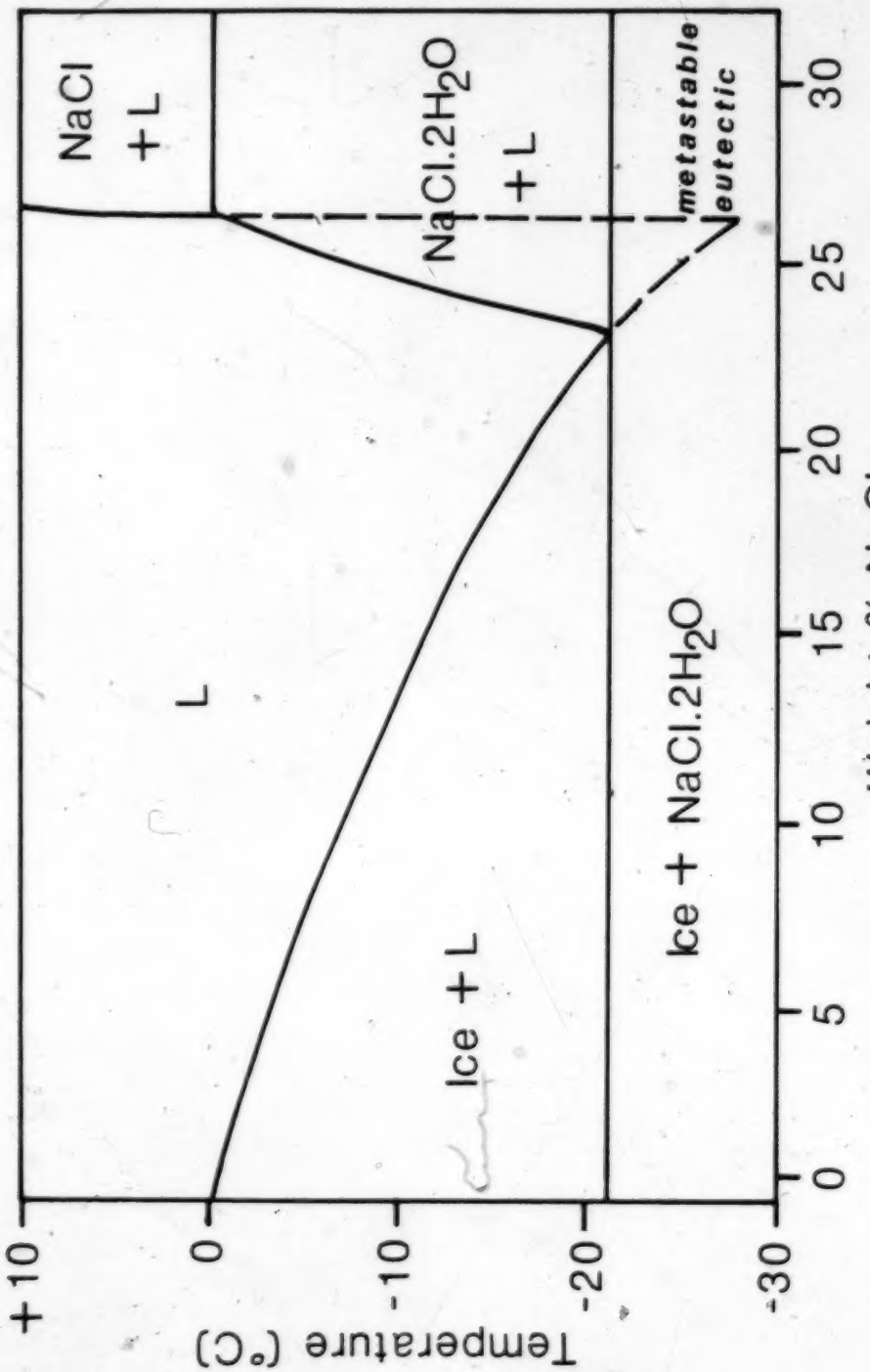

Table 5. Salinities of Type 1 inclusions

Sample number	Inclusion number	Salinity (wt.% NaCl equiv.)
Ankerite		
TU60-18	1/4/1	6.4
TU60-24	1/1/1	5.9
	1/2/1	6.1 - 2.0
TU40-92	3/1	13.1
TU15-10A	3/1/7	6.5
	3/2/1	5.8
TU70-7	1/1	11.9
	1/3	18.3
TU70-8	2/1/2/1	14.7
	2/3/a	8.8 - 7.5
TU70-16A	2/2	5.0
TU71-13	1/1/1	9.4
	2/1/2	9.8
	AVERAGE	9.1
Quartz		
TU60-10A	1/1/2	6.1
TU60-12	1/2/4/a	2.6 - 1.6
TS38-44	1/1	4.0 - 2.4
	2/1	5.5 - 4.6
	2/2	5.8
TS12-36	1/4	7.7 - 5.1
	1/6	4.9
	1/7	6.9
TU70-17	1A/6/1	5.5
	1A/6/2	4.5
	1A/6/3	5.8
	1A/6/4	4.5
	1A/6/5	4.2

Table 5. cont.

Sample number	Inclusion number	Salinity (wt.% NaCl equiv.)
TU71-15	1/1	3.9
	3/3	3.4
TS84-80	1/3/1	7.9 - 5.4
Calcite		
TS84-77	2/2	0.1
	2/3	8.5 - 6.7
	1/1	7.2 - 5.4
	1/2	2.6
	AVERAGE	4.8

Bozzo et al. (1975) fitted their experimental data to an equation (see below) which can be used to determine the salinity of a H_2O-CO_2-NaCl inclusion. The CO_2-clathrate in a H_2O-CO_2 inclusion will melt at 10.0°C.

$$W = 15.52023 - 1.02342(TmClath) - 0.05286(TmClath)^2$$

TmClath measurements are tabulated in Appendix 4 and plotted as a histogram in Figure 11. Although most measurements plot on the low temperature side of the +10.0°C peak, there is a range from +7.5° to 19.2°C. There is never more than a 5°C range in a given sample though. This range in TmClath is probably due to the presence of another gas, e.g. CH_4, as well as NaCl. Methane is completely miscible with the CO_2-rich fluid, and the CO_2 hydrate (Robinson and Hutton, 1962) and, for a given salinity, will increase the TmClath (Burruss, 1981a). Thus, since the effects of NaCl and CH_4 are opposite, TmClath measurements alone do not tie down the composition of the inclusion. The amount of reduction in $TmCO_2$ from -56.6°C gives a semi-quantitative estimate of the amount of CH_4 present in the CO_2-rich phase, and thus in the whole inclusion, since the solubility of H_2O in CO_2-CH_4 phases is negligible (Hollister and Burruss, 1976). Most $TmCO_2$ measurements plot between the triple point of pure CO_2 and -58.0°C (Fig. 11) which gives a maximum mole fraction CH_4 of 0.12 (Swanenberg, 1979). To calculate the mole fraction CH_4 accurately using Swanenberg's (1979) method, the degree of filling at $TmCO_2$ has to be estimated. This was not attempted in this study. Sample TS83-28 contained the most CH_4-rich inclusions with $TmCO_2$ varying from -59.5° to -86.0°C implying up to 85 mole % CH_4 in the CO_2-rich phase. This low $TmCO_2$ is consistent with a high TmClath in this sample of between +17.4° and +19.2°C.

A quantitative determination of the mole fraction of CH_4 in the CO_2-rich phase was attempted using the approach outlined by Burruss (1981b) and the data of Arai et al. (1971). The CO_2-CH_4 relations in the inclusion can be characterized accurately by observing the $TmCO_2$, $ThCO_2$, and the phase to which homogenization occurred. $ThCO_2$ are tabulated in Appendix 4, and plotted as an histogram in Figure 12. The calculated mole fractions of CH_4 in CO_2 are tabulated in Table 6. As can be seen there is a wide variation in mole fractions of CH_4 although the composition of a given sample does not vary

Table 6. Composition of Type 2 inclusions

Sample number	Inclusion number	CO_2	CH_4	H_2O	Minimum salinity	Bulk fluid density
		mole %	mole %	mole %	wt.% NaCl equiv.	mole/l
TU60-10A	1/1/1	12.6	0.4	87.0	---	41.5
TU60-12	1/2/5/1	7.5	2.5	90.0	3.2	48.6
TS38-44	2/4	29.4	0.6	70.0	3.6	33.0
	3/5	33.8	0.7	65.5	1.6	29.2
TU77-108	2	1.3	0.4	98.5	---	54.6
	3	16.4	1.6	82.0	---	41.4
	2/1	20.2	2.8	77.0	0.8	38.9
	2/2	6.6	1.4	92.0	---	50.5
	15/1	11.9	2.6	85.5	---	43.3
	15/2	49.3	3.7	47.0	---	27.5
	15/3	33.3	2.5	64.2	---	32.2
	15/4	16.7	1.8	81.5	---	41.1
	1/1	5.0	0.0	95.0	4.9	49.5
	1/2	3.9	0.1	96.0	2.1	51.9
TS12-36	1/1	24.0	1.0	75.0	1.3	37.5
	1/2	3.8	0.2	96.0	0.6	49.5
	1/3	6.2	0.3	93.5	0.3	48.6
	1/5	10.1	0.4	89.5	2.0	45.5
	1/8	13.4	0.6	86.0	0.8	41.4
	2/1	8.6	0.4	91.0	---	45.5
	C/1	3.8	0.2	96.0	1.3	49.0
	C/2	10.6	0.4	89.0	---	43.8
	C/5	9.0	---	91.0	---	45.5
	C/6	24.0	---	76.0	---	37.0
TU15-10A	2/1/2	2.9	0.1	97.0	---	51.4
	2/1/3	4.3	0.2	95.5	---	51.1
	3/1/8	8.2	0.3	91.5	---	47.0
TU70-6	1/1	6.7	1.3	92.0	---	48.0
	1/2	7.0	3.0	90.0	1.3	48.0
	1/a	4.8	0.7	94.5	0.0	49.7
	1/b	3.5	0.5	96.0	0.0	50.7
	1/c	2.2	0.3	97.5	---	53.8
	1/d	13.5	4.0	82.5	4.3	41.0
	1/e	6.6	1.9	91.5	---	49.5
	1/f	29.4	8.8	61.8	---	31.8
	1/3	20.6	3.4	76.0	---	37.2
	1/4	2.8	0.7	96.5	0.2	52.8
TU70-7	2/1	21.6	0.9	77.5	1.1	33.7
TU70-11	1/1	35.0	1.0	64.0	1.0	31.7
	1/2	3.8	0.2	96.0	1.8	51.5
	1/3	11.5	0.5	88.0	3.1	44.2
	1/4	2.4	0.1	97.5	0.8	52.8
	1/5	90.0	10.0	---	---	18.9
	1/6	3.9	0.1	96.0	1.8	49.5

Table 6. cont.

Sample number	Inclusion number	CO_2	CH_4	H_2O	Minimum salinity	Bulk fluid density
		mole %	mole %	mole %	wt.% NaCl equiv.	mole/l
	1/7	2.9	0.1	97.0	---	51.9
TU70-16A	2/2/1	3.4	0.1	96.5	0.4	50.7
	2/2/4	6.3	0.2	93.5	2.2	47.2
TU71-15	1/3	8.4	0.6	91.0	---	45.0
	1/4	45.5	---	54.5	---	25.0
	2/2	7.2	0.3	92.5	---	47.0
	2/3	7.7	0.3	92.0	0.8	46.0
	2/4	7.5	---	92.5	---	47.5
	2/5	8.0	---	92.0	---	47.2
	3/1	3.4	0.1	96.5	0.3	51.4
	3/2	3.4	0.1	96.5	0.5	51.0
	3/4	10.5	0.5	89.0	3.2	45.0
	3/6	35.5	1.5	63.0	---	29.1
TS83-28	1	8.5	3.5	88.0	---	45.5
	2	4.8	7.2	88.0	---	41.0
	3	25.2	37.8	37.0	---	21.5
	4	6.3	9.5	84.2	---	37.2
	6	19.8	29.7	50.5	---	24.6
TS84-79	2	27.5	1.5	71.0	2.8	32.1
TS84-80	1/1/1	5.0	0.0	95.0	3.4	50.0
	1/3/2	4.9	0.1	95.0	0.4	49.0
	1/3/3	10.5	0.0	89.5	---	44.2
	1/3/4	14.0	---	86.0	---	39.5
	1/1/2	2.0	0.0	98.0	1.8	52.0
	1/1/3	2.5	0.0	97.5	3.0	52.6
	1/2/1	29.1	0.9	70.0	---	30.6
	1/2/2	5.9	0.1	94.0	---	47.5
TS4-79	1/1/1	15.0	1.0	84.0	0.4	41.4
	1/1/2	7.0	0.5	92.5	0.2	48.9
	1/1/3	7.3	0.2	92.5	0.8	47.1
	2/1/1	47.9	3.6	48.5	---	27.5

substantially.

Obviously, the ubiquitous presence of CH_4 invalidates the accurate determination of salinity using the freezing point depression of CO_2 hydrate. However, minimum salinities were calculated using the equation of Bozzo et al. (1975), and are shown in Table 6. The average minimum salinity is 1.6 ± 1.1 weight percent NaCl equivalent, which is lower than that of Type 1 inclusions. If inclusions with $TmCO_2$ between -56.6° and -57.0°C are considered, i.e. those with minimal CH_4, the maximum salinity is 4.9 weight percent NaCl equivalent (Inclusion number TU77-108 1/1). But, as can be seen in Figure 14, the salinity of these inclusions vary from this maximum to pure water.

The data in Figure 14 does indicate the presence of a number of spurious measurements where an increased TmClath is not associated with a freezing point lowering of the CO_2-rich phase. The reason for this ambiguity is unknown.

Only one inclusion had a TmClath above the $ThCO_2$. In this inclusion the TmClath was at an extremely high temperature of +19.2°C. Other inclusions in this sample had similar TmClath, associated with a marked decrease in the $TmCO_2$, down to -86°C in one case. Such extreme temperatures implies a much greater amount of CH_4 and/or N_2, and heavier hydrocarbons (e.g. ethane, propane) dissolved in the CO_2-rich phase than is found elsewhere. Similar complex mixtures have been recognized by Hollister and Burruss (1976), Mullis (1979), Kreulen and Schuiling (1982), and Touret (1982).

4.5 Heating measurements

$ThCO_2$, Th, and Td are tabulated in Appendix 4, and plotted as histograms in Figures 12 and 15. Homogenization temperatures define the density of the phase to which the inclusion has homogenized. This defines a line of constant density or molar volume (isochore), if the volumetric properties of the one-phase fluid are known, along which the original fluid was trapped. The pressure at the time of entrapment needs to be known before the actual trapping temperature can be determined. The decrepitation temperature is the temperature at which the internal pressure of the inclusion exceeds the strength of the walls of the host mineral. This temperature is a function of the inclusion size (Leroy, 1979) and composition of the inclusion fluid (Burruss, 1981a). In this study the decrepitation temperature also represents the temperature of minor leakage from an

Figure 14. CO_2 clathrate melting temperatures plotted against the melting temperature of CO_2. The data points show the affect of adding NaCl and CH_4 to the H_2O-CO_2 system.

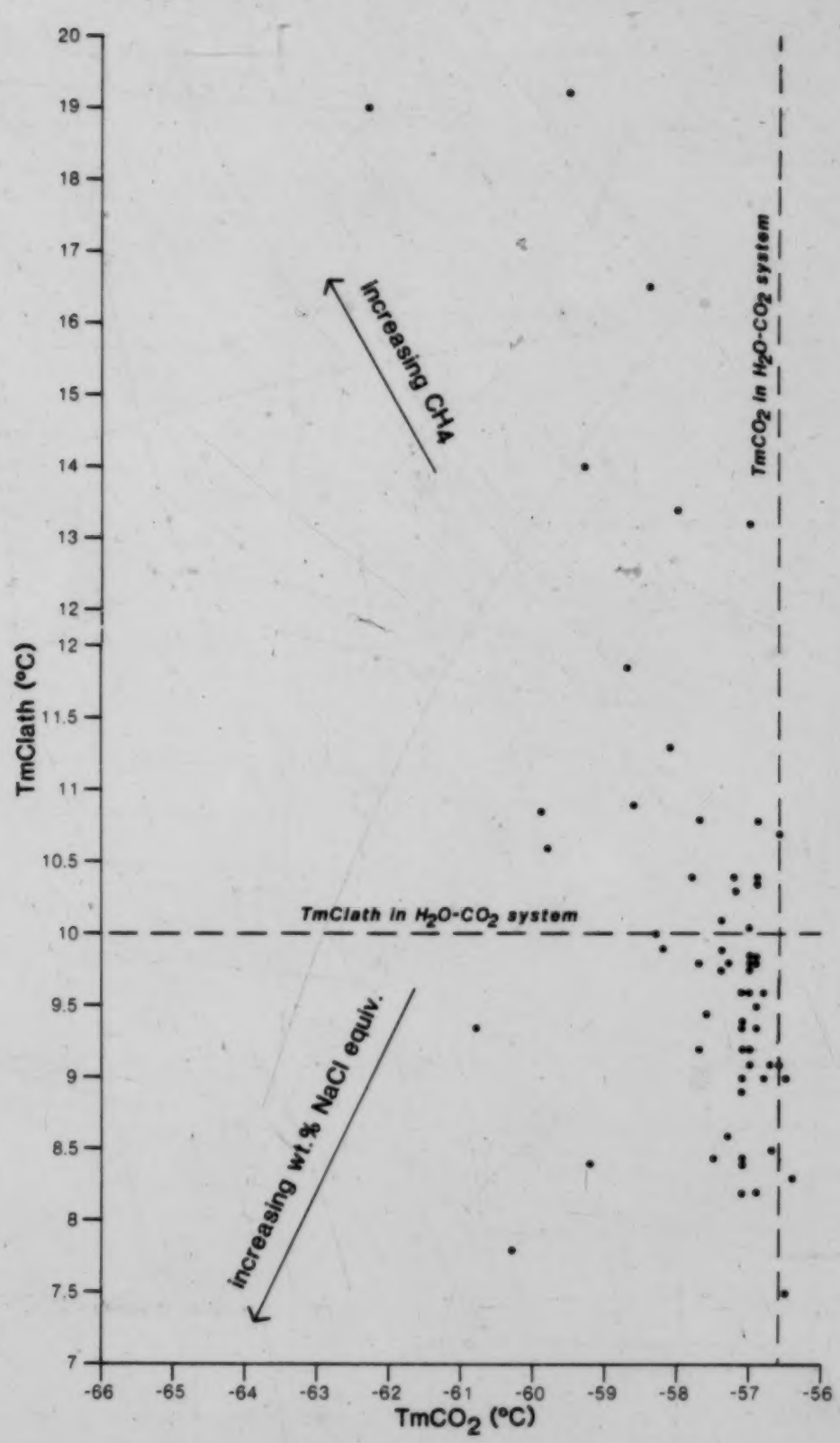
TmClath (°C)
TmCO2 (°C)
TmClath in H2O-CO2 system
TmCO2 in H2O-CO2 system
increasing CH4
increasing wt.% NaCl equiv.
20
19
18
17
16
15
14
13
12
12
11.5
11
10.5
10
9.5
9
8.5
8
7.5
7
-66
-65
-64
-63
-62
-61
-60
-59
-58
-57
-56

Figure 15. Homogenization and decrepitation temperatures from Type 1 and 2 inclusions.

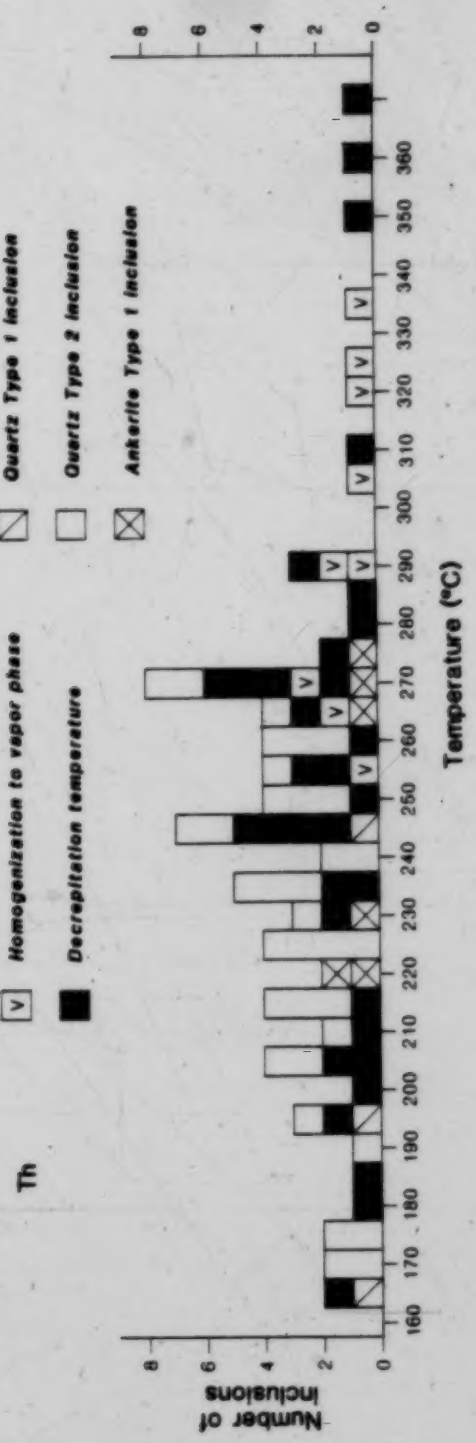

inclusion. An increase in size of the vapor bubble at room temperature, and an inability to reproduce homogenization temperatures were taken as an indication of leakage. However, reproducibility does not rule out the possibility of undetected changes in inclusion volume or composition since trapping as a result of the thermal history of the inclusion (Bodnar and Bethke, 1984), crystallization on inclusion walls, necking, or leakage by diffusion of hydrogen or submicroscopic fractures (Roedder, 1981).

The heating of Type 2 inclusions to homogenization is likely to induce decrepitation because of the high internal pressures that develop. To allow determination of the bulk density of these inclusions, the graphical method described by Burruss (1981b) was utilized. This involves the estimation of the volume percent of the CO_2-rich and H_2O-rich phases at a constant temperature (e.g. 40°C) in the two-phase region. The problems involved with volume estimates are outlined by Roedder (1967), and an unknown error is obviously introduced with this method. Also, the method relies on three assumptions :

(1) the solubility of H_2O in CO_2, and vice versa, is negligible at temperatures slightly greater than the CO_2 critical point (e.g 40°C),

(2) the bulk molar volume of an inclusion is an ideal solution of the endmembers,

(3) H_2O is incompressible up to 40°C, and thus the inclusion pressure is fixed by the isochore for the CO_2-phase at 40°C.

This method also assumes a pure H_2O-CO_2 system. Most Type 2 inclusions contain CH_4 and NaCl which affect the density determinations. Swanenberg (1979) shows that for a given $ThCO_2$ to the liquid phase, the density of the isochore having its origin at that temperature will decrease with increasing mole fraction CH_4. For example, at a $ThCO_2$ to liquid of +20°C the isochore density for a CO_2-rich phase with mole fraction CH_4 = 0.10 will be 0.18 g/cm^3 less than the density for a pure CO_2-phase. Hollister and Burruss (1976) used a similar method and assumed pure CO_2 for all inclusions with less than 10 mole % CH_4 in the CO_2-rich phase. The Burruss (1981b) method is used to calculate bulk inclusion densities and mole % H_2O, but only for inclusions with less than 10 mole % CH_4 in the CO_2-rich phase (Table 6). The magnitude of the error outlined above must be noted, although this does not affect the range of values seen. The densities and compositions calculated using this method are shown in Table 6.

Examination of Figure 15 reveals a wide range of decrepitation and homogenization temperatures in both quartz and ankerite. Most measurements lie between 200° and 275°C but there is no distinct peak or distinction between temperatures from quartz and ankerite, or between the two inclusion types. Temperatures of homogenization to the vapor phase range from 235° to 335°C, whereas temperatures of homogenization to the liquid phase range from 125° to 275°C. Decrepitation temperatures show the widest range, 165° to 370°C, with a small peak between 240° and 270°C. Decrepitation was most commonly encountered in Type 2 inclusions.

4.6 Discussion of results

The original objective of the fluid inclusion study was to determine the composition and temperature of the hydrothermal fluids from which the ore and gangue minerals were deposited. Gardner (1983), in a study of the Jason Pb-Zn deposit, concentrated on stockwork quartz, siderite, and ankerite, and secondary minerals in the laminated ore (quartz, ankerite, barite, fluorite, barytocalcite). Gardner's (1983) results, when averaged, gave salinities of 9.4 ± 1.7 weight percent NaCl equivalent and a temperature of 251 ± 22°C. Large (1981) indirectly suggested a similar temperature for the Tom ore-forming fluids from mineralogical reasoning and comparison with present geothermal systems.

Primary fluid inclusions in stockwork ankerites were chosen as being most likely to represent remnants of the original hydrothermal fluid. This was based upon consideration of the paragenesis of the footwall veins. As indicated in Chapter 3, quartz veins are late in the paragenetic sequence, although the timing of many of the veins relative to definite tectonic, quartz veins is difficult to determine. It was thought that quartz veins, formed at different times, may exhibit differences in the fluid inclusion type and composition. No such distinctions could be made and so it is probable that all the quartz veins formed during post-mineralization, tectonic activity. The fluid inclusions in these quartz veins thus provide samples of the fluid in the rock during deformation and remobilization of the sulfides.

The average salinity and homogenization temperature for fluid inclusions in ankerite is 9.1 ± 3.4 weight percent NaCl equivalent and 258 ± 33°C respectively, which is very

similar to the values quoted by Gardner (1983). The salinity range (5.0 to 18.3 wt.% NaCl equiv.) is also very similar. This would suggest that the two deposits were formed from very similar hydrothermal fluids as would be expected considering their temporal and spatial proximity.

As stated above, all the quartz veins are probably tectonic in origin. The area of the Tom deposit has undergone three phases of post-mineralization deformation (McClay, 1984). The quartz veins exhibit internal deformational features, e.g. undulose extinction, and subgrains, which are the result of dislocation creep mechanisms (White, 1973), although the extent of deformation varies from sample to sample. Kerrich (1976) showed that with increasing intracrystalline deformation, primary inclusions become sparser, smaller, and have a decreased degree of filling as a result of fluid leakage out of the inclusions. Homogenization temperatures can thus be significantly increased. Leakage out of inclusions increases the water content of the surrounding quartz, thus enabling deformation by hydrolytic weakening to proceed at a faster rate (Griggs and Blacic, 1965; Blacic, 1975). Although the ankerites do not exhibit any obvious deformational features, they must have been affected by these later deformation events.

The large range in homogenization temperatures in quartz from 164° to 335°C, and the complete overlap with the ankerite homogenization temperatures (Fig. 15) is probably a function of leakage during deformation which results in a decrease in the degree of filling by varying amounts from sample to sample. The average homogenization temperature for fluid inclusions in ankerite of 258°C, which in most fluid inclusion studies would be termed the temperature of the mineralizing fluids, is also erroneous. The initial homogenization temperature of the mineralizing fluids was probably much less. Unfortunately this temperature cannot be determined from this study, because the affect of leakage on the degree of filling of an inclusion is unquantifiable.

To determine the true trapping temperature of a given inclusion, the pressure at the time of entrapment has to be determined, so that a pressure correction can be added to the measured homogenization temperature (Potter, 1977). The pressure at the time of trapping can be determined directly from fluid inclusion data (the various methods are critically reviewed by Roedder and Bodnar 1980), or by independent methods based on, for example, metamorphic mineral assemblages or stratigraphic thickness estimates. The

addition of a pressure correction is only relevant if the measured homogenization temperatures are accurate. As explained above, leakage has occurred from inclusions in both quartz and ankerite, making homogenization temperatures erroneous. Thus, the addition of a pressure correction would be meaningless in this case, and would only serve to increase the error in the determination of the true trapping temperature of the inclusions.

Even though deformation and associated leakage from fluid inclusions make temperature estimates from the fluid inclusion data impossible, there does appear to be a general difference between the ankerite and quartz inclusion in terms of inclusion type and salinity (Fig. 10). Ankerites have a higher percentage of Type 1 inclusions and a higher inclusion salinity than quartz. Ankerite is paragenetically early, and so must be affected by the later deformation events and have been in contact with the quartz-forming fluids. To explain the distinct salinity differences between primary inclusions in ankerite and quartz, it is suggested that complete mixing between the deformation fluids from which the quartz veins precipitated and the primary fluids in ankerite did not occur. Complete mixing would have resulted in the salinities of inclusions in quartz and ankerite being the same, with the actual value being determined by the relative volumes of the two fluids. This observation also implies that complete dissolution and recrystallization of the ankerite did not occur. The salinity of the fluid at the time of ankerite deposition can therefore be approximated by the salinity of the ankerite inclusions.

The inclusions in ankerite exhibit no evidence for boiling, and consequently, a minimum seawater depth at the time of mineralization can be estimated. A boiling point curve corresponding to the average salinity (9.1 wt.% NaCl equiv.) of the mineralizing fluid is constructed from data by Haas (1971) (Fig. 16). If boiling was taking place then the intersection of the temperature of the fluid with the boiling point curve would give the seawater depth, and thus the hydrostatic pressure. This intersection gives the minimum seawater depth in the case of no boiling. The average homogenization temperature obtained from the Tom ankerites is 258°C, which coincides with a minimum seawater depth of 400 m (Fig. 16). This temperature is an upper limit for mineralization, which suggests that the minimum seawater depth was probably much less.

Figure 16. Boiling point curve for a H_2O-NaCl solution containing 9 wt.% NaCl, calculated from data of Haas (1971). The diagram indicates that a fluid of this salinity and a temperature of 258°C would boil if the depth of seawater was less than 400 m.

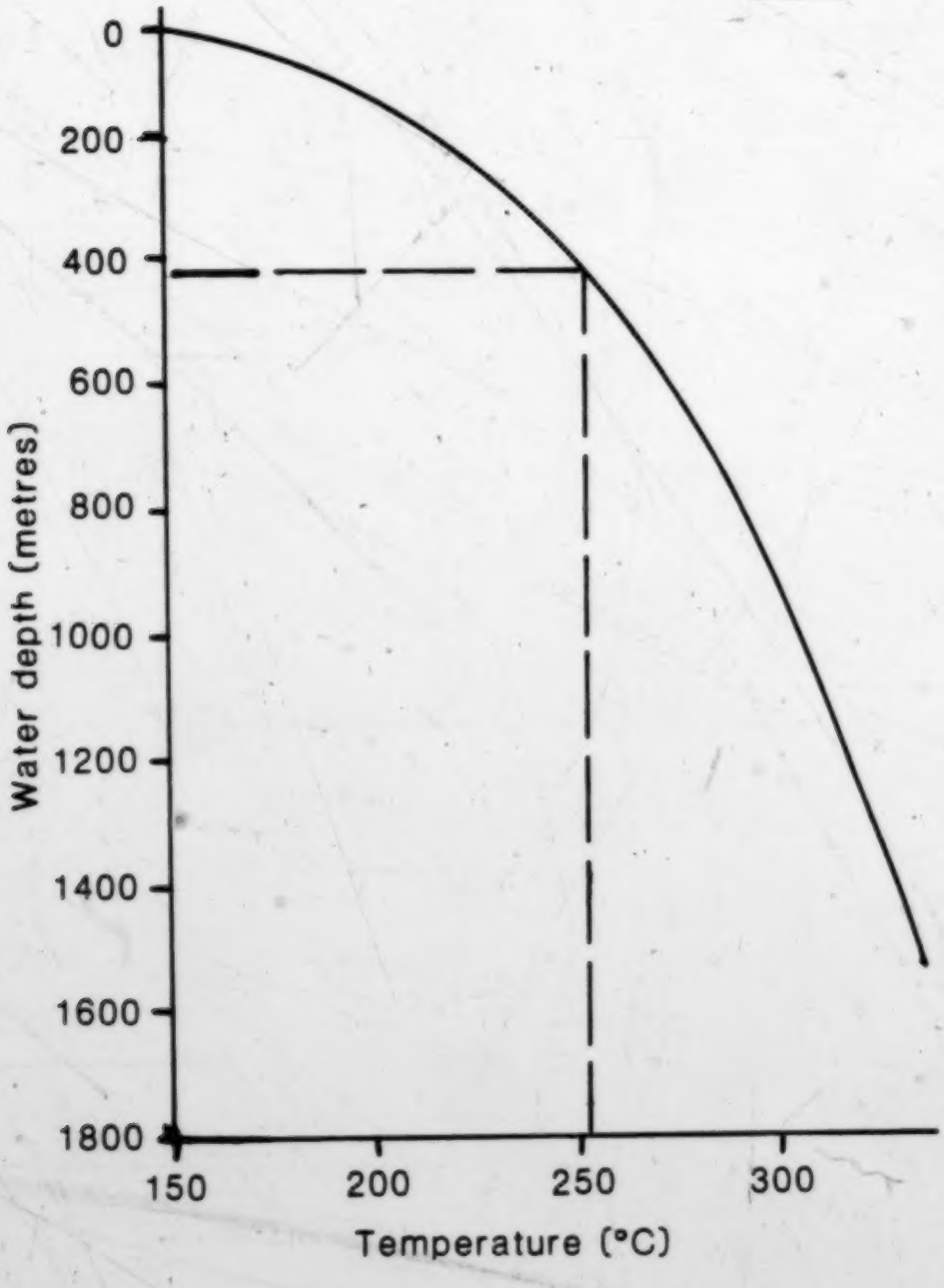

Many quartz grains contain inclusions that have apparently trapped a fairly uniform H_2O-CO_2-(NaCl-CH_4) fluid. However, there are variations from grain to grain, and in a few areas there was noted a distinct intragrain variation in inclusion type, homogenization temperature, and degree of filling among the assumed primary inclusions. An example is TS83-28 where the Td/Th varies from 166° to 271°C, and the volume % H_2O varies from 0 to 60 %. Other areas contain both Type 1 and 2 inclusions. If the inclusions originally trapped an homogeneous fluid, these variations would imply marked differences in the amount of leakage from inclusions adjacent to each other.

A possible explanation for the above could be the trapping of locally heterogeneous fluids. Konnerup-Madsen (1979) suggests such an idea to explain variable H_2O/CO_2 ratios in adjacent primary inclusions in quartz in amphibolites associated with molybdenite mineralization in southern Norway. Ramboz et al. (1982) state that the criteria for heterogeneous trapping are simultaneous trapping of the inclusions, and a scatter in the degree of filling, homogenization temperatures, and compositions. All these conditions are met by the inclusions. As explained above, there is evidence for undetected leakage, but it is postulated that all the inclusions in a given small area have leaked to a similar extent and so the general, initial compositional relationship between inclusions has remained.

The predominance of Type 2 inclusions in quartz shows that CO_2 and CH_4 were important constituents of the deformation fluids. The possible sources of CO_2 are :

(1) decarbonation of carbonates,

(2) oxidation of organic matter,

(3) a deep-seated mantle degassing,

while the CH_4 was probably produced by a mixture of thermal degradation of organic matter, and reduction of already formed CO_2.

An isotopic investigation of the CO_2 in the inclusion fluid could be used to determine the relative importance of these three possible sources. Because of the large sample (50 g) required in order to obtain a reasonable volume of CO_2, and the high percentage of secondary inclusions in all samples it was decided that any results obtained would be, at best, semi-quantitative, and so no analyses were attempted.

4.7 Conclusions

The usual objective of a fluid inclusion study of an ore deposit is to determine the composition and temperature of the mineralizing fluids (Spooner, 1981). Unfortunately, at the Tom deposit, the effects of later strain and low temperature recrystallization have been superimposed on the original mineralogy making interpretation of fluid inclusion data difficult. Temperature estimates particularly, are erroneous whenever any deformation-induced leakage is suspected (Kerrich, 1976). Nevertheless, certain conclusions can be reached concerning the fluids present during mineralization, and during later deformation.

The aqueous inclusions in the paragenetically early ankerite veins, which are thought to represent feeder veins, have an average salinity of 9.1 weight percent NaCl equivalent and an average homogenization temperature of 258°C. Complete recrystallization of the ankerite has been ruled out, but because of the unknown effect of leakage during deformation on the degree of filling this temperature is termed the maximum value for the minimum temperature of the mineralizing fluids. Small amounts of CO_2 and CH_4 are present in some ankerite inclusions. Although the number of primary inclusions in a given grain was small, there did not appear to be any evidence for boiling. The small volume of stockwork veining relative to stratiform mineralization also implies that boiling was minor (Large, 1983).

The paragenetically later, tectonic quartz veins contain primary inclusions exhibiting a wide range in homogenization temperature, but an average salinity in Type 1 inclusions of 4.8 weight percent NaCl equivalent. CO_2-rich inclusions dominate, although mole % CO_2 varies from 0 to 100 %. The average minimum salinity in CO_2-rich inclusions is 1.6 weight percent NaCl equivalent. The CO_2-phase frequently contains up to 10 mole % CH_4, although in certain areas up to 60 mole % CH_4 is found. Usually the inclusion compositions in a given grain are constant, but inter-grain and inter-sample variation is often distinct. This might imply local variations in fluid composition. In a few grains adjacent inclusions exhibit very variable degrees of filling and homogenization temperatures, which are interpreted to result from leakage during deformation superimposed on inclusions which originally trapped a locally heterogeneous, unmixed fluid.

5. ISOTOPE GEOCHEMISTRY

5.1 Introduction

The aim of this study is to determine the nature of the fluids involved in the development of the Tom deposit. To achieve this objective the oxygen isotopic composition of ankerite veins, quartz veins, whole rock and <2 μm mineral fractions have been examined. The isotopic composition of ankerite veins and bands within the massive sulphides are used to provide information on the isotopic composition of the hydrothermal fluids related to mineralization. The analysis of fluid inclusions indicated that probably all the quartz veins were formed during deformation. If the isotopic composition of various quartz veins support this hypothesis, then the oxygen isotopic compositions of the quartz veins can be used to give information as to the probable source of the fluids present during deformation. Variations in the oxygen isotopic composition of whole rock, and <2 μm fractions of footwall and hangingwall mudstones provide information on the extent of fluid / wall rock exchange related to mineralization.

Oxygen-isotope analyses of the rocks hosting the Jason deposit showed a distinct alteration halo around the mineralization, which was marked by a zone of ^{18}O depletion (Longstaffe et al., 1982). A similar relationship was anticipated around the Tom considering the temporal and spatial proximity of the two deposits.

5.2 Analytical procedure

Ankerite and quartz samples were hand-crushed and purified using conventional separation techniques. Mudstones were crushed in a swing-mill and the <2 μm fraction obtained by standard sedimentation procedures. Mineralogy and purity of the separates were checked by X-ray diffraction (Appendix 3).

Oxygen was quantitatively removed from the silicates using the BrF_5 oxidation technique of Clayton and Mayeda (1963). The oxygen was then subsequently converted to carbon dioxide for mass spectrometry. Carbon dioxide was obtained from ankerite by reaction with 100 % H_3PO_4 at 25°C (McCrea, 1950) for 11 days. A long reaction time ensured a yield close to 100 %.

Carbon dioxide was analyzed with a Nier-type, 90°-sector, double-collecting, Micromass 602D mass spectrometer. The results are reported in the usual δ-notation with respect to Standard Mean Ocean Water (SMOW) for oxygen (Craig, 1961), and PDB for carbon (Craig, 1957). A CO_2-H_2O fractionation factor of 1.0412 was used.

Samples were chosen so that any vertical and lateral variation in isotopic composition away from the proposed feeder zone could be detected. Sample locations are indicated in Table 7, and can be located relative to the feeder zone on Figure 17.

5.3 Results

Mineralogy and stable isotope data for all samples are tabulated in Table 7, along with their position relative to the stratiform mineralization.

The mineralogy of the whole rock samples is dominated by quartz. Petrographic observation suggests that the samples furthest from the mineralization are dominated by detrital quartz, while those nearest the mineralization are dominated by fine-grained silica that is interpreted to have been deposited from the hydrothermal fluids. Barium-bearing minerals are prevalent in many samples, with cymrite being especially common in hanging-wall rocks.

The oxygen isotopic composition of the whole rock samples vary from +17.9 to +20.8 ‰ . This range falls within the typical range of clastic sedimentary rocks (Eslinger and Savin, 1973; Magaritz and Taylor, 1976), and is similar to the range seen at Jason (Longstaffe et al., 1982) While Longstaffe et al. (1982) detected a small depletion in ^{18}O in the whole rock samples at the upper and lower contacts of the Jason Main Zone mineralization, no such depletion is seen above the West Zone of the Tom deposit. Nevertheless, the sample with the lowest $\delta^{18}O$ values occurs within 0.5 m of the base of the West Zone.

The <2 μm mineral fractions were obtained to try and determine the isotopic composition of the clay minerals. The <2 μm mineral fraction at Tom consists mostly of quartz with varying proportions of illite and/or kaolinite. Attempts to isolate the clay minerals proved unsuccessful. The kaolinite/illite ratio, which was determined approximately by using X-ray diffraction peak height intensities, increases towards the mineralization (Appendix 4). This relationship was also noted at Jason (Longstaffe et al.,

Table 7. Oxygen and carbon isotope data from the Tom deposit.

Sample number	Section	Distance from deposit[1]	Mineralogy[2]	$\delta^{18}O$	$\delta^{13}C$
Whole rock					
TS83-11	60	9.0 h	Qtz-Cym-Ill-Pyr-Dol	+20.2	---
TS83-16.1	60	4.0 h	Qtz-Cym-Dol-Pyr-Ill	+19.7	---
TS83-50	60	1.0 f	Qtz-Sd-Pyr-Kln	+19.3	---
TS83-55.7	60	7.0 f	Qtz-Sd-Dol-Ill	+18.5	---
TS83-65	60	15.0 f	Qtz-Dol-Ill	+20.2	---
TS88-46	68	6.0 h	Qtz-Cym-Pyr-Ill-Dol	+19.8	---
TS88-56	68	0.5 h	Qtz-Cym	+19.9	---
TS88-90.5	68	0.0 f	Qtz-Brt	+17.9	---
TS88-92	68	1.0 f	Qtz-Pyr-Cel	+20.8	---
TS88-100	68	5.5 f	Qtz-Cym-Pyr	+18.2	---
TS88-107	68	9.0 f	Qtz-Ill-Fsp-Pyr	+19.3	---
<2 μm fraction					
TU60-(-1)	52	1.0 h	Qtz-Ill-Kln	+21.5	---
TU60-(-2)	52	1.5 h	Qtz-Ill-Kln	+19.5	---
TU60-(-6)	52	4.0 h	Qtz-Ill-Kln	+19.7	---
TU28-14	54	2.5 f	Qtz-Ill	+18.8	---
TU28-20	54	6.0 f	Qtz-Ill	+18.4	---
TS38-65	54	60.0 h	Qtz-Ill-Kln	+20.7	---
TS38-90	54	36.0 h	Qtz-Ill-Kln	+19.8	---
TS38-120	54	7.0 h	Qtz-Ill	+20.0	---
TS38-178A	54	30.0 f	Qtz-Ill	+19.8	---
TU39-29	55.5	1.5 h	Qtz-Kln-Ill	+14.3	---
TU15-18	56	6.5 f	Qtz-Ill-Kln	+19.1	---
TU15-21	56	9.5 f	Qtz-Ill	+18.6	---
TU70-22	56	8.5 f	Qtz-Ill	+19.8	---
TU70-26	56	12.0 f	Qtz-Ill	+18.7	---
TU70-31A	56	16.5 f	Qtz-Ill	+19.3	---
TS40-69	58	4.0 h	Qtz-Ill	+20.7	---
TS40-276	58	3.5 f	Qtz-Ill	+18.5	---
TS84-83	60	1.0 f	Qtz-Kln-Ill	+16.0	---
TS84-96	60	7.0 f	Qtz-Ill-Kln	+19.6	---

Table 7. cont.

Sample number	Section	Distance from deposit[1]	Mineralogy[2]	$\delta^{13}O$	$\delta^{13}C$
Ankerite					
TU40-92	55.5	vein	Ank	+19.6	-3.0
TU70-6	56	vein	Ank	+20.0	-2.6
TU71-13	56	band	Ank	+19.7	-2.9
TU67-48	64	vein	Ank	+20.2	-2.2
Quartz (± carbonate) veins					
TU60-10A	52	vein	Qtz	+21.8	---
TU38-8	55	vein	Qtz	+22.3	---
TU39-47	55.5	vein	Qtz	+22.6	---
TU70-11	56	vein	Qtz	+21.9	---
TU71-15	56	vein	Qtz	+22.5	---
			Fe-dol	+19.7	-5.5
TS12-36	56	vein	Qtz	+21.3	---
TS84-80A	60	vein	Qtz	+21.5	---
TS84-80B	60	vein	Qtz	+21.7	---
TS4-79	62	vein	Qtz	+21.4	---

All stable isotope analyses performed by D. Caird.
[1] Distance from mineralization in metres, h - hangingwall, f - footwall.
[2] Qtz-Quartz, Cym-Cymrite, Ill-Illite, Pyr-Pyrite, Dol-Dolomite, Fsp-Feldspar, Sd-Siderite, Kln-Kaolinite, Brt-Barite, Cel-Celsian, Ank-Ankerite, Fe-dol-Ferroan dolomite.

Figure 17. Simplified longitudinal cross-section through the Tom West Zone to allow easy location of stable isotope samples relative to the feeder zone (modified after Carne, 1979).

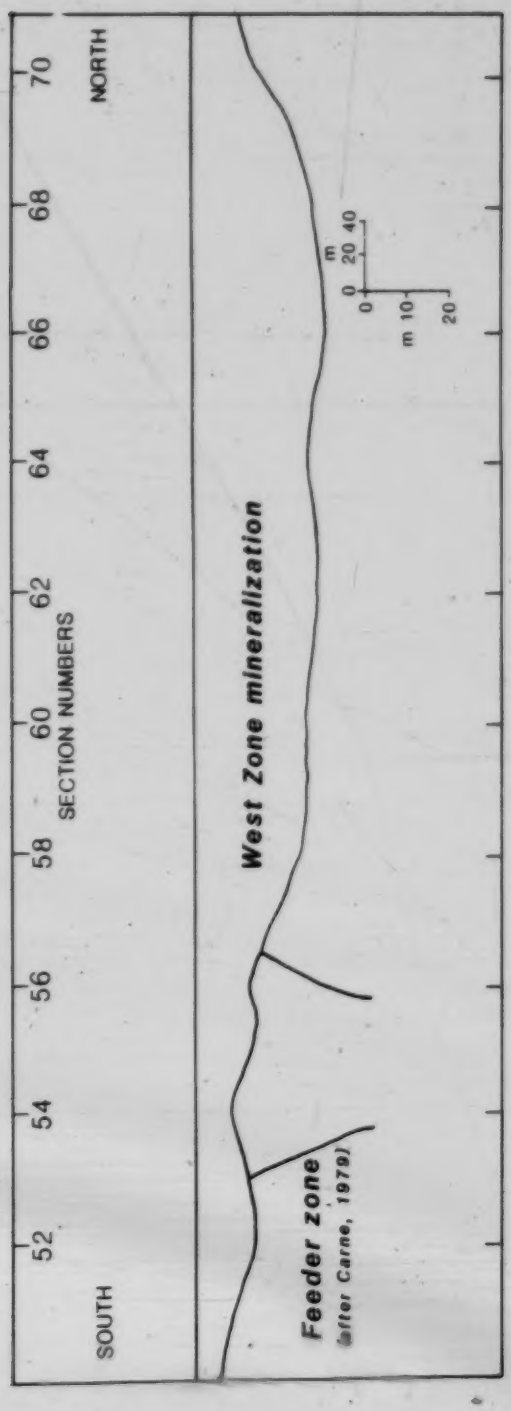

1982). In a few samples, kaolinite becomes the dominant clay mineral.

With the exception of two samples, the <2 μm fractions range in $\delta^{18}O$ from +18.4 to +21.5 ‰ (average $\delta^{18}O$ = +19.6 ± 0.6 ‰). These values are very similar to that shown by the whole rock samples, and again there is no distinct depletion in ^{18}O about the mineralization. However, samples TS84-83 and TU39-29, which are relatively rich in kaolinite, have lower $\delta^{18}O$ values (+16.0 ‰ and +14.3 ‰ , respectively). This suggests that the kaolinite in these samples is depleted in ^{18}O relative to typical, detrital clay minerals (Savin and Epstein, 1970). Low ^{18}O kaolinites were characteristic of the depletion halo around Jason (Longstaffe et al., 1982). The absence of a recognizable ^{18}O-depletion halo about the Tom deposit probably reflects the abundance of quartz rather than hydrothermal clays in the <2 μm mineral fraction.

Ankerite veins and bands are concentrated at the southern end of the West Zone. To the north, no ankerite bands are found interbedded with laminated sulfide mineralization, but veins are found cutting the chert pebble conglomerate.

Ankerites have a tight range in $\delta^{18}O$ and $\delta^{13}C$ values (Table 7), averaging +19.9 ± 0.2 ‰ and -2.7 ± 0.3 ‰ respectively. No spatial variations in the $\delta^{18}O$ or $\delta^{13}C$ values of the ankerites are evident (Table 7).

The oxygen isotopic composition of the tectonic quartz veins fall within a very narrow range from +21.3 to +22.6 ‰ (average $\delta^{18}O$ = +21.9 ± 0.5 ‰ . Sample TU71-15 is a tectonic quartz-ferroan dolomite vein, with the quartz being enriched in O^{18} relative to the dolomite by 2.8 ‰ (Table 7). Assuming equilibrium fractionation, an isotopic temperature of formation of 220 K is indicated from the fractionation curves of Clayton et al. (1972) for quartz-water, and Northrop and Clayton (1966) for dolomite-water. This low temperature implies that isotopic equilibrium between the quartz and ferroan dolomite has not been maintained.

5.4 Discussion of results

From the results obtained, it is possible to calculate the isotopic composition of both the ankerite-forming and quartz-forming fluids. The isotopic composition of the fluid from which a mineral crystallizes can be determined, if the fractionation factor between the mineral and water and the temperature of formation of the mineral are

known. The oxygen isotopic composition of the quartz-forming, deformation fluids can be calculated using the quartz-water fractionation curve of Clayton et al. (1972). Unfortunately, there are no experimental data available on the oxygen or carbon isotope fractionation between ankerite and water. Since ankerite is a dolomite isotype (Reeder, 1983), ankerite-water fractionation is probably similar to the fractionation between dolomite and water. Northrop and Clayton (1966) experimentally determined oxygen isotope fractionations between 300 and 510°C, and this fractionation has been extrapolated to lower temperatures by Land (1983). O'Neil et al. (1969) showed that in alkaline-earth carbonates there is a tendency to concentrate ^{18}O relative to ^{16}O with decreasing mass and/or size of cation. If this observation is applicable to ankerites they would be expected to have lower $^{18}O/^{16}O$ ratios than dolomites crystallizing from a given fluid at constant temperature. Determination of the temperature of formation of the ankerites and the quartz is a problem however, that will be discussed below.

Primary fluid inclusions in the ankerites indicate an average homogenization temperature of 258°C, which compares favorably with the temperature of the mineralizing fluids at Jason (Gardner, 1983). However, these temperatures are interpreted to have been increased by an unknown amount as a result of leakage during deformation. Isotopic and fluid inclusion evidence from other sediment-hosted Pb-Zn deposits indicate a wide range in temperatures, ranging from 150° to 310°C (Rye and Williams, 1981; Longstaffe et al., 1982; Samson and Russell, 1983; Nesbitt et al., 1984). Lydon (1983), in a review of the geochemical characteristics of sediment-hosted Pb-Zn deposits, implies that the hydrothermal fluids from which these deposits formed may vary from 100° to 250°C, depending on the salinity of the solution.

Since no unambiguous temperatures are available, a number of hypothetical temperatures are used to determine the possible isotopic composition of the ankerite-forming hydrothermal fluid (Table 8). The following two methods are utilized:

(1) the theoretical fractionation curve constructed by Rye and Williams (1981, their Figure 8) using the equilibrium fractionation curves of Sheppard and Schwarz (1970) (dolomite-calcite), O'Neil et al. (1969) (calcite-water), and Bottinga (1969) (calcite-CO_2),

(2) the empirical dolomite-water fractionation curve of Northrop and Clayton (1966):

Table 8. Calculated isotopic composition of the ankerite-forming fluid

Temperature °C	Method (1) $\delta^{18}O(H_2O)$	$\delta^{13}C$(fluid)	Method (2) $\delta^{18}O(H_2O$
250	+11.3	-2.3	+10.2
200	+8.7	-3.3	+7.6
150	+5.1	-5.0	+4.0
100	+0.1	-7.5	-1.1

$$1000 \ln \alpha \text{ dol-}H_2O = 3.20 \times 10^6 / T^2 - 2.00$$

where α is the fractionation factor, and T is temperature in Kelvin.

A similar procedure is used to determine the possible isotopic compositions of the quartz-forming, deformation fluids. The fluid compositions calculated using the equilibrium fractionation curve of Clayton et al. (1972) are listed in Table 9.

Comparison of the calculated fluid compositions from Tables 8 and 9 at a given temperature, suggests that the quartz-forming fluids are enriched in ^{18}O relative to the ankerite-forming fluids. The significance of this difference is unknown given the errors that may be introduced by the use of inaccurate equilibrium fractionation curves, by the use of the dolomite-water fractionation curve as an approximation for an ankerite-water curve, and the assumption that the tectonic quartz grew in isotopic equilibrium with the fluids present during deformation. Another problem is suggested by the isotopic disequilibrium suggested by the quartz-dolomite pair in sample TU71-15 (Table 7). If it is assumed that the quartz and dolomite originally grew in isotopic equilibrium, then the lack of equilibrium seen now must be a function of differential re-equilibration of the two minerals. Clayton et al. (1968) showed that calcite attains isotopic equilibrium at a temperature of 150°C, whereas quartz is resistant to isotopic exchange up to 340°C. Thus, the dolomite may have partially, or completely re-equilibrated with later fluids. The isotopic composition of the ankerite-forming fluids is calculated assuming that the isotopic composition of the ankerites has not changed significantly from the time of formation. Since tectonic dolomite has isotopically re-equilibrated, the earlier-formed ankerites may also have been affected. The accuracy of the calculated isotopic composition of the ankerite-forming fluid is thus unknown. However, the isotopic compositions calculated are typical of formation waters (Taylor, 1979), which are suggested as being the possible origin of the fluids in both sedimentary, exhalative systems (Badham, 1981; Sawkins, 1984), and low-grade metamorphic environments (Magaritz and Taylor, 1976; Kerrich et al., 1978).

The oxidized carbon species in the ankerite-forming hydrothermal fluid can be derived by way of redox, or hydrolysis reactions from organic matter, decarbonation of sedimentary carbonates, or from a magmatic source. CO_2 produced by the above

Table 9. Calculated isotopic composition of the quartz-forming fluid

Temperature °C	$\delta^{18}O(H_2O)$
250	+12.4
200	+9.7
150	+5.9
100	+0.5

processes have distinctive ranges in $\delta^{13}C$ (Rye and Ohmoto, 1979). CO_2 produced by the breakdown of organic matter usually has a $\delta^{13}C$ of less than -10 ‰, while decarbonation of limestones produces CO_2 with a $\delta^{13}C$ value of just over 0 ‰. CO_2 having a magmatic source, has a $\delta^{13}C$ value of about -5 ‰. A magmatic source cannot be ruled out, but is unlikely to be dominant because of the lack of igneous activity in the region at the time of ore deposition. It seems probable that the calculated carbon isotopic composition of the hydrothermal fluid (-2.3 to -7.5 ‰, Table 8) results from mixing of CO_2 derived from organic matter, and limestones, in the sedimentary pile underlying the Tom.

The lack of variation in the oxygen isotopic compositions of the whole rock and <2 μm mineral fractions, plus the absence of an alteration package around the mineralization, implies that the extent of interaction between the mineralizing fluids and the country rock was small. Nesbitt et al. (1984) show that there is a similar lack of isotopic variation associated with the Sullivan Pb-Zn deposit, and used this to suggest that the temperature of the mineralizing fluid was low (150°C). The lack of interaction at Tom may be the result of a similar low temperature. It could also be explained by a low water / rock ratio during mineralization, with the isotopic composition of the mineralizing fluid being controlled by the isotopic composition of the country rock. A high fluid flow rate during mineralization could also have prevented substantial isotopic exchange, since the time available for interaction between the fluids and the country rock would have been much reduced.

However, the two samples (TU39-29, TS84-83) richest in kaolinite do appear to have been depleted in ^{18}O relative to all the other samples. Since typical detrital clay minerals have an oxygen isotopic composition ranging from +15 to +30 ‰ (Savin and Epstein, 1970), the oxygen isotopic composition of these two samples suggests that the kaolinites are depleted in ^{18}O. Kaolinite formed in isotopic equilibrium with seawater ($\delta^{18}O$ = 0 ‰) at 25°C will have a $\delta^{18}O$ value of +25 ‰ (Longstaffe, 1983). Thus, the reduction in the oxygen isotopic composition of these two samples, plus the suggestion that the fluids involved in the development of the Tom deposit were formation waters enriched in ^{18}O relative to seawater, implies that the kaolinite probably formed during high temperature, hydrothermal activity. Further attempts at obtaining pure kaolinite samples would be useful, so that an isotopic temperature for the hydrothermal activity could be

determined.

6. DISCUSSION AND CONCLUSIONS ON THE DEVELOPMENT OF THE TOM DEPOSIT

6.1 Genesis of the deposit

6.1.1 Features relevant to the formation of the deposit

The Tom deposit is a typical, sediment-hosted, exhalative, massive sulfide deposit (Large, 1983). Such deposits are believed to have precipitated from exhaled, metal-bearing brines that have been ponded in small, fault-bounded basins (Finlow-Bates, 1980; Russell et al., 1981; Lydon, 1983). This mode of formation for the Tom deposit has been suggested in previous studies by Carne (1979) and Large (1981).

The features of the Tom deposit which typify a sediment-hosted, massive sulfide deposit, and which have a bearing on the genesis of the Tom, are summarized below. The mineralization consists of laminated sphalerite, galena, barite and chert overlying a zone of massive sulfides, which is situated towards the southern end of the West Zone. Carne (1979) identified an area of stockwork mineralization below the massive sulfides, but the density of ankerite veins in this area is no higher than that seen to the north. However, the presence of massive sulfides, the thickest zone of sugary replacement by ankerite, and the element zonation of (Cu) - Pb - Zn - Ba centred on the massive sulfides suggests that this area was a focus for vertical movement of the mineralizing fluids. A strong horizontal flow of fluids through the footwall rocks is also indicated by pervasive silicification of these rocks, and later replacement by ankerite. The latter is concentrated within the coarser-grained horizons, probably as a result of the greater permeability of these horizons. Thus, there may have been a continuous percolation of fluids from these coarser-grained units upwards into the depositional basin, although the volume of fluid exhaled away from the main vent was probably minor. It may have been important though in providing a medium for early diagenetic reactions.

The mineral zonation away from the massive sulfides (pyrrhotite - pyrite, Fe-rich sphalerite - Fe-poor sphalerite, galena - sphalerite - barite) typically develops as a result of the mixing of a hot, reducing hydrothermal fluid with cooler, more oxygenated seawater (Large, 1977). However, the high organic carbon content of the footwall and hangingwall mudstones does suggest that the depositional environment was also anoxic at the time of

exhalation. The development of a locally anoxic environment in the Upper Devonian may have been influenced by the seafloor topography at the time. Lateral facies and thickness variations in the lower Earn Group are indicative of synsedimentary faulting during the Middle and Upper Devonian (Abbott, 1982))

6.1.2 Composition, temperature and origin of the mineralizing fluid

Limits on the nature of this exhalative fluid can be made using fluid inclusion and stable isotope data. The mineralizing fluid is a sodium chloride brine with an average salinity of 9.1 weight percent NaCl equivalent (1.7 mole % NaCl), which is similar to the mineralizing fluids at Jason (Gardner, 1983). Eutectic melting temperatures down to -45°C imply the presence of minor $CaCl_2$ and $MgCl_2$. The presence of KCl cannot be ruled out from the fluid inclusion study, since the eutectic melting temperature for a H_2O-NaCl-KCl mixture is similar to the eutectic melting temperature for a H_2O-NaCl mixture (Crawford, 1981). The salinity of the fluids probably developed by the process of membrane filtration (Graf, 1982), since the sedimentary sequence underlying the Tom is evaporite-poor (Large, 1981).

The average homogenization temperature for primary inclusions in the vein ankerites is 258°C, which is very similar to the temperature observed at Jason (Gardner, 1983). He interpreted these temperatures as representing the temperature of the mineralizing fluid. However, the MacMillan Pass area has experienced several phases of post-mineralization deformation, and so these temperatures have been increased by an unknown amount as a result of leakage. Gardner (1983) applied a pressure correction of 25°C to his measurements, inferring a temperature of trapping of 276°C. This temperature represents the upper limit for the temperature of the mineralizing fluids at both Tom and Jason. The actual temperature of the fluids is suggested to have been between 150° and 200°C for the following reasons :

(1) there is no variation in the oxygen isotopic composition of whole rock and <2 μm mineral fractions as the mineralization is approached, which implies that the extent of isotopic exchange between the fluids and the country rock was minor. Nesbitt et al. (1984) detected a similar lack of variation in the footwall of the Sullivan Pb-Zn deposit, and interpreted this to be a function of the temperature of the hydrothermal fluids.

Detectable isotopic exchange would only be expected if the temperature was above 200°C (Clayton et al., 1968, 1978; O'Neil and Kharaka, 1976; Yeh and Savin, 1977). Alternatively, this could be explained by rapid movement of the fluids through the country rock, which thus prevents significant interaction between the two, or by a low water / rock ratio and so the isotopic composition of the hydrothermal fluid is controlled by the isotopic composition of the country rock.

(2) Lydon (1983) states that the solubility of copper minerals in a 3 molal NaCl fluid is very dependent on temperature, and so the absence or presence of Cu in reduced, hydrothermal fluids can be used as a rough geothermometer. High concentrations of Cu would be expected above 200°C, while no copper is indicative of temperatures below 150°C. Minor chalcopyrite is observed in the feeder zone and in the massive sulfides at Tom, and so these temperatures may represent the upper and lower limits for the temperature of the mineralizing fluid. The lack of significant Cu may also suggest that the salinity of the mineralizing fluid was less than 3 molal NaCl.

The source of sedimentary, exhalative brines is generally considered to be formation waters (Badham, 1981; Sawkins, 1984). Since the formation water has been held within the sedimentary sequence long enough for its composition to have been affected by reaction with adjacent minerals, the pH of such a fluid is dependent on the mineralogy of the rocks. The typical mineralogy of the clastic sedimentary rocks underlying the Tom are quartz, illite and feldspar. Solutions buffered by this assemblage are usually slightly acidic (Ellis, 1979).

This pH favours chloride complexes as the dominant metal carrier (Barnes, 1979). Sulfur complexes are also unlikely because, based on a consideration of the paragenesis and mineral assemblages present in the footwall veins and the massive sulfides, it appears that the total sulfur molality of the mineralizing fluid was extremely low. The first three stages in the paragenesis of the footwall are silicification, deposition of ankerite in veins and as a secondary cement, and formation of pyrrhotite veins (Fig. 8). The first stage requires a temperature decrease, while the second stage is probably the result of an increase in pH. Both these changes in the conditions would destabilize Fe-chloride complexes, and so the initial lack of Fe-sulfides associated with the silica and the ankerite may indicate that there was little sulfur available in the mineralizing fluid or in the

depositional environment. The actual sulfur molality is difficult to determine although it probably lies at the lower end of the range indicated by Giordano and Barnes (1981) for Mississippi Valley-type Pb-Zn deposits, i.e. 10^{-4} to 10^{-5} molal. Lydon (1983) also states that the Zn/ Zn+Pb ratio of 0.6 seen at Tom is typical of sulfur-deficient, hydrothermal fluids. The lack of sulfur indicates that chloride complexes are the dominant metal carriers.

The presence of ankerite in the feeder zone and in the massive sulfides indicates the importance of dissolved CO_2 in the mineralizing fluid. Little CO_2 was observed in fluid inclusions, although, as Roedder (1984) states, this does not rule out the presence of CO_2 in the original fluid. Large (1981) argues that the total activity of carbon was probably at least 0.1 molal, which corresponds to a CO_2 fugacity of 10 atm. This is the maximum CO_2 fugacity measured in modern geothermal systems (Ellis, 1979). The solubility data for CO_2 in sodium chloride solutions of Ellis and Golding (1963) is used to estimate the molality of CO_2 in a solution of temperature, 150°C, and salinity, 1.5 mole % NaCl. The calculated CO_2 molality is of the order of 0.5 molal.

The deposition of pyrrhotite prior to deposition of pyrite in both the footwall veins and the massive sulfides implies that the mineralizing fluids were very reducing ($fO_2 = 10^{-30} - 10^{-60}$). Under these reducing conditions, and a slightly acid pH, the dominant species of sulfur and carbon are H_2S and H_2CO_3 respectively.

The calculated carbon isotopic composition of the mineralizing fluid (Table 8) suggests that the dissolved CO_2 may have been derived from two sources :

(1) decarbonation of marine limestones,

(2) breakdown of organic matter.

Also, from lead isotope analyses of galena at Tom, the metals were probably leached from the underlying rocks (Large, 1981; Godwin and Sinclair, 1982).

6.1.3 Constraints on the depositional environment

Metal-bearing, chloride complexes become unstable as a result of a decrease in temperature, an increase in H_2S concentration, an increase in pH, or a decrease in chloride concentration (Barnes, 1979). The solubility of silica is reduced solely by a temperature decrease (Holland and Malinin, 1979), while the solubility of barite also decreases with

temperature at the salinity of the Tom mineralizing fluid (Blount, 1977). Since there are no published thermodynamic data for ankerites the solubility pattern of dolomite can be used as an approximation for ankerites. The solubility of dolomite decreases with increasing temperature, and increases with fO_2 (Holland and Malinin, 1979).

Silicification is early at Tom and affects all footwall rocks. The extent of silicification decreases away from the mineralization. Silica solubility decreases with temperature and so the silica was probably deposited as a result of mixing of silica-saturated, hydrothermal fluids with cool, seawater trapped in the sediment during burial. There are no associated sulfides because of the low sulfur concentration in the depositional environment at this time.

The pure ankerite veins seen in the footwall were probably deposited from a H_2O-CO_2 fluid as a result of an increase in pH. A likely method is by the boiling off of the CO_2 (Holland and Malinin, 1979). No sulfides are found associated with these early ankerites, although ankerite is found interbanded with sulfides within the massive sulfides higher up the succession. This change in associated mineralogy may represent an upward change in the depositional environment. The increase in pH, and the slight temperature decrease may have destabilized metal-bearing, chloride complexes, but no sulfides formed initially because of the low reduced sulfur activity. The observation that pyrrhotite-sphalerite-galena-chalcopyrite veinlets cut the ankerite veins, and the change upwards from ankerite veins to interbanded ankerite-sulfides can be explained by an increase in the concentration of reduced sulfur. A temperature decrease is not required to explain the variation in mineral association with time, although there may have been some interaction with downward-percolating seawater in the massive sulfides.

The lack of interaction with seawater is a major problem if the massive sulfides are interpreted to have been deposited on the seafloor proximal to the vent zone (Carne, 1979; Large, 1981). However, textures observed in this study suggest that some of the massive sulfides may represent replacement of the silicified, and carbonate-rich footwall rock, rather than all the sulfides being deposited on the seafloor as the result of rapid cooling of the mineralizing fluid.

The behaviour of the hydrothermal fluid after discharge into seawater is a function of its density. A maximum fluid temperature of 200°C combined with a salinity of 9.1

weight percent NaCl equivalent, gives a minimum density of 0.95 g/cm^3 for the exhaled fluid. This density is less than seawater and such a fluid will rise through the water column until the water surface is reached, or until it becomes infinitely diluted (Sato, 1972). Sulfides precipitated from this light brine will be dispersed and show no relationship to the seafloor topography. However, Figure 6 indicates that the laminated mineralization at Tom is concentrated within a basin. A buoyant brine plume would be expected, but the concentration of mineralization within a basin is explained by the rapid quenching of the hydrothermal fluids above the vent zone as a result of mixing with seawater, with the formation of a dense bottom-hugging brine (Turner and Gustafson, 1978; Solomon and Walshe, 1979).

The laminated ore exhibits a typical zonation pattern away from the massive sulfides with barite dominating in the distal portions of the deposit. This zonation pattern is generally interpreted to be a function of temperature, oxidation state, and sulfur fugacity. Temperature most likely decreases away from the zone of exhalation which is the dominant control on the stability of Pb and Zn-chloride complexes (Barnes, 1979). Galena laminae are concentrated proximal to the massive sulfides, while sphalerite becomes more dominant distally. The low iron-content of the sphalerites in the laminated ore relative to the massive sulfides, and the change in the dominant iron sulfide mineralogy from pyrrhotite to pyrite can be explained by a temperature decrease, an increase in the sulfur fugacity, or a mixture of the two (Scott, 1983). The presence of barite suggests a more oxidizing environment away from the vent area.

Sulfur and oxygen isotopic compositions of barite in the Selwyn Basin shows that the sulfate is derived directly from the seawater (Cecile et al., 1983). Preliminary sulfur isotopic analysis of sulfides at Tom and Jason (Large, 1981; Gardner, 1983) suggests that the source of the sulfur was the hydrothermal fluid, which suggests that little or no reduced sulfur needed to be produced locally to allow sulfide deposition. This does not fit with the suggested composition of the mineralizing fluid, and a number of features at Tom indicates that local production of reduced sulfur by sulfate-reducing bacteria was probably the major source of sulfide-sulfur. The high organic content of the sedimentary rocks is considered to be related to the development of euxinic conditions, which enhances the bacterial and/or chemical reduction of sulfur (Berner, 1974; Orr, 1974).

The presence of pyrite framboids in the stratiform mineralization, as well as in the hangingwall and footwall rocks indicates that sulfate-reduction was an important process in the early stages of diagenesis. Since the rate of barite dissolution is very dependant on the bacterial reduction of organic matter (McCready and Krouse, 1980), the presence of barite indicates that the rate of precipitation of barite was greater than the rate of dissolution (Cecile et al., 1983). Reduced sulfur is still produced within the barite-rich sequences, since framboidal pyrite, and sphalerite are still deposited. The efficiency of the sulfate-reducing bacteria may be reduced as a result of the more oxidizing conditions away from the vent area, thus allowing a greater percentage of the hydrothermal barite to be deposited as a sulfate. Any dissolution of barite by sulfate reduction results in the release of barium. The barium may diffuse upwards, and be involved in further precipitation of barite in more oxidizing conditions, or it may remain within the sediment and become available for the formation of diagenetic, barium-bearing minerals. Celsian, and barium carbonates are the main diagenetic minerals and imply high Ba^{2+} / Ca^{2+} and CO_3^{2-} / SO_4^{2-} activity ratios (Large, 1981).

Periodic exhalations of hydrothermal fluid are suggested by the laminated form of the ore body, but there were probably more than one major periods of exhalation as indicated by the peaks in zinc grade seen through the stratiform mineralization (Figure 5).

Continued hydrothermal activity after the deposition of the stratiform mineralization is indicated by the high silica content and the high Ba concentration in the hangingwall rocks. The major barium mineral in the hangingwall is cymrite.

6.2 Determination of the timing of quartz veins

An interesting facet of this study was the determination of the timing of the numerous quartz (± carbonate, sulfide) veins seen cutting the footwall rocks. In all samples these veins are late in the paragenesis, although relationships between samples are difficult to determine because observations are restricted to drillcore. Carne (1979) suggested that these veins represented the feeder zone, and there does appear to be a slight increase in density of veining below the massive sulfides. Microscopically, some of the quartz veins exhibit textures typical of crack-seal deformation (Ramsay, 1980), and thus were definitely formed during post-mineralization deformation. Due to the varied

mineralogy of the veins it was difficult to classify the veins unambiguously, although it was thought at first that quartz plus sulfide veins may be related to mineralization. Representative samples from the different types of quartz veins were subjected to fluid inclusion and stable isotope analysis. The results are explained in detail in Chapters 4 and 5, but it was found that the quartz veins could be convincingly classified after these studies. The fluid inclusion data indicated that the fluid from which the quartz was deposited was different in composition from the ankerite-forming fluid. The oxygen isotopic composition of the sampled quartz veins showed a very small range from 21.3 to 22.6 ‰ suggesting also that all the quartz veins were deposited from the same fluid. Since some of the veins are definitely related to post-mineralization deformation, it seems reasonable to assume that all the quartz veins are tectonic in origin. Usually, fluid inclusion and stable isotope studies require accurate knowledge of the paragenetic position of a sample prior to analysis. However, this study shows the usefulness of these analytical tools in helping to identify, and classify different generations of veining.

6.3 Conclusions on the nature of the fluids present during deformation

As explained above, the quartz veins are interpreted to be tectonic in origin. The quartz in these veins also exhibit features indicative of later strain (e.g., undulose extinction, subgrains), which suggests that leakage has probably occurred. Because of this unquantifiable leakage, the temperature of the quartz-forming, deformation fluids cannot be conclusively determined by fluid inclusion analysis. A temperature range of 150° to 200°C is estimated by McClay and Ellis (1983) for the sub-greenschist metamorphism at the Tom deposit. This temperature falls at the lower end of the range of homogenization temperatures observed in quartz and is thus consistent with an increase in homogenization temperatures as a result of leakage.

Since the composition of the ankerite, and quartz fluid inclusions are distinctly different, little or no mixing of the ankerite-forming and quartz-forming fluids occurred during straining and partial recrystallization of the minerals. After consideration of fluid leakage from inclusions, the composition of the inclusions in quartz must approximate the fluid composition at the time of deformation. The inclusions will have lost some fluid, but if the amount of leakage from inclusions within a given grain is assumed constant, then the

initial compositional relationship between these inclusions can be assumed to have remained.

CO_2-rich inclusions dominate, and in some areas there is up to 60 mole % CH_4 in the CO_2-phase. The composition of adjacent inclusions within a given grain are usually similar, although there are distinctive inter-grain and inter-sample variations, which implies local variations in fluid composition. These variations may be partially explained by considering the mechanism of formation of the bulk of the quartz veins. The textures seen in the veins, plus the presence of pressure solution fabrics in the adjacent rocks suggests that the crack-seal mechanism as described by Ramsay (1980) was probably operative. This process requires that successive microfractures were filled with fluids that contained components in solution which were chemically closely-related to the components forming the main body of the rock. These components are derived by local chemical solution, followed by diffusional mass transport towards the opened microfractures. Although much of the CO_2 was probably derived from the oxidation of organic matter and the decarbonation of limestones at depth within the sedimentary column, a secondary source could well have been the pressure solution of hydrothermal carbonates. Local variations in the mole % CO_2 could thus be a function of local variations in the carbonate content of the adjacent rocks.

The calculated oxygen isotopic composition of the quartz-forming, deformation fluids (Table 9) suggests that they were probably derived from formation waters. Formation waters are also the source of the mineralizing fluids, but the latter have a salinity of 9.1 weight percent NaCl equivalent as opposed to the lower salinity (4.8 weight percent NaCl equivalent), deformation fluids. The lower salinity of the deformation fluids may be the result of greater compaction of the sedimentary column, which thus restricts the membrane filtration process from effectively increasing the fluid salinity.

REFERENCES

Abbott, J.G., 1982, Structure and Stratigraphy of the MacMillan Fold Belt; Evidence for Devonian faulting: Yukon Exploration and Geology 1981, p. 22-33.

-----, 1983, Geology of the MacMillan Fold Belt, D.I.A.N.D. Open File Report.

Arai, Y., Kaminishi, G., and Saito, S., 1971, The experimental determination of the P-V-T-X relations for the carbon dioxide-nitrogen and the carbon dioxide-methane systems: J. Chem. Eng. Jap., v. 4, p. 113-122.

Badham, J.P.N., 1981, Shale-hosted Pb-Zn deposits: products ofexhalation of formation waters?: Inst. Mining and Metallurgy Trans., v. 90, sec. B, p. B70-B76.

Barnes, H.L., 1979, Solubilities of ore minerals, *in* Barnes, H.L., ed., Geochemistry of hydrothermal ore deposits: New York, Wiley, p. 404-460.

Berner, R.A., 1974, Iron sulfides in Pleistocene deep Black Sea sediments and their palaeo-oceanographic significance: Am. Assoc. Petroleum Geologists Mem. 20, p. 524-531.

Blacic, J.D., 1975, Plastic-deformation mechanisms in quartz: the effect of water: Tectonophysics, v. 27, p. 271-294.

Blount, C.W., 1977, Barite solubilities and thermodynamic quantities up to 300°C and 1400 bars: Am. Mineralogist, v. 62, p. 942-957.

Blusson, S.L., 1976, Selwyn Basin: Yukon and District of MacKenzie: Geol. Survey Canada, Paper 76-1A, p. 131-132.

Bodnar, R.J., and Bethke, P.M., 1984, Systematics of stretching of fluid inclusions I: Fluorite and Sphalerite at 1 atmosphere confining pressure: Econ. Geol., v. 79, p.141-161.

Bottinga, Y., 1969, Calculated fractionation factors for carbon and hydrogen isotope exchange in the system calcite-carbon dioxide-graphite-methane-hydrogen-water vapor: Geochim. et Cosmochim. Acta, v. 33, p. 49-64.

Bozzo, A.T., Chen, H-S., Kass, J.R., and Barduhn, A.J., 1975, The properties of the hydrates of chlorine and carbon dioxide: Desalination, v. 16, p. 303-320.

Burruss, R.C., 1981a, Analysis of phase equilibria in C-O-H-S fluid inclusions: Mineralog. Assoc. Canada, Short Course Handbook 6, p. 39-74.

-----, 1981b, Analysis of fluid inclusions: phase equilibria at constant volume: Am. J. Sci., v. 281, p. 1104-1126.

Carne, R.C., 1979, Upper Devonian stratiform barite-lead-zinc-silver mineralization at Tom claims, MacMillan Pass, Yukon Territory: Unpub. M. S. thesis, Univ. of British Columbia, 149 p.

Carne, R.C., and Cathro, R.J., 1982, Sedimentary exhalative (sedex) zinc-lead-silver deposits, northern Canadian Cordillera: C.I.M. Bull, v. 75, p. 66-78.

Cecile, M.P., Shakur, M.A., and Krouse, H.R., 1983, The isotopic composition of Western Canadian barites and the possible derivation of oceanic sulphate $\delta^{34}S$ and $\delta^{18}O$ age curves: Canadian Jour. Earth Sci., v. 14, p. 476-489.

Clayton, R.N., and Mayeda, T.K., 1963, The use of bromine pentafluoride in the extraction of oxygen from oxides and silicates for isotopic analysis: Geochim. et Cosmochim. Acta, v. 27, p. 43-52.

Clayton, R.N., Jackson, M.L., and Sridhar, K., 1978, Resistance of quartz silt to isotopic exchange under burial and intense weathering conditions: Geochim. et Cosmochim. Acta, v. 42, p. 1517-1522.

Clayton, R.N., Muffler, L.J.P., and White, D.E., 1968, Oxygen isotope study of calcite and silicates of the River Ranch No. 1 Well, Salton Sea geothermal field, California: Am. J. Sci., v. 266, p. 968-979.

Clayton, R.N., O'Neil, J.R., and Mayeda, T.K., 1972, Oxygen isotope exchange between quartz and water: Jour. Geophys. Research, v. 77, p. 3057-3067.

Clynne, M.A., and Potter, R.W., II, 1977, Freezing point depression of synthetic brines: Geol. Soc. America, Abstracts with Programs, v. 9, p. 930.

Collins, P.L.F., 1979, Gas hydrates in CO_2-bearing fluid inclusions and the use of freezing data for estimation of salinity: Econ. Geol., v. 74, p. 1435-1444.

Craig, H., 1957, Isotopic standards for carbon and oxygen and correction factors for mass spectrometric analysis of carbon dioxide: Geochim. et Cosmochim. Acta, v. 12, p. 133-149.

-----, 1961, Standard for reporting concentrations of deuterium and oxygen-18 in natural waters: Science, v. 133, p. 1833-1834.

Crawford, M.L., 1981, Phase equilibria in aqueous fluid inclusions: Mineralog. Assoc. Canada, Short Course Handbook 6, p. 75-100.

Dawson, K.M., 1983, A review of barite in the northern Cordillera: Program with Abstracts, C.I.M. Mineral Deposits of northern Cordillera, p. 18.

Dawson, K.M., and Orchard, 1982, Regional metallogeny of the northern Cordillera: biostratigraphy, correlation and metallogenic significance of bedded barite occurrences in eastern Yukon and western District of Mackenzie: Geol. Survey Canada Paper 82-1C, pt. C; p.31-38.

Douglas, R.J.W., Gabrielse, H., Wheeler, J.O., Stott, D.F., and Belyea, H.R., 1970, Geology of Western Canada: *in* Douglas, R.J.W., ed., Geology and Economic Minerals of Canada: Geol. Survey Canada, p. 367-546.

Ellis, A.J., 1979, Explored geothermal systems: *in* Barnes, H.L., ed., Geochemistry of hydrothermal ore deposits: New York, Wiley, p. 632-683.

Ellis, A.J., and Golding, R.M., 1963, The solubility of carbon dioxide above 100°C in water and in sodium chloride solutions: Am. Jour. Sci., v. 261, p. 47-60.

English, P.J., 1981, Gold-quartz veins in metasediments of the Yellowknife Supergroup, Northwest Territories: A fluid inclusion study: Unpub. M. S. thesis, Univ. of Alberta, 107 p.

Eslinger, E.V., and Savin, S.M., 1973, Oxygen isotope geothermometry of the burial metamorphic rocks of the Precambrian Belt Supergroup, Glacier National Park, Montana: Geol. Soc. America Bull., v. 84, p. 2549-2560.

Finlow-Bates, T., 1980, The chemical and physical controls on the genesis of submarine exhalative orebodies and their implications for formulating exploration concepts. A review: Geol. Jahrb., v. D40, p. 131-168.

Gabrielse, H., Blusson, S.L., and Roddick, J.A., 1973, Geology of the Flat River, Glacier Lake, and Wrigley Lake map-areas, District of Mackenzie and the Yukon Territory (95 E, L, M): Geol. Survey Canada Mem. 366, 153 p.

Gardner, H.P., 1983, Petrologic and geochemical constraints on the genesis of the Jason Pb-Zn deposits, Yukon Territory: Unpub. M. S. thesis, Univ. of Calgary, 212 p.

Giordano, T.H., and Barnes, H.L., 1981, Lead transport in Mississippi Valley-type ore solutions: Econ. Geol., v. 76, p. 2200-2211.

Godwin, C.I., and Sinclair, A.J., 1982, Average lead isotope growth curves for shale-hosted zinc-lead deposits, Canadian Cordillera: Econ. Geol., v. 77, p. 675-690.

Gordey, S.P., 1980, Stratigraphic cross-section, Selwyn Basin to Mackenzie Platform, Nahanni map area, Yukon Territory and District of Mackenzie: Geol. Survey Canada Paper 80-1A, pt. A, p. 353-355.

Gordey, S.P., Abbott, J.G., and Orchard, M.J., 1982, Devono-Mississippian (Earn Group) and younger strata in east-central Yukon: Geol. Survey Canada Paper 82-1B, pt. B, p. 93-100.

Gordey, S.P., Wood, D.,and Anderson, R.G., 1981, Stratigraphic framework of southeastern Selwyn Basin, Nahanni map area, Yukon Territory and District of Mackenzie: Geol. Survey Canada Paper 81-1A, pt. A, p. 395-398.

Graf, D.L., 1982, Chemical osmosis, reverse chemical osmosis, and the origin of subsurface brines: Geochim. et Cosmochim. Acta, v. 46, p. 1431-1448.

Griggs, D.T., and Blacic, J.D., 1965, Quartz - anomalous weakness of synthetic crystals: Science, v. 147, p.292-295.

Haas, J.L., 1971, The effect of salinity on the maximum thermal gradient of a hydrothermal system at hydrostatic pressure: Econ. Geol., v. 66, p. 940-946.

Holland, H.D., and Malinin, S.D., 1979, The solubility and occurrence of non-ore minerals: *in* Barnes, H.L., ed., Geochemistry of hydrothermal ore deposits: New York, Wiley, p. 461-508.

Hollister, L.S., and Burruss, R.C., 1976, Phase equilibria in fluid inclusions from the Khtada Lake metamorphic complex: Geochim. et Cosmochim. Acta, v. 40, p. 163-175.

Hollister, L.S., and Crawford, M.L., 1981, Fluid inclusions: Applications to petrology: Mineralog. Assoc. Canada, Short Course Handbook 6, 304 p.

Ignasiuk, T.M., Kotlyar, L., Longstaffe, F.J., Strausz, O.P., and Montgomery, D.S., 1983, Separation and characterization of clay from Athabasca asphaltene: Fuel, v. 62, p. 353-362.

Jefferson, C.W., Kilby, D.B., Pigage, L.C., and Roberts, W.J., 1983, The Cirque barite-lead-zinc deposits, northeastern British Columbia: Mineralog. Assoc. Canada, Short Course Handbook 8, p. 121-140.

Jennings, D.S., Jilson, G.A., and Pigage, L.C., 1980, Anvil Range stratigraphy, south-central Yukon Territory: Program with Abstracts, Geol. Assoc. Canada Cordilleran Section, p. 16.

Jennings, D.S., and Jilson, G.A., 1983, Geology and sulphide deposits of Anvil Range, Yukon Territory: Program with abstracts, C.I.M. Mineral Deposits of northern Cordillera, p. 11.

Kerrich, R., 1976, Some effects of tectonic recrystallization on fluid inclusions in quartz veins: Contr. Mineralogy Petrology, v. 59, p. 195-202.

Kerrich, R., Beckinsale, R.D., and Shackleton, N.J., 1978, The physical and hydrothermal regime of tectonic vein systems: evidence from stable isotope and fluid inclusion

studies: Neues Jahrb. Mineral. Abh., v. 131, p. 225-239.

Konnerup-Madsen, J., 1979, Fluid inclusions associated with a metamorphosed molybdenite mineralization in Vest-Agder, south Norway: Econ. Geol., v. 74, p. 1221-1230.

Kreulen, R., and Schuiling, R.D., 1982, N_2-CH_4-CO_2 fluids during formation of the Dome de l'Agout, France: Geochim. et Cosmochim. Acta, v. 46, p.193-203.

Land, L.S., 1983, The application of stable isotopes to studies of the origin of dolomite and to problems of diagenesis of clastic sediments: S.E.P.M., Short Course 10, p. 4-1 - 4-22.8.

Large, D.E., 1981, On the geology, geochemistry, and genesis of the Tom Pb-Zn-Barite deposit, Yukon Territory, Canada: unpub. Ph.D. thesis, University of Braunschweig, 152 p.

-----, 1983, Sediment-hosted massive sulphide lead-zinc deposits: An empirical model: Mineralog. Assoc. Canada, Short Course Handbook 8, p. 1-29.

Large, R.R., 1977, Chemical evolution and zonation of massive sulfide deposits in volcanic terrains: Econ. Geol., v. 72, p. 549-572.

Lawler, J.P., and Crawford, M.L., 1983, Stretching of fluid inclusions resulting from a low-temperature microthermometric technique: Econ. Geol., v. 78, P.527-529.

Leroy, J., 1979, Contribution a l'etalonnage de la pression interne des inclusions fluides lors de leur decrepitation: Bull. Mineral., v. 102, p 584-593.

Longstaffe, F.J., 1983, Diagenesis-4: Stable isotope studies of diagenesis in clastic rocks: Geosci. Canada, v. 10, p. 43-58.

Longstaffe, F.J., Nesbitt, B.E., and Muehlenbachs, K., 1982, Oxygen isotope geochemistry of the shales hosting Pb-Zn-Ba mineralization at the Jason prospect, Selwyn Basin, Yukon: Geol. Survey Canada Paper 82-1C, pt. C, p. 45-49.

Lydon, J.W., 1983, Chemical parameters controlling the origin and deposition of sediment-hosted stratiform lead-zinc deposits: Mineralog. Assoc. Canada, Short Course Handbook 8, p. 175-250.

Lydon, J.W., Lancaster, R.D., and Karkkainen, P., 1979, Genetic controls of Selwyn Basin stratiform barite / sphalerite / galena deposits: An investigation of the dominant barium mineralogy of the Tea deposit, Yukon: Geol. Survey Canada Paper 79-1B, pt. B, p. 223-229.

MacIntyre, D.G., 1983, Geology and stratiform barite-sulphide deposits of the Gataga district, northeast British Columbia: Mineralog. Assoc. Canada, Short Course Handbook 8, p. 85-119.

Magaritz, M., and Taylor, H.P., Jr., 1976, Oxygen, hydrogen and carbon isotope studies of the Franciscan Formation, Coast Ranges, California: Geochim. et Cosmochim. Acta, v. 40, p. 215-234.

McClay, K.R., 1982, Tectonic and sedimentary structure in the sulphide orebodies of Mount Isa (Australia) and Sullivan (Canada): Inst. Mining Metallurgy Trans., v. 91, sec. B., p. B146-151.

-----, 1984, The geology of the Tom deposit, MacMillan Pass, Yukon Territory, Canada: Geol. Assoc. Canada (Cordilleran Section), Short Course Notes 2 (Part 2), p. 60-96.

McClay, K.R., and Ellis, P.C., 1983, Deformation and recrystallization of pyrite: Mineral.

Mag., v. 47, p. 527-538.

McCrea, J.M., 1950, On the isotopic chemistry of carbonates and a palaeotemperature scale: Jour. Chem. Physics, v. 18, p. 849-857.

McCready, R.B.L., and Krouse, H.R., 1980, Sulfur isotope fractionation by *Desulfovibrio vulgaris* during metabolism of $BaSO_4$: Geomicrobiology Jour., v. 6, p. 55-61.

Morganti, J.M., 1983, Geology and mineralization of the Howard's Pass zinc-lead deposits, Yukon-Northwest Territories: Program with Abstracts, C.I.M. Mineral Deposits of Northern Cordillera, p. 12-13.

Mullis, J., 1979, The system methane-water as a geologic thermometer and barometer from the external part of the Central Alps: Bull. Mineral., v. 102, p. 526-536.

Nesbitt, B.E., Longstaffe, F.J., Shaw, D.R., and Muehlenbachs, K., 1984, Oxygen isotope geochemistry of the Sullivan massive sulfide deposit, Kimberley, Canada: Econ. Geol., v. 79, p. 933-946.

Northrop, D.A., and Clayton, R.N., 1966, Oxygen-isotope fractionations in systems containing dolomite: Jour. Geol., v. 74, p. 174-196.

O'Neil, J.R., Clayton, R.N., and Mayeda, T.K., 1969, Oxygen isotope fractionation in divalent metal carbonates: Jour. Chem. Physics, v. 51, p. 5547-5558.

O'Neil, J.R., and Kharaka, Y., 1976, Hydrogen and oxygen isotope exchange reactions between clay minerals and water: Geochim. et Cosmochim. Acta, v. 40, p. 241-246.

Orr, W.L., 1974, Changes in sulfur content and isotopic ratios of sulfur during petroleum maturation - study of Big Horn basin Palaeozoic oils: Am. Assoc. Petroleum

Geologists Bull., v. 58, p. 2295-2318.

Potter, R.W., II, 1977, Pressure corrections for fluid inclusion homogenization temperatures based on the volumetric properties of the system NaCl-H_2O: U. S. Geol. Survey Jour. Res., v. 5, p. 603-607.

Potter, R.W., II, Clynne, M.A., and Brown, D.L., 1978, Freezing point depression of aqueous sodium chloride solutions: Econ. Geol., v. 73, p. 284-285.

Poty, B., Leroy, J., and Jachimowicz, L., 1976, A new device for measuring temperature under the microscope : the Chaixmeca microthermometry apparatus: COFFI Fluid Inclusion Research, v. 9, p. 173-178.

Ramboz, C., Pichavant, M., and Weisbrod, A., 1982, Fluid immiscibility in natural processes: use and misuse of fluid inclusion data, II. Interpretation of fluid inclusion data in terms of immiscibility: Chemical Geology, v. 37, p. 29-48.

Ramsay, J.G., 1980, The crack-seal mechanism of rock deformation: Nature, v. 284, p. 135-139.

Reeder, R.J., 1983, Crystal chemistry of the rhombohedral carbonates: Mineralog. Soc. America, Reviews in Mineralogy, v. 11, p 1-48.

Robinson, D.B., and Hutton, J.M., 1967, Hydrate formation in systems containing methane, hydrogen sulphide, and carbon dioxide: Can. Jour. Petroleum Technology, v. 6, p. 6-9.

Roddick, J.A., and Green, L.H., 1961, Geology of Sheldon Lake map sheet (105-J), Yukon Territory: Geol. Survey Canada Prelim. Map 12.

Roedder, E., 1967, Fluid inclusions as samples of ore fluids: *in* Barnes, H.L., ed.,

Geochemistry of Hydrothermal Ore Deposits : Holt, Rinehart, and Winston, New York, p. 515-574.

-----, 1979, Fluid inclusions as samples of ore fluids: *in* Barnes, H.L., ed., Geochemistry of Hydrothermal Ore Deposits : Wiley, New York, p. 684-737.

-----, 1981, Origin of fluid inclusions and changes that occur after trapping: Mineralog. Assoc. Canada, Short Course Handbook 6, p. 101-137.

-----, 1984, Fluid inclusions: Mineralog. Soc. America, Reviews in Mineralogy, v. 12, 644 p.

Roedder, E., and Bodnar, R.J., 1980, Geologic pressure determinations from fluid inclusion studies: Ann. Rev. Earth. Planet. Sci., v. 8, p. 263-301.

Russell, M.J., Solomon, M., and Walshe, J.L., 1981, The genesis of sediment-hosted, exhalative zinc + lead deposits: Mineralium Deposita, v. 16, p. 113-127.

Rye, R.O., and Ohmoto, H., 1974, Sulfur and carbon isotopes and ore genesis: a review: Econ. Geol., v. 69, p. 826-842.

Rye, D.M., and Williams, N., 1981, Studies of the base metal sulfide deposits at McArthur River, Northern Territory, Australia: III. The stable isotope geochemistry of the H.Y.C., Ridge, and Cooley deposits: Econ. Geol., v. 76, p. 1-26.

Samson, I.M., and Russell, M.J., 1983, Fluid inclusion data from Silvermines base metal-baryte deposits, Ireland: Inst. Mining Metallurgy Trans., sec. B, v. 92, p. 867-871.

Sato, T., 1972, Behaviour of ore-forming solutions in sea water: Mining Geology, v. 22, p. 31-42.

Savin, S.M., and Epstein, S., 1970, The oxygen and hydrogen isotope geochemistry of clay minerals: Geochim. et Cosmochim. Acta, v. 34, p. 25-42.

Sawkins, F.J., 1984, Ore genesis by episodic dewatering of sedimentary basins: Application to giant Proterozoic lead-zinc deposits: Geology, v. 12, p. 451-454.

Scott, S.D., 1983, Chemical behaviour of sphalerite and arsenopyrite in hydrothermal and metamorphic environments: Mineral. Mag., v. 47, p. 427-436.

Sheppard, S.M.F., and Schwarz, H.P., 1970, Fractionation of carbon and oxygen isotopes and magnesium between coexisting metamorphic calcite and dolomite: Contr. Mineralogy Petrology, v. 26, p. 161-198.

Smith, D.G.W., and Gold., C.M., 1979, EDATA2: a FORTRAN IV computer program for processing wavelength- and/or energy-dispersive microprobe analyses: *in* Newbury, D.E., ed., Proceedings of the 14th Annual Conference of the Microbeam Analysis Society: Microbeam Analysis Society, p. 273-278.

Solomon, M., and Walshe, J.L., 1979, The formation of massive sulfide deposits on the sea floors: Econ. Geol., v. 74, p. 797-813.

Spooner, E.T.C., 1981, Fluid inclusion studies of hydrothermal ore deposits: Mineralog. Assoc. Canada, Short Course Handbook 6, p. 209-240.

Swanenberg, H.E.C., 1979, Phase equilibria in carbonic systems, and their application to freezing studies of fluid inclusions : Contr. Mineralogy Petrology, v. 68, p. 303-306.

Taylor, H.P., Jr., 1979, Oxygen and hydrogen isotope relationships in hydrothermal mineral deposits: *in* Barnes, H.L., ed., Geochemistry of Hydrothermal Ore Deposits:

New York, Wiley, p. 236-277.

Templeman-Kluit, 1977, Stratigraphic and structural relations between the Selwyn Basin, Pelly-Cassiar Platform, and Yukon Crystalline Terrane in the Pelly Mountains, Yukon: Report of Activities, Part A, Geol. Survey Canada, Paper 77-1A, p. 223-22

Templeman-Kluit, D.J., and Blusson, S.L., 1977, Pelly-Cassiar Platform an d Selwyn Basin: Neither without the other: G.A.C./M.A.C. Program with Abstracts, v. 2, p. 52.

Touret, J.L.R., 1981, Fluid inclusions in high grade metamorphic rocks: Mineralog. Assoc. Canada, Short Course Handbook 6, p. 182-208.

-----, 1982, An empirical phase diagram for a part of the N_2-CO_2 system at low temperature: Chemical Geology, v. 37, p. 49-58.

Turner, J.S., and Gustafson, L.B., 1978, The flow of hot saline solutions from vents in the sea floor - some implications for exhalative massive sulfides and other deposits: Econ. Geol., v. 73, p. 1002-1100.

White, S., 1973, The dislocation structures responsible for the optical effects in some naturally-deformed quartzes: Jour. Materials Science, v. 8, p.490-499.

Winn, R.D., Jr., Bailes, R.J., and Lu, K.I., 1981, Debris flows, turbidites, and lead-zinc sulfides along a Devonian submarine scarp, Jason Prospect, Yukon Territory: *in* S.E.P.M. Core Workshop 2, San Francisco, p. 396-416.

Yeh, H-W., and Savin, S.M., 1977, Mechanism of burial metamorphism of argillaceous sediments: 3. O-isotope evidence: Geol. Soc. America Bull., v. 88, p. 1321-1330.

APPENDIX 1. SECTIONS ACROSS THE TOM WEST ZONE

LEGEND

Referenced samples ●

Other samples ○

Mineralization

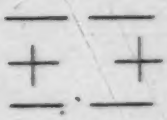

Replaced by ankerite

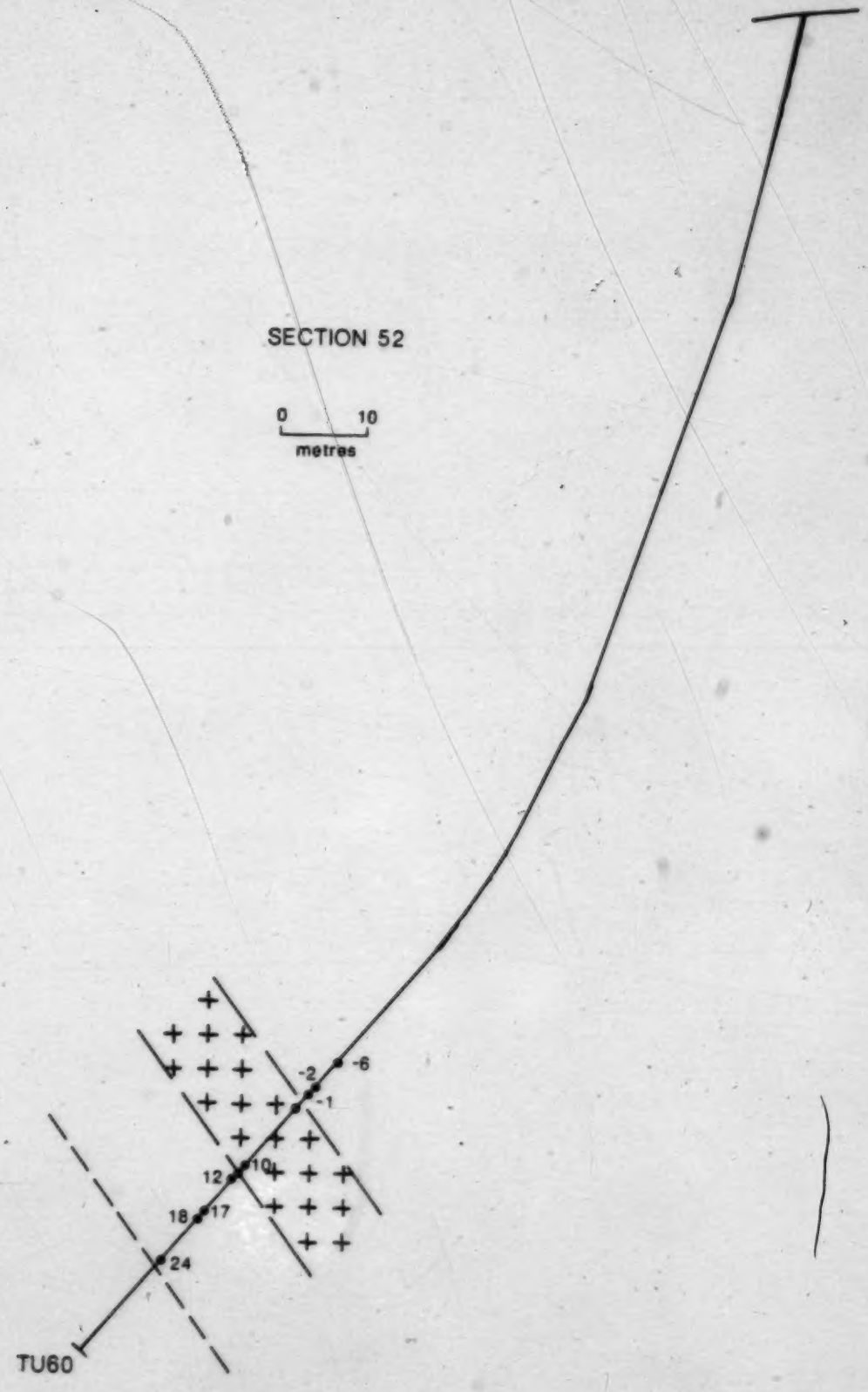
SECTION 52
0
10
metres
-6
-2
-1
10
12
17
18
24
TU60

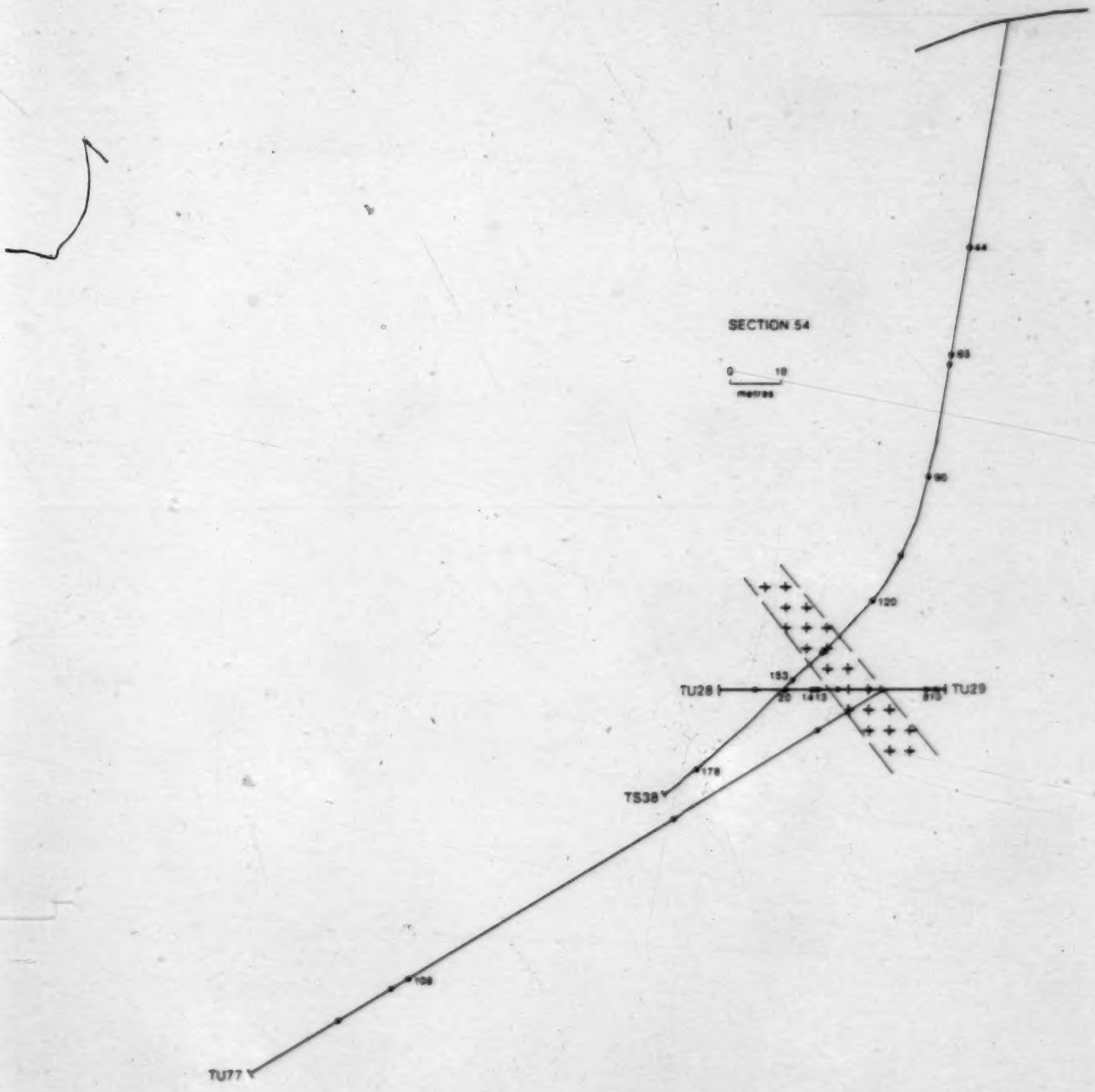
SECTION 54
0
10
metres
44
65
90
120
153
TU28
20
1413
TU29
178
TS38
109
TU77

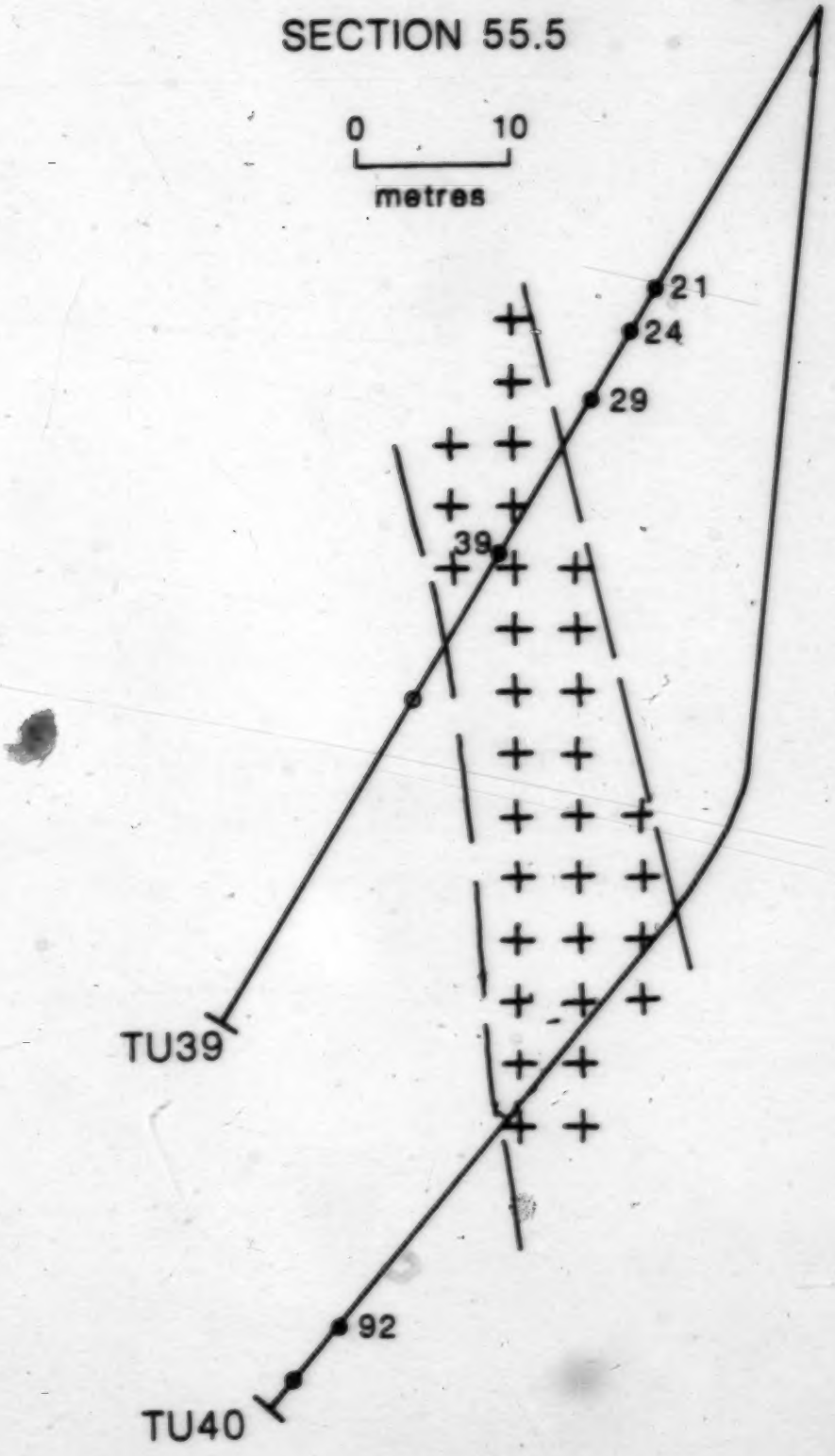
SECTION 55.5
0
10
metres
21
24
29
39
TU39
92
TU40

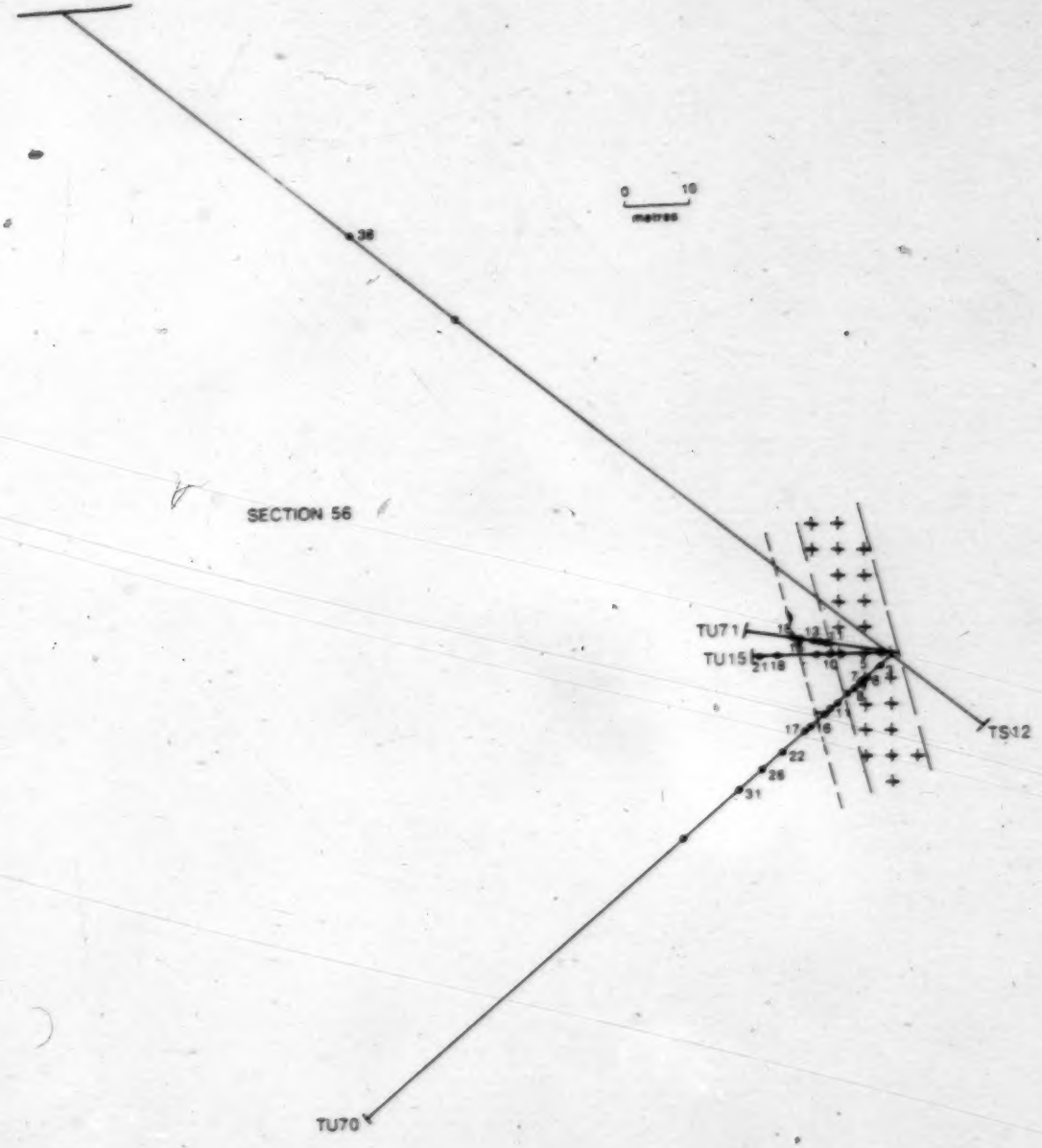
0
10
metres
SECTION 56
TU71
TU15
TU70
TS12

SECTION 58

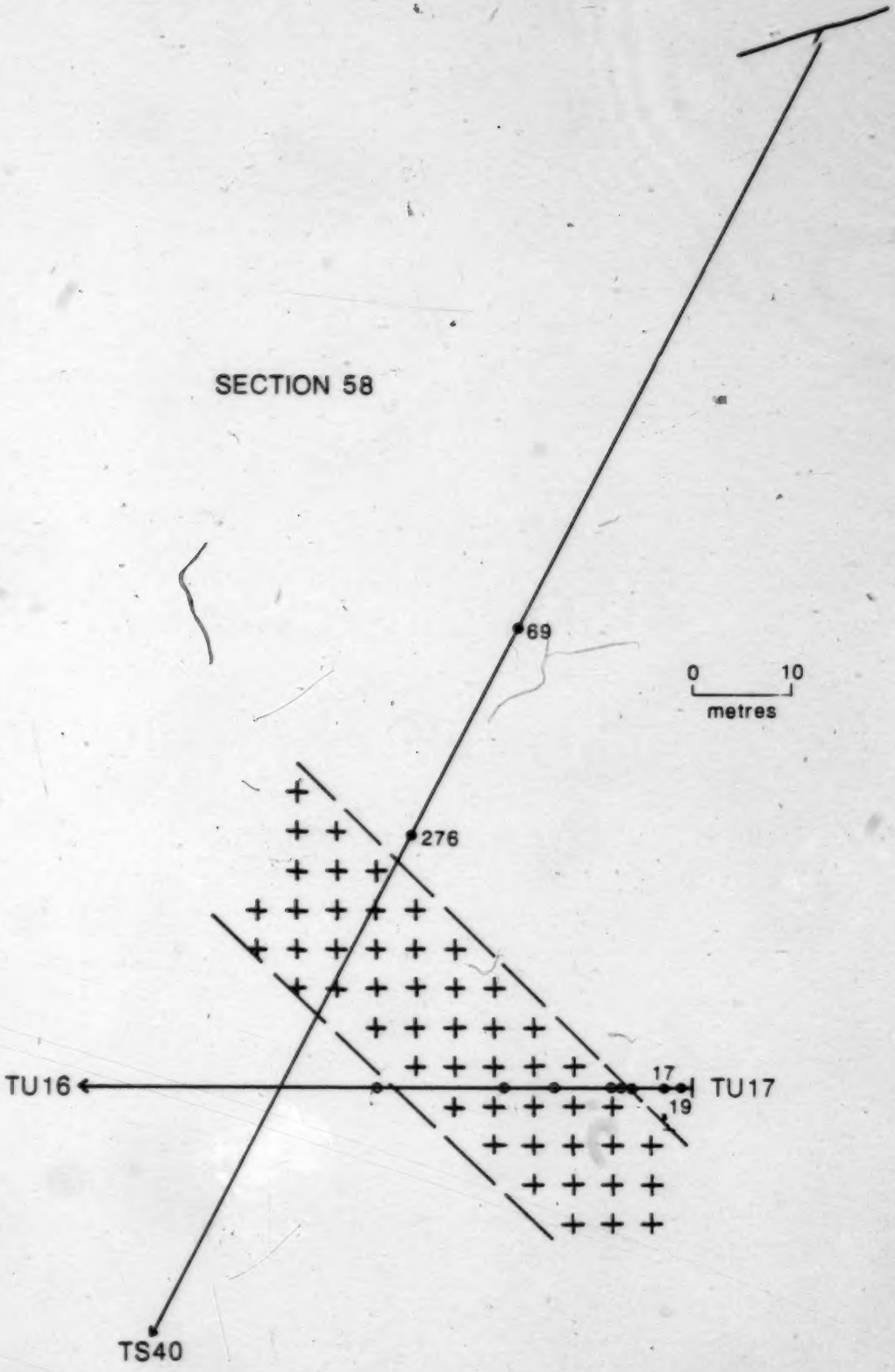

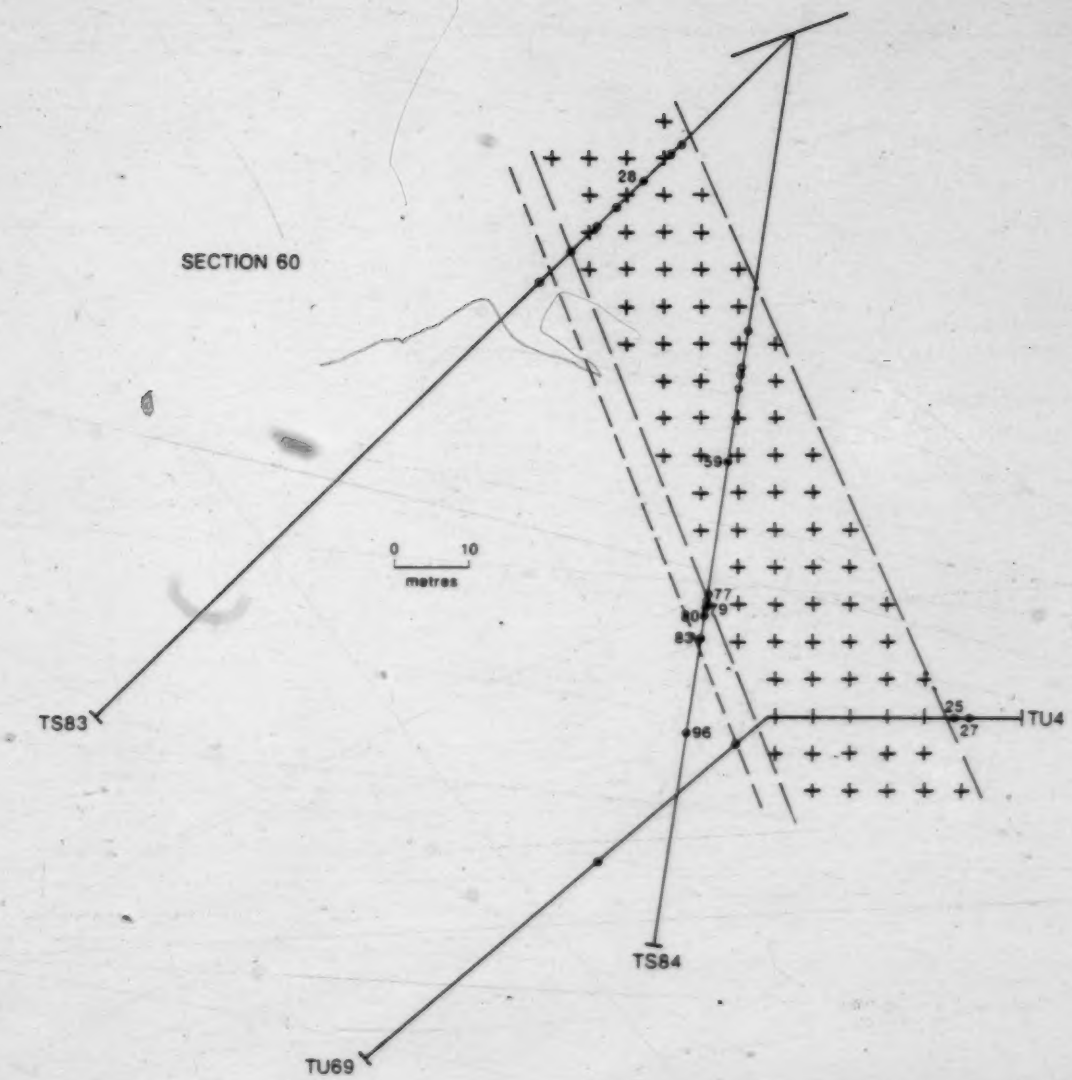
SECTION 60
0
10
metres
28
59
77
9
80
83
96
25
27
TS83
TU4
TS84
TU69

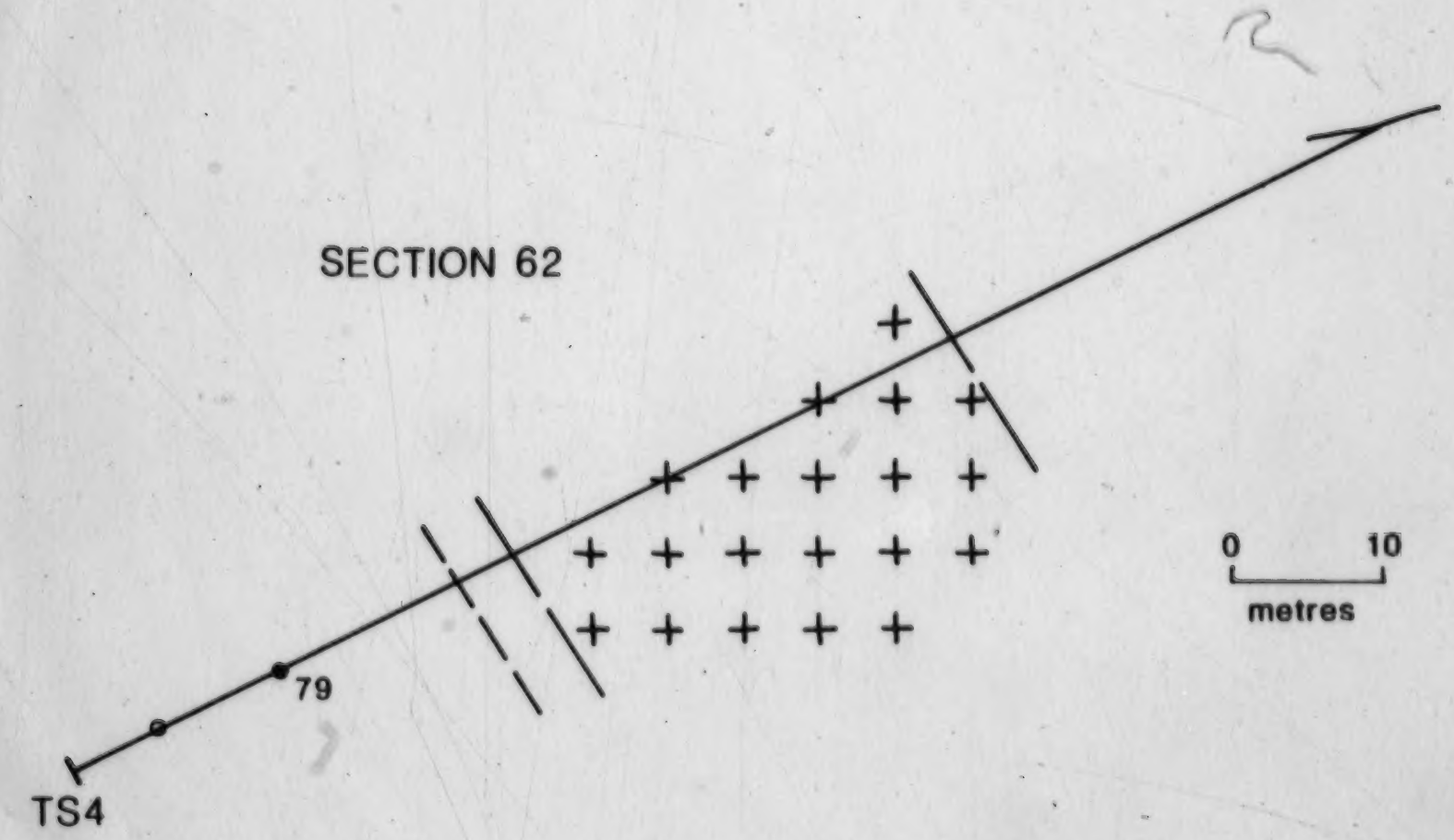
SECTION 62
79
TS4
0
10
metres

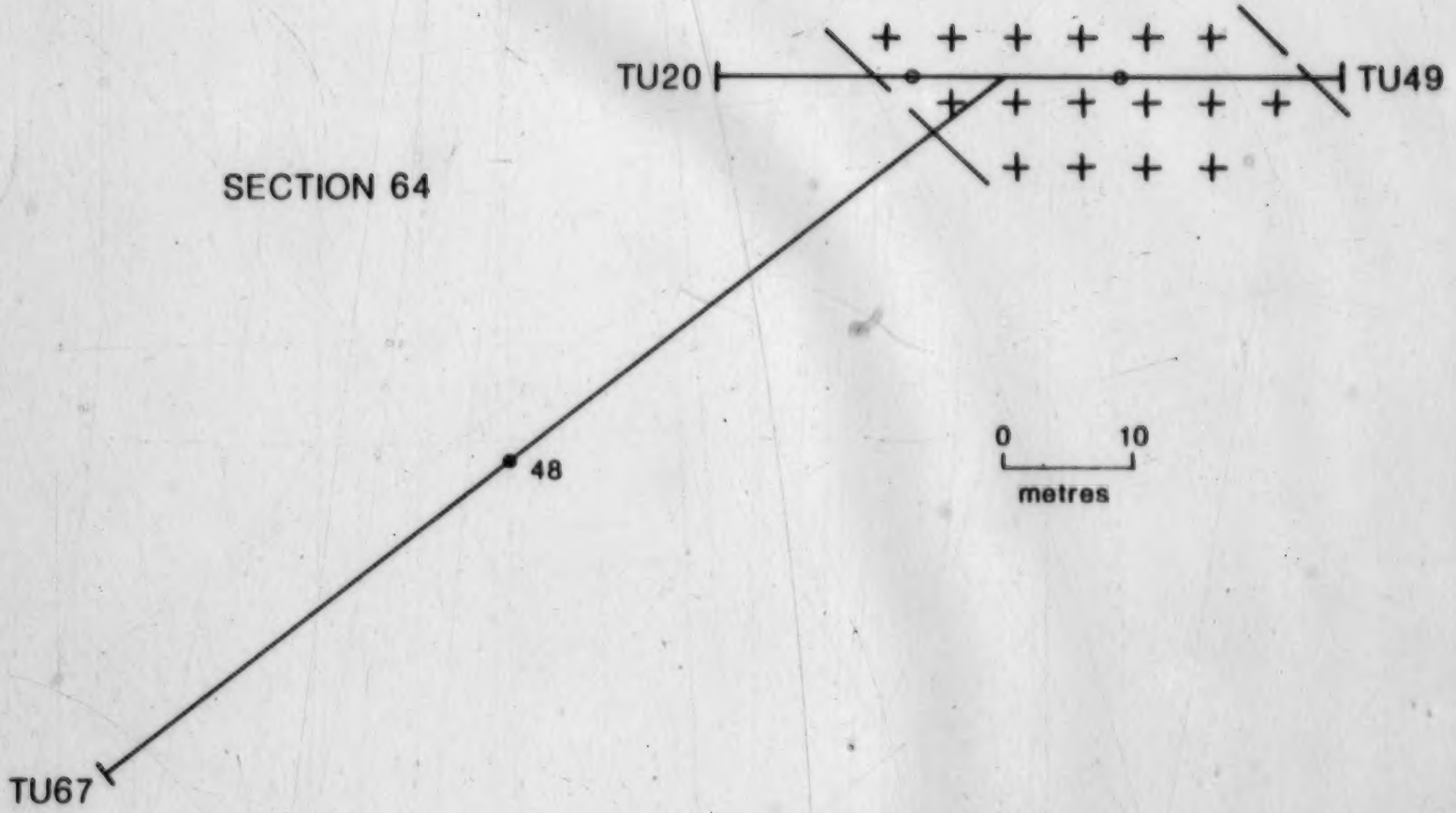
TU20
TU49
SECTION 64
48
TU67
0
10
metres

All sections oriented ENE - WSW perpendicular to the base line shown on Figure 5.

APPENDIX 2. PREPARATION OF CLAY SAMPLES

1. Disaggregation of samples.

Attempts were made to disaggregate the mudstones by crushing with a hammer and slaking in distilled water, followed by vigorous stirring with an ultrasonic probe. This process was unsuccessful, because of the highly silicified nature of the mudstones.

The method finally used was to swingmill the samples for 5 seconds. Unfortunately, this mechanical disaggregation may have artificially affected the grain size characteristics of the sample resulting in a spuriously high amount of quartz in the <2 μm fraction. The relative proportions of extremely fine-grained silica cement and artificially produced <2 μm quartz cannot be estimated however.

2. Clay mineral recovery and identification

A test sample (TS38-65) was split and both halves Ca^{2+} and K^{+}-saturated following the procedure of Ignasiuk et al. (1983). One half was treated with 3 % sodium hypochlorite solution prior to grain settling, while the other half was treated after settling. The former treatment was utilized to determine whether any of the clay minerals were being bound together by organic matter. The difference in the quantity of clay minerals obtained by the two methods and thus the effect of organic matter, was minimal. The latter treatment was used for the remaining samples since it was less time-consuming.

The clay mineralogy of the test sample was simple (illite and kaolinite) and could be identified without using all the six X-ray patterns indicated below :

(1) Ca-disc, 54 % relative humidity, 2°-35° 2θ ,

(2) Ca-disc glycolated, 54 % relative humidity, 2°-80° 2θ ,

(3) K-disc, 0 % relative humidity, 2°-25° 2θ ,

(4) K-disc, 54 % relative humidity, 2°-25° 2θ ,

(5) K-disc, 0 % relative humidity, 300°C, 2°-25° 2θ ,

(6) K-disc, 0 % relative humidity, 550°C, 2°-25° 2θ .

For the remaining samples the <2 μm fraction was analyzed unsaturated at 54 % relative humidity.

All samples were gravity-settled through calgonated, distilled water. Test samples (TU39-29, TS38-90) showed that although all the clay minerals were not recovered in the <2 μm fraction, the relative proportions of illite and kaolinite were the same in the <2 μm fraction and the residue after settling.

APPENDIX 3. RELATIVE INTENSITIES OF KAOLINITE AND ILLITE PEAKS ON X.R.D. CHARTS

Sample number	Section	Location	Kaolinite peak height intensity	Illite peak height intensity
TU60-(-6)	52	HW	5.0	76.5
TU60-(-2)		HW	4.0	57.0
TU60-(-1)		HW	4.0	28.0
TS38-65	54	HW	6.0	43.0
TS38-90		HW	8.0	43.0
TS38-120		HW	---	68.0
TS38-153		FW	12.5	12.0
TS38-178		FW	---	79.0
TU29-10		HW	4.5	26.5
TU29-8		HW	5.5	22.5
TU28-14		FW	---	21.5
TU28-20		FW	---	83.0
TU39-21	55.5	HW	6.0	42.0
TU39-24		HW	---	22.5
TU39-29		HW	74.0	19.0
TU70-22	56	FW	---	37.0
TU70-26		FW	---	96.0
TU70-31		FW	---	79.0
TU15-18		FW	5.0	18.5
TU15-21		FW	---	31.0
TU17-17	58	HW	---	17.5
TU17-19		HW	---	23.0
TS40-276		FW	---	68.0
TS40-69		FW	---	64.01
TU4-25	60	HW	4.5	8.0
TU4-27		HW	6.0	26.0
TS84-83		FW	44.0	15.0
TS84-96		FW	4.5	29.5

APPENDIX 4. FLUID INCLUSION MEASUREMENTS

* degree of filling estimated at 40°C

Sample number	Incl. number	Incl. type	Host mineral	$TmCO_2$	Te	Tmice	TmClath	$ThCO_2$	D.F.	Th	Td
TU60-10A	1/1/1	2	Q	-57.4	---	---	10.1	22.7	63*	324(V)	---
	1/1/2	1	Q	---	<-24	-3.8	---	---	85-90	171	---
	1/1/3	2	Q	-57.4	---	-3.0	---	---	85	---	203
TU60-12	1/2/5/1	2	Q	-59.2	---	---	8.4	11.2	80*	---	---
	1/2/4/a	1	Q	---	---	-1.2±0.3	---	---	95	---	---
	1/2/4/b	2	Q	-59.8	---	---	10.6	---	20*	---	---
TU60-18	1/5/1	1	A	---	-36±8	---	---	---	75	---	---
	1/5/2	1	A	---	---	---	---	---	91	194	---
	1/4/1	1	A	---	---	-4.0	---	---	82.5	---	---
TU60-24	1/1/1	1	A	---	-32±7	-3.7	---	---	88	---	<335
	1/1/2	1	A	---	---	---	---	---	90	---	<335
	1/1/3	1	A	---	---	---	---	---	90	---	<335
	1/1/5	1	A	---	---	---	---	---	93	---	<335
	1/2/1	1	A	---	---	-2.5±1.3	---	---	90	>253	---
	2	1	Q	---	---	-0.7	---	---	90	---	310
TS38-44	1/1	1	Q	---	-25±2	-1.9±0.5	---	---	80	---	<309
	2/4	2	Q	-56.9	-24±4	---	8.2	21.1	40*	291(V)	---
	3/5	2	Q	-57.0	---	---	9.2	22.1	30*	335(V)	---
	2/1	1	Q	---	---	-3.1±0.3	---	---	80	---	---
	2/2	1	Q	---	---	-3.6	---	---	95	---	---
TU77-108	2	2	Q	-86.5	---	---	---	12.0	98*	---	---
	3	2	Q	-57.7	---	---	10.8	16.2	60*	---	---
	2/1	2	Q	-58.1	---	---	11.3	14.1	40*	---	---
	2/2	2	Q	-58.7	-25±5	-5.0	11.9	18.6	85*	---	---
	15/1	2	Q	-58.8	---	---	---	12.9	65*	---	---
	15/2	2	Q	-57.4	---	---	---	12.7	25*	---	---
	15/3	2	Q	-57.4	---	---	---	12.7	35*	---	---
	15/4	2	Q	-57.8	---	---	---	12.0	60*	---	---
	1/1	2	Q	-56.5	---	---	7.5	21.0	82*	---	---
	1/2	2	Q	-56.8	---	---	9.0	19.6	90*	---	268
TU40-92	2/1/1	1	A	---	-23±2	---	---	---	88	---	279
	3/1	1	A	---	-39±6	-9.2	---	---	83	---	286
	4/1	1	A	---	---	---	---	---	89	---	272
TS12-36	1/1	2	Q	-57.1	---	---	9.4	15.9	50*	221	---
	1/2	2	Q	-57.4	---	---	9.7	22.9	83*	278	---
	1/3	2	Q	-56.9	---	---	9.9	23.6	81*	264	---

Sample number	Incl. number	Incl. type	Host mineral	$TmCO_2$	Te	Tmice	TmClath	$ThCO_2$	D.F.	Th	Td
	1/4	1	Q	---	-31±4	-4.0±0.9	---	---	95	---	---
	1/5	2	Q	-57.1	---	---	9.0	20.6	72*	268	278
	1/6	1	Q	---	-26±2	-3.0	---	---	85	---	<278
	1/7	1	Q	---	-26±2	-4.3	---	---	95	---	<278
	1/8	2	Q	-57.0	---	---	9.6	23.0	63*	---	---
	2/1	2	Q	-57.8	---	---	10.4	21.9	73*	---	---
	C/1	2	Q	-56.9	---	-1.9	9.4	26.3	83*	---	---
	C/2	2	Q	-56.9	---	---	10.4	26.7	70*	---	---
	C/3	2	Q	---	---	---	---	24.4	---	---	---
	C/4	2	Q	---	---	---	---	25.2	---	---	---
	C/5	2	Q	---	---	---	10.0	26.3	75*	---	---
	C/6	2	Q	---	---	---	---	19.6	50*	---	---
	C/7	2	Q	---	---	---	---	-2.1(V)	0	---	---
	C/8	1	Q	---	---	---	---	---	90	157	---
	C/9	2	Q	---	---	---	---	---	80	263	---
	C/10	2	Q	---	---	---	---	---	50	278	---
TU15-10A	2/1/2	2	A	---	---	---	---	17.4	88*	---	---
	2/1/3	2	A	---	---	---	---	16.8	87*	---	---
	3/1/1	1	A	---	-30±5	---	---	---	80	---	---
	3/1/3	2	A	-57.2	---	---	10.3	---	60*	---	---
	3/1/6	2	A	-57.1	---	---	9.4	---	45*	---	---
	3/1/7	1	A	---	---	-4.1	---	---	95	---	---
	3/1/8	2	A	-57.2	---	---	10.4	21.4	76*	---	---
	3/2/1	1	A	---	---	-3.6	---	---	85	---	---
	2/2/1	1	A	---	---	---	---	---	93	235	---
TU70-6	1/1	2	Q	-58.6	---	---	10.9	23.0	80*	---	262
	1/2	2	Q	-60.8	---	---	9.4	11.4	77*	---	---
	1/a	2	Q	-58.3	---	---	10.0	13.6	83*	---	269
	1/b	2	Q	-58.3	---	---	10.0	13.6	86*	---	271
	1/c	2	Q	-58.0	---	---	13.4	16.6	94*	---	270
	1/d	2	Q	-60.3	---	---	7.8	13.6	59*	---	---
	1/e	2	Q	-59.3	---	---	14.0	10.6	82*	---	---
	1/f	2	Q	-59.3	---	---	14.0	12.1	32*	---	---
	5/1	1	A	---	-25±4	-5.4±0.6	---	---	90	230	359
	1/3	2	Q	-58.4	---	-4.2±0.8	16.5	19.2	50*	---	324
	1/4	2	Q	-58.9	---	---	10.9	14.5	92*	---	349

Sample number	Incl. number	Incl. type	Host mineral	$TmCO_2$	Te	Tmice	TmClath	$ThCO_2$	D.F.	Th	Td
	4	2	A	-58.2	---	---	9.9	16.6(C)	60*	---	---
	3/4	2	A	-57.7	---	---	9.8	21.5(V)	40*	---	---
	A	1	A	---	---	---	---	---	75	215	---
	C	1	A	---	---	---	---	---	70	204	---
TU70-7	1/1	1	A	---	-30±5	-8.2	---	---	86	---	---
	1/3	1	A	---	---	-14.5	---	---	91	---	---
	1/4	1	A	---	---	---	---	---	92	269	---
	2/1	2	A	-57.6	---	---	9.4	28.0	44	---	253
	A	1	A	---	---	---	---	---	87	216	---
TU70-8	2/1/2/1	1	A	---	-38±2	-10.7	---	---	86	---	---
	2/1/2/2	2	A	-56.5	---	-4.8±0.6	9.0	24.3(V)	66*	---	---
	2/3/a	1	A	---	-36±5	-5.2±0.4	---	---	91	272	---
	2/3/d	1	A	---	---	---	---	---	---	258	---
TU70-11	1/1	2	Q	-56.9	---	---	9.5	18.2	35*	---	---
	1/2	2	Q	-57.0	---	---	9.1	22.1	90*	---	---
	1/3	2	Q	-57.5	-29±1	-4.7	8.4	19.6	69*	---	186
	1/4	2	Q	-56.8	-30±4	-5.0	9.6	24.2	92*	---	202
	1/5	2	Q	-56.7	---	---	---	17.3	0	---	---
	1/6	2	Q	-56.7	---	---	9.1	24.6	84*	---	247
	1/7	2	Q	---	---	---	---	24.5	90*	---	---
	1/8	2	Q	---	---	---	---	---	80	---	246
	1/9	2	Q	---	---	---	---	---	98	226	---
	1/10	2	Q	---	---	---	---	---	95	240	---
	1/11	2	Q	---	---	---	---	---	85	---	244
	1/12	2	Q	---	---	---	---	---	85	---	245
	1/13	2	Q	---	---	---	---	---	90	---	248
	1/14	2	Q	---	---	---	---	---	65	236	---
	1/15	2	Q	---	---	---	---	---	75	238	---
	1/16	2	Q	---	---	---	---	---	75	233	---
	1/17	2	Q	---	---	---	---	---	70	---	195
	1/18	2	Q	---	---	---	---	---	55	303(V)	---
TU70-16A	2/1/1	2	Q	-57.7	---	---	9.2	25.0	70*	---	---
	2/2	1	A	---	---	-3.1	---	---	93	---	---
	2/2/1	2	Q	-57.0	---	-6.6	9.8	25.6	87*	---	---
	2/2/2	2	Q	-57.1	-35±4	-5.5	8.4	26.1	82*	---	---
	2/2/3	2	Q	-57.1	---	-5.9	8.2	25.2	82*	---	---

Sample number	Incl. number	Incl. type	Host mineral	$TmCO_2$	Te	Tmice	TmClath	$ThCO_2$	D.F.	Th	Td
	2/2/4	2	Q	-57.1	---	---	8.9	25.4	78*	---	---
	2/2/5	2	Q	-57.1	-30±2	-5.5	9.2	26.0	82*	---	---
TU70-17	1A/6/1	1	Q	---	---	-3.4	---	---	95	164	---
	1A/6/2	1	Q	---	---	-2.7	---	---	90	---	---
	1A/6/3	1	Q	---	---	-3.6	---	---	90	---	---
	1A/6/4	1	Q	---	---	-2.7	---	---	88	---	---
	1A/6/5	1	Q	---	---	-2.5	---	---	80	---	---
TU71-13	1/1/1	1	A	---	-33±4	-6.2	---	---	97	---	---
	2/1/2	1	A	---	<-26	-6.5	---	---	96	210	---
TU71-15	1/1	1	Q	---	-26±2	-2.3	---	---	85	195	---
	1/2	1	Q	---	-27	---	---	---	90	---	---
	1/3	2	Q	-57.4	---	---	10.1	21.9	72.5*	---	---
	1/4	2	Q	---	---	---	10.4	24.5	20*	---	---
	1/5	1	Q	---	---	---	---	---	65	226	---
	1/6	1	Q	---	---	---	---	---	75	207	---
	1/7	1	Q	---	---	---	---	---	85	209	---
	1/8	1	Q	---	---	---	---	---	80	250	---
	2/1	2	Q	---	---	---	---	---	65*	---	267
	2/2	2	Q	-57.0	---	---	13.2	27.0	78*	---	---
	2/3	2	Q	-57.1	---	---	9.6	27.0	76.5*	271	---
	2/4	2	Q	---	---	---	---	22.6	74*	233(V)	---
	2/5	2	Q	---	---	---	---	27.2	80*	---	<251
	3/1	2	Q	-57.0	---	-3.1	9.9	25.8	89.5*	258	---
	3/2	2	Q	-57.0	---	---	9.8	26.3	89*	253	---
	3/3	1	Q	---	---	-2.0	---	---	70	---	---
	3/4	2	Q	-57.1	---	---	8.4	25.6	72*	239	---
	3/6	2	Q	-57.0	---	---	10.1	22.3	30*	243	---
TS83-28	1	2	Q	-59.5	---	---	19.2	16.1	71*	256(V)	---
	1a	2	Q	---	---	---	---	---	65*	271(V)	---
	2	2	Q	-86.0	---	---	17.4	28.3	60.4*	---	230
	3	2	Q	-62.3	-25±1	---	19.0	23.6	10*	---	216
	4	2	Q	-73.0	-22	-6.6	19.0	29.5	55.5*	---	166
	6	2	Q	-69.9	---	---	19.1	24.2	18*	---	---
	7	2	Q	-64.5	---	---	---	23.1	0	---	---
	8	2	Q	---	---	---	---	23.2	0	---	---
TS84-77	2/1	1	C	---	---	---	---	---	70	260	<297

Sample number	Incl. number	Incl. type	Host mineral	$TmCO_2$	Te	Tmice	TmClath	$ThCO_2$	D.F.	Th	Td
	2/2	1S	C	---	-22	-0.1	---	---	90	115	<297
	2/3	1	C	---	---	-4.9±0.6	---	---	95	---	---
	1/1	1	C	---	---	-3.9±0.6	---	---	90	---	---
	1/2	1	C	---	---	-1.5	---	---	90	---	---
TS84-79	2	2	Q	-57.3	---	---	8.6	24.1	24*	291(V)	---
TS84-80	1/1/1	2	Q	-56.5	---	-5.9±0.4	8.3	26.7	86*	---	---
	1/3/1	1	Q	---	---	-4.1±0.8	---	---	80	244	---
	1/3/2	2	Q	-56.9	---	---	9.8	25.5	83*	---	---
	1/3/3	2	Q	-56.6	---	---	10.7	25.1	70*	266(V)	---
	1/3/4	2	Q	---	---	---	---	27.2	60*	266	---
	1/3/5	1	Q	---	---	---	---	---	80	195	---
	1/3/6	2	Q	---	---	---	---	---	60	253	---
	1/3/7	1	Q	---	---	---	---	---	80	243	---
	1/1/2	2	Q	-56.6	---	---	9.1	28.8	88*	---	---
	1/1/3	2	Q	-56.7	---	---	8.5	24.3	92*	251	---
	1/1/4	2	Q	---	---	---	---	---	65	---	292
	1/1/5	2	Q	---	---	---	---	---	85	189	---
	1/2/1	2	Q	-56.9	---	---	10.4	24.9	33*	---	---
	1/2/2	2	Q	-56.9	---	---	10.8	26.5	80*	---	---
	1	2	Q	---	---	---	---	---	40	---	268
	3	2	Q	---	---	---	---	---	70	---	278
	4	2	Q	---	---	---	---	---	65	---	254
TS4-79	1/1/1	2	Q	-57.3	---	---	9.8	19.8	62*	---	---
	1/1/2	2	Q	-57.4	---	---	9.9	19.0	67*	318(V)	---
	1/1/3	2	Q	-57.0	---	---	9.6	21.7	77*	---	---
	2/1/1	2	Q	-57.4	---	---	10.1	12.3	23*	---	207